Non-Equilibrium Stochastic Models:
Random Average Process and Diffusion with Resetting

Inaugural-Dissertation

zur
Erlangung des Doktorgrades
der Mathematisch-Naturwissenschaftlichen Fakultät
der Universität zu Köln

vorgelegt von

Christos Christou
aus Athen

Köln 2019

Berichterstatter: Prof. Dr. Andreas Schadschneider
Prof. Dr. Joachim Krug

Tag der letzten mündlichen Prüfung: 04.09.2018

Contents

List of Figures . . . iii

List of Tables . . . ix

Abstract . . . xi

Zusammenfassung . . . xiii

1 Introduction . . . 1

2 Condensation in Truncated Random Average Processes . . . 5
2.1. Introduction . . . 5
2.2. Markov Processes and Master Equation . . . 6
2.3. Mass Transport Models with Factorized Steady States . . . 8
2.3.1. Zero Range Process . . . 12
2.3.2. Asymmetric Random Average Process . . . 16
2.4. Truncated processes . . . 18
2.4.1. TARAP . . . 21
2.4.2. ZRRAP . . . 24
2.4.3. SRAP . . . 25
2.5. Discussion and Conclusions . . . 29

3 Continuous Mass Transport Models with $\gamma = -\infty$ . . . 31
3.1. Introduction . . . 31
3.2. Large Deviation Theory . . . 32
3.2.1. Basic Elements of Large Deviation Theory . . . 32
3.2.2. Connection to the Boltzmann Formalism . . . 36
3.3. Canonical Ensemble Approach for Mass Transport Systems . . . 38
3.3.1. Model and general approach . . . 39
3.4. Restricted Processes . . . 41
3.4.1. Examples . . . 48
3.5. Partial Asymmetric Case . . . 51
3.6. Unbounded Transport . . . 52
3.7. Discussion and Conclusions . . . 54

4 Diffusion with Resetting in Bounded Domains . . . 57
4.1. Introduction . . . 57
4.1.1. Background and Motivation . . . 58

4.2. Model 60
4.3. Stationary solution 64
4.4. Survival Probability 66
4.4.1. Existence of the optimal rate 68
4.4.2. Special cases 71
4.4.3. Numerical Results 74
4.5. Discussion and Conclusions 75

5 Diffusion with Resetting inside a two-dimensional Circle . 79
5.1. Introduction 79
5.1.1. General Approach 81
5.2. Diffusion with Resetting in one-dimensional periodic domain . 82
5.3. Hard Resetting 85
5.4. Partial Resetting 89
5.5. Persistent Resetting 92
5.6. Monte Carlo simulation 96
5.7. Discussion and Conclusions 98

6 Conclusions 101

Appendix A Mean Field Approach for the Random Average Process 105

Appendix B Extreme Value Distribution of the Random Average Process 109

Appendix C Effect of Resetting on the Hitting Probability 115

Appendix D Optimal Search Strategy for Intermittent Search Process 119

Bibliography 121

Danksagung 125

Erklärung 127

Curricilum Vitae 129

List of Figures

2.1 Diagrammatic representation of the mapping between the ASEP and the ZRP. 14

2.2 Mapping between the particles on a circle and mass exchange between different sites picture for the asymmetric random average process 16

2.3 Characteristic representation of the dynamics of the TARAP. The mass fraction μ_1 cannot be transported to site 2 since $\mu_1 > \Delta$. On the other side the transport from site 2 to site 3 takes place since $\mu_2 < \Delta$. 19

2.4 Characteristic representation of the function $m^{1-\gamma}$ for different values of the parameter γ. This representation helps us evaluate the function $R(m) = \min\{m, m^{1-\gamma}\}$ used extensively in the next sections. 21

2.5 Schematic diagram for the TARAP model in the ρ-γ plane for $L = 100$. The dashed line describes the crossover between **LF1**-**LF2**. The characteristics of these corresponding states are described by the same dynamics and thus we choose a distinct way of displaying the crossover line between them. 22

2.6 Mean largest value of the TARAP in the stationary limit for $L = 100$ and different values of γ. 22

2.7 Time evolution of the largest mass for the TARAP for $L = 100$, $\gamma = 1$ and different densities. 23

2.8 Mean largest value of the ZRRAP in the stationary limit for different values of γ. 24

2.9 Schematic diagram for the ZRRAP model in the ρ-γ plane for $L = 100$. The dashed line describes the crossover between **LF1**-**LF2**. The characteristics of these two states are described by the same dynamics and thus we choose a distinct way of displaying the crossover line between them. 26

2.10 Mean transported mass per time-step for a site with mass m for the ZRRAP and the SRAP and different parameters γ. We can see that for these two models the first moment μ_1 is described by the same function (Eq. (2.87) and (2.89)). 27

2.11 Mean largest value of the SRAP in the stationary limit for different values of γ. 27

2.12 Schematic diagram for the SRAP model in the ρ-γ plane for $L = 100$. The dashed lines do describe the crossover between **LF1**-**LF2** and **HLF1**-**HLF2** correspondingly. 29

3.1 Numerical evaluation of the probability density function for a random process described by the equation (3.50) for different $q's$ and $\xi_i \sim \varphi(\xi)$ with $\varphi(\xi) = \Theta(1-\xi)$. As we can see for increasing values of q we have a convergence to the expected weight function. 43

3.2 Rate of sites with more than three updates for the uniform density function $\varphi(\mu) = 1$ for a periodic boundary system with $\rho = 0.7$. . . 45

3.3 Single site excess mass (in logarithmic scale) as function of the number of the update steps (also in logarithmic scale) for the algorithm described in detail in the text. The presented results were derived for a system with $\varphi(\mu|m) = 1$ and $\rho = 0.7$. 46

3.4 Single site mass distribution for a system with $L = 100, \rho = 0.7$ and a uniform distribution of the transported masses. The results of the Monte Carlo simulation rely on 10^6 realizations and each trial showed excellent agreement to our analytical result of $p(m) \simeq 1.3m\exp(0.627m)$. 48

3.5 Analytical and numerical description of the single site mass distribution for a system with $L = 100$. The fraction density is given by $\varphi(\mu) = \exp(-\mu)$ and we consider two different densities. For the derived weight function we have a critical density of $\rho_c = 0.6961$. As we can see the described analytical method shows an excellent agreement to the Monte Carlo simulation for values of ρ well above the critical regime, while a deviation can be observed for $\rho = 0.7$. We considered in both cases 10^6 realizations. 49

3.6 Single site mass distribution for the Gaussian-like probability density functions. The numerical results were derived by a Monte Carlo simulation over 10^4 samples where the dynamics of periodic systems with $L = 100$ were simulated. We have chosen here to set $\sigma = 0.2$ and $\rho = 0.75$. For these parameters we have the critical value $\rho_c = 0.73$ and $s_0 = -1.3$. 50

3.7 The mean increment of the excess mass for a system with a uniform distribution $\varphi(\mu) = 1$ and $\rho = 0.7$. We can see that for decreasing asymmetry coefficients the mean value decreases to the point where the increament is negative. This means that for specific values of ρ and a no unique stationary value for the single site distribution can be achieved even if we choose to set $L \to \infty$. 51

3.8 Single site mass distribution for a system with $L = 50$ and $\rho = 0.7$. The results of Monte Carlo simulation rely on 10^6 realizations

and show excellent agreement to our analytical result of $p(m) \simeq 0.2\exp(2.647m)$. 53

4.1 Characteristic path of a diffusion process X_t with resetting. The red lines correspond to the path of the stochastic process while the blue lines indicate the jumps performed due to the resetting to the initial position X_0. 59

4.2 Plot of $f(s) = s + \frac{r\alpha G_r(x_B,x_r;s)}{1+\alpha G_r(x_B,x_B;s)}$ for $r = 0.1$, $D = 10^{-4}$, $L = 1$, $\alpha = 10^7$, $x_B = 0.54$ and $x_r = 0.44$. In the limit $s \to \infty$ we get $f(s) \to s$, while for $s \to -r$, $f(s)$ approaches negative value proportional to r. 67

4.3 Plot of s_0 in dependence of r for $\alpha = 10^7$, $L = 1$, $D = 10^{-4}$, $x_B = 0.54$ and $x_r = 0.44$. We see that in the limit $r \to 0$ the behaviour of s_0 approximates that of $-r$. The limit of zero is approached for big resetting rates. 68

4.4 The MTA as a function of the resetting rate r for different values of $|x_B - x_0|$. We set $x_B = 0.54$, $L = 1$, $D = 10^{-4}$ and $\alpha = 10^7$. We see that the existence of an optimal resetting rate for $T(x_0)$ is evident only for the smallest value of $|x_B - x_0|$. 70

4.5 Phase diagram for the existence of an optimal resetting rate r^* for a random walk taking place in a bounded domain with reflecting walls. In the region between the two lines (blue and red) resetting can be beneficial. The blue line is given by the formula $x_0 = (1-g_r)+g_r x_B$ and the red line is of the form $x_0 = g_r x_B$. 71

4.6 Proportionality factor g_r introduced in Fig. 4.5 as function of the absorption constant α. 72

4.7 Optimal resetting rate as a function of the initial position. We show the behavior of the optimal resetting rate for $L = 1$, $x_B = 0.5$, $\alpha = 1$ and $D = 10^{-4}$. Numerical calculations for different combinations of the parameters ($L = 1; 2; 3$, $x_B = 0.5 \cdot L$, $D = 10^{-4}; 4 \cdot 10^{-4}; 9 \cdot 10^{-4}$, $\alpha = 1$) show the same behavior. The critical value is estimated at $x_0^* = (0.448 \pm 0.004)x_B$. 72

4.8 MTA in dependence of the mean free path $1/\sqrt{r}$. For this simulation we set $x_0 = x_r = 44$ and $x_B = 64$. The numerical results are calculated based on the values of 100 different random walks. . . . 75

4.9 MTA as a function of the mean free path $1/\sqrt{r}$. For this simulation we set $x_0 = x_r = 34$ and $x_B = 74$. The numerical results are calculated based on the values of 100 different random walks. . . . 76

5.1 Characteristic paths of a diffusion process with resetting inside a circle with $R = (2\pi)^{-1}$. The red line on the left figure correspond to the first excursion of the Brownian particle starting from the center of the circle and diffusing inside the circle. Upon arriving on

the boundary an one-dimensional stochastic process starts that gets interrupted by stochastic resets. Directly after this resetting a new diffusive excursion from the center of the circle starts (indicated by the green line in the left figure) which ends again at the boundary. As in the last chapter we represent these resetting effects on the boundary by blue lines. Starting an one-dimensional excursion at the position $x = 0/1$ would require a two-dimensional path ending at the position $\vec{R} = \left((2\pi)^{-1}, \pi\right)$. 80

5.2 Inverse of the optimal mean free path length vs the starting position of the searcher for a system of length $L = 1$. We can see that for $0.276L < x_0 < 0.724L$ the optimal mean free path length is equal to ∞. This fact changes if we consider a starting position which is closer to the boundaries and thus a finite value for the mean free path length tends to be optimal. 85

5.3 Numerical evaluation of the formula (5.27) for $x_0 = 0.5$ with $L = 1$. We have chosen here, as before, $D_1 = 5 \cdot 10^{-7}$. 87

5.4 MTA for the hard resetting problem in the special case of $D_2/D_1 = 2$ for $R = (2\pi)^{-1}$ and $D_1 = 5 \cdot 10^{-7}$. 88

5.5 MTA for the hard resetting problem in the special case of $D_2/D_1 = 0.25$ for $R = (2\pi)^{-1}$ and $D_1 = 5 \cdot 10^{-7}$. 89

5.6 Mean time to absorption for a Brownian process starting inside a two-dimensional circle for different initial conditions (R_0, θ_0). The points were determined by a Monte-Carlo simulation with $D_2 = 10^{-6}$, $2D_1 = D_2$ and $R = 1/2\pi$. The lines correspond to our theoretical values for these parameters. 90

5.7 Different regimes with regard to the existence of an optimal resetting rate for different initial position for a Brownian particle in search for a target located at **A**. The left figure corresponds to the choice of parameters with $D_2/D_1 = 0.25$ and on the right to $D_2 = D_1$. The shaded area (red) describes initial positions for which no positive optimal resetting rate can be found. We can see that for $D_2/D_1 = 1$ a particle starting from the center of the circle can be optimized through a positive resetting rate. 91

5.8 MTB for two-dimensional Brownian motion in a circle of radius $R = 1$ starting from the radius $R_0 = 0.9$ for different inverse mean path lengths. We can clearly see that there exists an optimal resetting rate for which this time is minimized. 94

5.9 Inverse of the optimal mean free path length for different ratios of the initial radius to the total radius of the circle. We can see that for $R_0 > 0.578R$ the optimal resetting rate is greater than zero. We have used here a circle of radius $R = (2\pi)^{-1}$. 94

5.10 MTA for a particle starting from the center of the circle of radius $R = (2\pi)^{-1}$ for different inverse mean path lengths and $D_2 = D_1$. We can clearly see that there exists an optimal resetting rate for which this time is minimized. The results of the Monte-Carlo simulation show a very good agreement to the analytical expectations derived from the formula (5.52). 95

5.11 Numerical and analytical evaluation of the targeting problem with no resetting. We calculate the mean time to absorption for a Brownian particle starting from $x_0 = 1/2$ with two absorbing boundary conditions $T(0) = T(1) = 0$. We can see that a comparison between our analytical and numerical results is only possible for low values of σ. 97

A.1 Second moment for random average process defined by Eq. (1) for different asymmetry coefficient and two distinct boundary conditions. We see a clear discrepancy between the mean field solution and the numerical results for $\alpha < 1$. We are therefore inclined to declare the product measure ansatz for $\alpha < 1$ as invalid. In the case of open boundary conditions we have chosen $\xi_{\ell,t}, \xi_{r,t}$ to have a uniform distribution in the interval $[0, 1]$. 107

A.2 Probability distribution for the process described by Equations (A.10)-(A.12). We can see a very good agreement between the predicted distribution, Eq. (A.14), and the Monte Carlo simulation. The Monte Carlo simulation is based on 10^4 different realizations. 108

B.1 Numerical (red circles) and analytical (black line) derivation of the largest value distribution density for a free ARAP system with $L = 100$ and $\rho = 1$. 110

B.2 Mean largest value for different lengths in the special case of $\rho = 1$. Each data point was calculated by averaging over 10^4 different Monte Carlo simulations. We have evolved hereby a periodic boundary system with random initial condition according of the dynamics of the free ARAP. The blue line was derived by a numerical evaluation of the integral in Eq. (B.11). 111

B.3 $\mathcal{N} = \int \mathrm{d}\rho \Pr\{\ell_2 < 1 < \ell_1\}$ vs the length of the system L. We find that for increasing lengths this weight tends to zero with an algebraic law. Numerically we find $\mathcal{N} \propto L^{-2.5}$ for $L \to \infty$. The blue line correspond to our numerical fit. 113

B.4 Density ρ^* as function of the length of the system. 114

C.1 Evaluation of the probability density functions $p^s(t)$ and $p^f(t)$ for process starting at $x_0 = 0.75$ with $L = 1$ and $D = 5 \cdot 10^{-4}$. The blue lines corresponds to the results of the Monte-Carlo simulation which ends at the boundary $x = L$ while the red lines describe the

distribution of the absorption times for process who end in fails (at the boundary $x = 0$). We can see a very good agreement between our numerical and analytical results. 116

C.2 Probability for a process to end at the boundary $x = 1$ if it started from the position x_0 with $D = 5 \cdot 10^{-5}$ and $r = 5 \cdot 10^{-3}$. 117

D.1 Mean time to absorption for a resetting process that performs a maximum jump of $a = 2R$. The numerical results were derived by a discrete time Monte-Carlo simulation where after each time-step the searcher performed a long range jump. 119

List of Tables

1 Characterization of the different characteristic regimes of the TARAP. 24

2 Characterization of the different characteristic regimes of the ZRRAP. 26

3 Characterization of the different characteristic regimes of the SRAP. No difference between the **HLF2** and **LF2** state can be determined if we observe only the parameters $\ell(\infty)$ and $J(\infty)$. 30

Abstract

In this work we consider two non-equilibrium models, the random average process and the diffusion with resetting. Both of these models have very interesting features and are relevant for a variety of fields.

The random average process is defined on one-dimensional periodic lattice and equipped with nearest neighbor interaction. The state of the system is described by continuous variables that are called masses. We focus here on totally asymmetric and discrete time dynamics. This means that at each time-step an asymmetric mass exchange between neighboring sites takes place. The fraction of the transported masses is defined by the probability density function ϕ which we call fraction density.

We start by introducing a special case of the random average process with state-dependent fraction density, the truncated random average process. We will give here a short overview over the different properties of three distinct truncated models with finite lattice size.

A new kind of random average process is introduced in this work that is characterized by the fact that only sites, who have a mass that is above a certain cutoff, can give a fraction of this mass to their neighboring sites. A special property of this model is the existence of a steady state that is an absorbing state. We determine analytically the exact form of this absorbing state in the thermodynamic limit by a canonical ensemble approach. This exact form also holds for systems that are partial asymmetric. Furthermore the provided single site distribution function is a good approximation for finite size systems.

The second class of models studied in this work are diffusive search processes with resets. The fact that random resetting may reduce the mean duration of a diffusive search process is rather intriguing. Here we re-evaluate this positive effect of resetting for the special case of stochastic processes that take place in bounded domains.

It will be shown here that for a diffusion process taking place in one-dimensional domain with reflecting boundaries an optimal resetting rate can be found. The exact value of this optimal value is provided by the solution to the Laplace Transform of the Fokker-Planck equation. Additionally we are in the position to calculate the non-equilibrium steady state for this process.

Finally we consider a diffusion search process inside a two-dimensional circular domain that switches between two phase of motion while also having

the property of resetting to the initial position. We calculate the mean time to absorption for several variations of this procedure by determining the corresponding survival probability. From the derived results we can define for which parameter values resetting is still beneficial for this kind of diffusive search.

Zusammenfassung

Wir haben uns in dieser Arbeit mit zwei verschiedenen Nichtgleichgewichtsystemen beschäftigt, den Random Average Process und Diffusion mit Rücksetzung. Beide Systeme haben nicht nur interessante Eigenschaften, sondern sind auch für eine Fülle von Anwendungen interessant.

Der random average process ist auf ein eindimensionales Gitter mit periodischen Randbedingungen definiert. Wir können uns hierbei vorstellen, dass jeder Gitterpunkt eine kontinuirliche Masse besitzt. Wir betrachten ein total asymmetrisches Model mit diskrete Zeitschritten. Bei jedem Zeitschritt wird eine zufällige Fraktion der Masse von einem Gitterpunkt zum nächsten Gitterpunkt übertragen. Die Grösse dieser Fraktion wird von der Verteilungsdichte ϕ bestimmt. Wir nennen diese Funktion im folgenden Fraktionsdichte.

Am Anfang betrachten den Spezialfall von einem Prozess mit einer Zustandsabhängige Fraktionsdichte, der als truncated random average process bezeichnet wird. Wir geben hier einen kleinen Überblick über die unterschiedliche Eigenschaften von drei verschiedenen Modellen mit 'truncation' Dynamik und endlicher Länge.

In dieser Arbeit führen wir eine neue Art von random average process ein. Er ist dadurch charakterisiert, dass nur Gitterpunkte, die eine Masse besitzen, die über einen bestimmten Wert liegen, Masse an ihren Nachbarn abgeben können. Für diese Art von Modellen können wir stationäre Zustände finden, die als absorbierend charakterisiert werden. Dieser absorbierende Zustand kann in den thermodynamischen Limit analytisch bestimmt werden. Wir nutzen hierbei den Formalismus der kanonischen Gesamtheit. Die hergeleiteten Formeln sind auch für partial asymmetrische Systeme gültig. Die Verteilungsfunktion von Konfigurationen von endlichen Systemen kann auf diese Weise auch bestimmt werden.

Die zweite Klasse von Prozessen, die wir in dieser Arbeit untersuchen, sind Diffusionsprozesse mit Rücksetzung. Der Grund unserer Beschäftigung mit dieser Klasse von Prozessen liegt in der Minimierung der Suchzeit für stochastische Suchprozesse, die durch zufällige Rücksetzung erreicht werden kann. Hier wollen wir diesen positiven Effekt für den speziellen Fall von stochastischen Suchprozessen in geschlossenen Berreichen überpüffen.

Es wird gezeigt, dass für einen eindimensionalen Diffusionprozess, der innerhalb von einem Interval mit zwei reflektierenden Randbedingungen stattfindet, wir eine optimale Rücksetzungsrate finden können. Wir können

den exakten Wert dieser optimaler Rate bestimmen, indem wir die Laplace Transformierte der Fokker-Planck Gleichung berechnen. Zudem sind wir in der Lage, den stationären Zustand von diesem Nichtgleichgewichtsystem zu finden.

Am Ende betrachten wir Diffusion innerhalb von einem zweidimensionalen Kreis, die zwischen zwei verschiedenen Phasen der Ausbreitung wechseln kann. Außerdem wird die Entwicklung dieser Diffusion durch zufällige Rücksetzungen auf den den Anfangszustand unterbrochen. Der Prozess endet sobald ein bestimmter Punkt am Rand des Kreises erreicht wird. Die Bestimmung der Überlebenswahrscheinlichkeit erlaubt uns die mittlere Suchzeit für verschiedene Variationen dieses Prozesses zu berechnen. Aus den hergeleiteten Ergebnisse können wir dann Parametergrößen bestimmen, für die eine Rücksetzung vorteilhaft sein kann.

CHAPTER 1

Introduction

Statistical mechanics is the physical theory which connects the observable behavior of complex systems with the dynamics of the microscopic parts constituting these objects. In order to apprehend the interplay between the two seemingly incompatible theoretical schemes of microscopic and macroscopic description the reduction of the degrees of freedom to a manageable size becomes necessary. This approach proves very successful when studying equilibrium states and has thus lead to the development of a powerful and general framework, equilibrium statistical mechanics.

Unfortunately a very large variety of phenomena and situations involves systems that are not in thermodynamic equilibrium. In general we can say that non-equilibrium phenomena are encountered whenever systems are relaxing towards an equilibrium steady state and also whenever systems are driven, i.e., maintained away from equilibrium by external forces. This often makes the determination of the probability distribution of the configurations in terms of a Boltzmann-Gibbs weight formalism impossible.

The different nature of such systems and their wide area of applications makes them more interesting that their equilibrium counterparts but does not allow for a unified approach. In spite of this difficulty numerous promising methods arose in the last decades. Many of them have in common several essential fundamental features on which they rely. In this work we will try to introduce such methods like the canonical ensemble approach for non-equilibrium systems, study their general features, and show their applications to models that have been developed in the last years. We concentrate hereby on driven diffusive systems and focus on the relation between the microscopic dynamics described by stochastic processes and the observable characteristics like condensation and minimization of search times.

Condensation is a concept that is familiar to us in everyday life, normally through the phase transition of water vapor from gaseous to liquid. Another prominent example is the Bose-Einstein condensation which can be treated in terms of the grand-canonical ensemble in equilibrium statistical mechanics. The term condensation is used in statistical mechanics in order to describe the occupation of a certain state by a macroscopic fraction of the particles in the system. The properties and occurrence of condensation has been investigated in the last years in terms of a particular driven diffusive system: the zero range process (ZRP). In the ZRP, particles hop from site to site on a lattice with a hop rate which depends on the number of particles

on the departure site. Here we will discuss the properties of condensation for a similar system where instead of particles we will consider the exchange of continuous quantities between different sites. This system is the random average process (RAP) and its dynamics are given by the so-called fraction density, which defines the amount of mass transported between different sites.

Stochastic search processes on the other side are also related to everyday experience but on a very unfathomable level. They may describe chemical reactions in cells, or foraging in ecological environments, activation times for call options etc. We are studying here the properties of such processes that take place in bounded domains. We know that for a diffusion process in a bounded domain the steady sate is described by the detailed balance condition. The implementation of a driven force in terms of a resetting mechanism, that forces the system back to its initial state, destroys the detailed balance condition and raises the question with regard to the existence and form of the new stationary state. Originating from this simple question several properties of this non-equilibrium stochastic search process may be analyzed.

In chapter 2 we start by presenting some general features of stochastic mass transport models and focus on the factorization property of the ZRP and the RAP. After that we consider a variation of the random average process with state-dependent fraction density. Truncation dynamics that control the maximum amount of the transported mass per site are implied. The effect of three distinct truncation dynamics on the condensation transition are illustrated by numerical simulations.

In chapter 3 a new form of the random average process is introduced. The special property of this process is the existence of an absorbing state. We will determine the single-site mass distribution for this absorbing state by using a canonical ensemble approach. The description of this state becomes possible by studying the stochastic dynamics induced by the state-dependent fraction density. We can furthermore determine sufficient conditions for the appearance of this stationary state. To demonstrate the utility of the proposed canonical approach we analyze a broad class of mass transport models and use numerical simulations of finite size periodic systems in order to show the validity of our results. Lastly we discuss briefly the relevance of asymmetry for the presented methods.

Starting with Chapter 4 we go over to the analysis of stochastic search processes. We consider the one-dimensional diffusion in a bounded domain with stochastic resetting that forces the Brownian motion to return to its initial position. Our motivation arises from the existence of an optimal resetting rate that minimizes the search time. We start our analysis by presenting a method to derive the Master equation for different resetting mechanisms. In the next step we compute the non-equilibrium steady state for a special case of this differential equation. Then we consider the existence of an absorbing point in the system and calculate the mean time to

absorption of the diffusive particle by the target. Numerical and analytical calculations will be used in order to determine the optimal resetting rate. Finally we discuss different special cases of the presented problem.

Lastly in chapter 5 we consider a Brownian particle that has the property to change between two different modes of motion. The idea for this implementation came from works focused around intermittent stochastic processes and surface mediated diffusion. Both of these processes are very relevant for biological and chemical systems. Here we study the Brownian motion of a particle in a bounded circular 2-dimensional domain, in search for a stationary target on the boundary of the domain. The process switches between a two-dimensional diffusion inside the circle and an one-dimensional diffusion along the boundary. During the diffusion, the Brownian particle resets to its initial position with a constant rate. The Fokker-Planck formalism allows us to calculate the mean time to absorption (MTA) as well as the optimal resetting rate for which the MTA is minimized. From the derived analytical results the parameter regions for which resetting reduces the search time can be specified. The MTA for a variety of different realizations is derived analytically and shows excellent agreement to our numerical results.

CHAPTER 2

Condensation in Truncated Random Average Processes

2.1. Introduction

In this chapter we focus on the properties of the condensation transitions that can be observed in truncated random average processes. Condensation is a phenomenon occurring in a plethora of physical systems and under different conditions. Our everyday experience is full of such phenomena whether it may be the appearance of water drops on a cold surface or formations of small clouds in low-pressure zones above aircraft wings in the case of damp weather conditions.

Although these examples describe a transition from a gas to a liquid phase we have to note hereby that in general condensation phenomena are not necessarily related to this transition. In statistical physics the notion of condensation is more widely used in order to describe any process in which a finite fraction of some conserved quantity becomes localized in the phase space. This means that if the system consists of many particles a macroscopic fraction of those particles will assume the same value for a given characteristic quantity of the system. The most prominent example is the Bose-Einstein Condensation [**2**], where a finite fraction of all bosons occupy the lowest energy state. This behavior is not limited to elementary particles or small molecules as a variety of works in fields as diverse as traffic models [**3, 4, 5**], quantum gravity [**6**], networks [**7, 8**], economics [**9, 10**], granular materials [**11**], and mass transport [**14**] in the last years has shown.

It is important to note here that many of these different instances of condensation share common basic features. The analysis of those universal properties has advanced greatly in the last years through the study of mass transport models like the zero-range process (ZRP) [**15**]. Mass transport models describe systems in which a conserved quantity, often called 'mass', is transferred from site to site of a lattice. Condensation is manifested in such models when, in the steady state, a finite fraction of the total mass condenses onto a single lattice site. The implied dynamics of mass transport often allow for a simple description of the steady state and build therefore a natural setup for the study of condensation transitions. This is especially true for the case of the ZRP which enjoys the convenient property of having a factorized steady state.

This property is also shared by the asymmetric random average process (ARAP) [**17, 18**], for which no condensation is expected. The ARAP is a special case of the random average process that was first introduced by Ferrari and Fontes in [**19**]. A condensation transition may be induced for this class of models by imposing a maximum threshold on the amount of mass that may be transported between two sites. Such a model was introduced in the past by Zielen and Schadschneider and was characterized as truncated random average process [**36**].

In this chapter we will focus on the properties of condensation arising for such truncated models of mass transfer. We start with a brief introduction on Markov Chains and Master Equations, allowing us to determine the conditions for a steady state. In section 2.3 we will see how grand canonical analysis can be used in order to determine the critical density for condensation for the special case of factorized non-equilibrium steady states as the ones occurring for the ZRP and ARAP. The concept of truncation will be presented in section 2.4. In the same section we present some numerical findings for finite and periodic one-dimensional systems for three different variations of the truncation dynamics. Some concluding remarks are presented in the last section of this chapter.

2.2. Markov Processes and Master Equation

One of the basic assumptions of statistical physics is the Markovian Postulate which states that "the current observational state embodies all the observational information about the past history of the system that is relevant to its observable future behavior" [**1**]. In this thesis we rely on an even stronger version of this postulate since we are dealing with the special class of stochastic processes called Markov processes. Markov processes can be characterized picturesquely as 'processes without memory' [**12**].

In order to characterize this property in a more rigorous way we use the definition of the conditional probability. Let $P(x,t)$ describe hereby the probability density of stochastic process at the time-point t. The conditional probability is then the probability density at a time-point t_1 provided that the state x_2 was observed at the time t_2. In the following we use therefore the notation $P(x_1,t_1|x_2,t_2)$. We assumed here that the times t_1 and t_2 are ordered: $t_1 < t_2$. The current definition can be generalized for more complicated histories. As example, an observation at the time t_n provided the history of the process is described by the measurements $x_1, x_2, ..., x_{n-1}$ at the corresponding times $t_1, t_2, ..., t_{n-1}$ with $t_1 < t_2 < ... < t_{n-1}$ is described by the function $P(x_n,t_n|x_{n-1},t_{n-1};...;x_1,t_1)$.

By providing this formalism we can describe a Markov process as a process fulfilling the equation

$$P(x_n,t_n|x_{n-1},t_{n-1};...;x_1,t_1) = P(x_n,t_n|x_{n-1},t_{n-1}). \tag{2.1}$$

This equation describes a property stronger then the one implied by the Markov Postulate. The probability of finding state x_n at the time t_n depends

only on the state of the system at the previous time-step and not on the whole previous history.

The Markovian property allows us to replace the formula for the joint probability by the following expression:

$$P\left(x_1, t_1; ...; x_n, t_n\right) = P(x_1, t_1)P(x_2, t_2|x_1, t_1)...P(x_n, t_n|x_{n-1}, t_{n-1}). \quad (2.2)$$

We see also that the whole evolution of the process is governed by the transition probabilities $P(x_k, t_k|x_{k-1}, t_{k-1})$ and the initial distribution. This property leads also to the so-called Chapman-Kolmogorov equation:

$$P(x_3, t_3|x_1, t_1) = \int \mathrm{d}x_2\, P(x_3, t_3|x_2, t_2)P(x_2, t_2|x_1, t_1) \quad (2.3)$$

with $t_1 < t_2 < t_3$. The Chapman-Kolmogorov equation is non-linear and thus not suited for defining the stationary state of the process. The master equation that will be derived in the following is far better suited in this regard.

For the processes discussed in this thesis we deal with processes evolving in a continuous phase space and discrete time setting. Since we are working in such a discrete time setting we often adopt the characterization time-step in order to describe the different relevant instances of times. We define hereby the distance between two sequential time-points as $\varepsilon = t_k - t_{k-1} = \Delta t$. For two subsequent time-points t_{k-1}, t_k the transition probability $P(x_k, t_k|x_{k-1}, t_{k-1})$ is fully described by the nature of the system and its specific properties. This mean that

$$P(x, t_k|x', t_{k-1}) = P(x, t_j|x', t_{j-1}) \quad (2.4)$$

for all time-points t_k and t_j.

The evolution of the Markov Process is described by the dynamical rule [**13**]

$$P(x, t_k) = \int \mathrm{d}x'\, P(x, t_k|x', t_{k-1})P(x', t_{k-1}) \quad (2.5)$$

which can be rewritten using the formula $\int \mathrm{d}x'\, P(x', t_k|x, t_{k-1}) = 1$ as

$$P(x, t_k) = P(x, t_{k-1}) - P(x, t_{k-1}) \int \mathrm{d}x'\, P(x', t_k|x, t_{k-1}) + \\ + \int \mathrm{d}x'\, P(x, t_k|x', t_{k-1})P(x', t_{k-1}) \quad (2.6)$$

Now it follows that

$$P(x, t_k) - P(x, t_{k-1}) = \int \mathrm{d}x'\, P(x, t_k|x', t_{k-1})P(x', t_{k-1}) - \\ - P(x, t_{k-1})P(x', t_k|x, t_{k-1}). \quad (2.7)$$

By dividing through Δt and taking the limit $\Delta t \to 0$ we can derive the master equation

$$\frac{\partial}{\partial t}P(x, t) = \int \mathrm{d}x'\, \left[P(x', t)W\left(x' \to x\right) - P(x, t)W\left(x \to x'\right)\right]. \quad (2.8)$$

with the terms $W(x \to x')$ describing the transition rates between different states

$$W(x \to x') = \lim_{\Delta t \to 0} \frac{P(x, t_k | x', t_{k-1})}{\Delta t} \tag{2.9}$$

Now this form is especially helpful when trying to determine the steady state

$$\frac{\partial}{\partial t} P(x, t) = 0. \tag{2.10}$$

The steady state condition is equivalent to the equation

$$\int \mathrm{d}x' \left[P(x', t) W\left(x' \to x\right) - P(x, t) W\left(x \to x'\right) \right] = 0. \tag{2.11}$$

This equation is easily fulfilled by the equation

$$P(x', t) W\left(x' \to x\right) = P(x, t) W\left(x \to x'\right), \tag{2.12}$$

which is known as detailed balance condition. Such a condition is to be expected for the stationary sate of an equilibrium system that is also ergodic.

On the other side a non-equilibrium steady state (NESS) fulfills Eq. (2.11) but not the detailed balance condition Eq. (2.12). This fact makes the characterization of NESS a difficult undertaking and will be the main goal of the next chapter.

2.3. Mass Transport Models with Factorized Steady States

In the introduction of this chapter we claimed that the study of mass transport models and especially of the ZRP and ARAP greatly improved our understanding of condensation transitions. The influence of these two models is mainly explained due to the fact that their respective steady states $\{m_i, ..., m_n\}$ are factorizable. This means that the probability to observe the state $\{m_i, ..., m_n\}$ can be expressed in terms of the single site functions $f(m_i)$:

$$P\left(m_1, ..., m_n\right) \sim \prod_{i=1}^{n} f\left(m_i\right). \tag{2.13}$$

In this section we will recapitulate some important results of the past with regard to the properties of those models and discuss the general conditions for the existence of a factorized steady state in a stochastic mass transport model.

We use a very general description of the class of one-dimensional mass transport models. Let us consider a one-dimensional lattice of L sites with periodic boundary conditions (site $L + 1$ corresponds to site 1). On each site i of the lattice resides a mass m_i and at each time-step a portion of this mass, $\mu_i \leq m_i$ is chipped off and transported to a different site of the system. The total mass

$$M = \sum_{i=1}^{L} m_i \tag{2.14}$$

is conserved. In this chapter we will consider only transport between nearest neighbors and only in one direction (total asymmetric process). The portion of the mass transported is given by the probability density function $\phi(\mu|m)$. This function is also called chipping kernel and it has to satisfy the obvious normalization condition

$$\int_0^m \mathrm{d}\mu\, \phi\left(\mu|m\right) = 1. \tag{2.15}$$

An appropriate choice of the chipping kernel $\phi(\mu|m)$ can recover the ZRP and the ARAP as we will see later. In this work we focus mostly on parallel update rules. This does not mean that continuous time dynamics (especially random sequential update) is excluded from the present formalism as will be shown for the specific cases studied below.

For the case of discrete time dynamics the evolution of the system is given by the master equation

$$\begin{aligned} P_{t+1}\left(m_1,...,m_L\right) = Z_t\left(L,M\right)^{-1} \prod_{i=1}^{L} \int_0^{\infty} \mathrm{d}m_i' \int_0^{m_i'} \mathrm{d}\mu_i\, \varphi\left(\mu_l|m_l'\right) \times \\ \times \prod_{j=1}^{L} \delta\left(m_j - m_j' + \mu_j - \mu_{j-1}\right) P_t\left(m_1',...,m_L'\right) \end{aligned} \tag{2.16}$$

where $Z_t\left(L,M\right)$ is the normalization constant with

$$Z_t\left(M,L\right) = \int_0^{\infty} \mathrm{d}m_1 .... \int_0^{\infty} \mathrm{d}m_L\, P_t\left(m_1,...,m_L\right) \delta\left(\sum_{i=1}^{L} m_i - M\right). \tag{2.17}$$

This expression can be considered as the equivalent of the canonical equilibrium partition function and is thus usually referred to as partition function. The conservation of the total mass is guaranteed by the δ-function.

In the long time limit ($t \to \infty$) the steady state distribution $P\left(m_1,...,m_L\right)$ is achieved. As it was shown in [**42**] this steady state factorizes if the dynamics of the system are described by a fraction density kernel of the form

$$\phi(\mu|m) \propto u(\mu) w(m-\mu). \tag{2.18}$$

This is easily proven by considering the Laplace transform of $P\left(m_1,...,m_L\right)$

$$G\left(s_1,...,s_L\right) = \int_0^{\infty} \mathrm{d}m_1 .... \int_0^{\infty} \mathrm{d}m_L\, \mathrm{e}^{-\sum_i s_i m_i} P\left(m_1,...,m_L\right) \tag{2.19}$$

and using the factorization property

$$P\left(m_1,...,m_L\right) = Z\left(M,L\right)^{-1} \prod_{i=1}^{L} f\left(m_i\right) \delta\left(\sum_{k=1}^{L} m_k - M\right) \tag{2.20}$$

with the normalization constant

$$Z\left(M,L\right) = \prod_{i=1}^{L} \int_0^{\infty} \mathrm{d}m_i\, f(m_i) \delta\left(\sum_{k=1}^{L} m_k - M\right). \tag{2.21}$$

By combining the two equations (2.19) and (2.20) we can derive the expression

$$G\left(s_1,...,s_L\right) = Z\left(M,L\right)^{-1}\prod_{i=1}^{L} g(s_i) \tag{2.22}$$

where

$$g(s) = \int_0^\infty \mathrm{d}m\, f(m)\mathrm{e}^{-sm}. \tag{2.23}$$

By taking the master equation into account we can see that

$$\prod_{i=1}^{L} g(s_i) = \prod_{i=1}^{L}\left[\int_0^\infty \mathrm{d}m_i'\, f(m_i')\int_0^{m_i'} \mathrm{d}\mu_i\, \phi(\mu_i|m_i')\mathrm{e}^{-s_i(m_i'-\mu_i+\mu_{i-1})}\right]. \tag{2.24}$$

We can now perform a change of the variable $\sigma = m - \mu$ in order to obtain

$$\prod_{i=1}^{L} g(s_i) = \prod_{i=1}^{L}\left[\int_0^\infty \mathrm{d}\mu_i \int_0^\infty \mathrm{d}\sigma_i\, \mathcal{P}(\mu_i,\sigma_i)\mathrm{e}^{-s_i\sigma_i - s_{i+1}\mu_i}\right] \tag{2.25}$$

with

$$\mathcal{P}(\mu_i,\sigma_i) = f(m_i)\phi(\mu_i|m_i). \tag{2.26}$$

A necessary and sufficient condition for the solution of (2.25) is [**42**]

$$\int_0^\infty \mathrm{d}\mu_i \int_0^\infty \mathrm{d}\sigma_i\, \phi(\mu_i|\sigma_i)\mathrm{e}^{-s_i\sigma_i - s_{i+1}\mu_i} = \ell(s_i)k(s_{i+1}) \tag{2.27}$$

where the two functions, k and ℓ, must satisfy

$$k(s)\ell(s) = g(s). \tag{2.28}$$

By applying now the inverse Laplace transform on this product we can see via the convolution theorem that

$$f(m) = \left[v * w\right](m) = \int_0^m \mathrm{d}\mu\, v(\mu)w(m-\mu) \tag{2.29}$$

where

$$k(s) = \int_0^\infty \mathrm{d}\mu\, \mathrm{e}^{-s\mu}v(\mu) \qquad \ell(s) = \int_0^\infty \mathrm{d}\sigma\, \mathrm{e}^{-s\sigma}w(\sigma). \tag{2.30}$$

Finally from the combination of Eq. (2.27) with (2.30) and (2.26) with (2.29) we obtain

$$\phi(\mu|m) = \frac{\mathcal{P}(\mu,\sigma)}{f(m)} = \frac{v(\mu)w(m-\mu)}{\left[v * w\right](m)}. \tag{2.31}$$

The importance of this proof with regard to the sufficient and necessary condition for a factorized steady state provided by Evans, Majumdar and Zia in [**42**] cannot be overstated. It not only allows for an easy characterization of the steady state since the weight functions are provided by a rather simple formula but also delivers an easy mechanism for the characterization of equivalent chipping distributions.

The provided condition might be elegant but at the same time it corresponds to an 'implicit test'. Hence a proof of it might be difficult. In order to overcome this difficulty a simple explicit test for ϕ was provided in [**43**].

One has to consider hereby that the condition provided by Eq. (2.31) is equivalent to asking whether

$$\frac{\partial}{\partial\mu}\Big|_{\sigma}\frac{\partial}{\partial\sigma}\Big|_{\mu}\ln\phi\left(\mu|\mu+\sigma\right) \tag{2.32}$$

is a function of $\mu+\sigma$ alone. The equivalence between the two conditions is shown by integrating with respect to μ and σ, from which a ϕ of the form (2.31) follows.

For mass transport models evolving in a discrete configuration space the corresponding chipping rates can be written as

$$\phi(\mu|m)=\sum_{n=1}^{\infty}\sum_{\ell=0}^{\infty}\phi_{\ell,n}\delta\left(\mu-\ell\right)\delta\left(m-n\right). \tag{2.33}$$

For discrete masses in a discrete time setting the factorization condition can be expressed as

$$\phi_{\ell,n}=\frac{v_\ell w_{n-\ell}}{f_n} \tag{2.34}$$

where f_n describes the single-site weight

$$f_n=\sum_{\ell=0}^{n}v_\ell w_{n-\ell} \tag{2.35}$$

with

$$f(m)=\sum_{n=1}^{\infty}f_n\delta\left(m-n\right). \tag{2.36}$$

It is not hard to see that the factorization text can now be rephrased in this case in terms of the cross ratio

$$R(\ell,n)\stackrel{!}{=}\frac{\phi_{\ell+1,n+2}\phi_{\ell,n}}{\phi_{\ell+1,n+1}\phi_{\ell,n+1}}, \tag{2.37}$$

defined when when all the ϕ's are positive. One can claim namely that the steady state factorizes if the cross ratio depends solely on n ($R(\ell,n)=R(n)$). Then, from (2.34), one derives

$$R(n)=\frac{f_{n+1}^2}{f_n f_{n+2}} \tag{2.38}$$

which implies the recursion

$$\frac{f_{n+2}}{f_{n+1}}=\frac{1}{R(n)}\frac{f_{n+1}}{f_n}. \tag{2.39}$$

Iterating this formula two times, which corresponds to a discrete version of 'integrating twice', yields

$$f_n=f_0\left(\frac{f_1}{f_0}\right)^n\left[\prod_{m=0}^{n-2}\frac{1}{R(m)^{n-m-1}}\right]\quad\text{for}\quad n\geq 2. \tag{2.40}$$

Now that we have discussed the necessary and sufficient conditions with regard to the factorization we turn to the issue of condensation and especially to the question: when does a condensation transition within a factorized state occur? A grand canonical ensemble approach is easily applied under the assumption of factorization [**45**]. In this approach we take the thermodynamic limit ($L, M \to \infty$ with fixed overall density $\rho = M/L$). In this limit the sites decoupled from each other and the single site mass distribution is given by $p(m) = f(m)\mathrm{e}^{-\mu m}$ where μ is the negative of the chemical potential and is chosen to fix the density through the relation

$$\rho = \rho(\mu) \stackrel{!}{=} \frac{\int_0^\infty \mathrm{d}m\, m f(m)\mathrm{e}^{-\mu m}}{\int_0^\infty \mathrm{d}m\, f(m)\mathrm{e}^{-\mu m}}. \tag{2.41}$$

This function $\rho(\mu)$ allows us now to easily derive the criterion for condensation. We can consider hereby three different cases with regard to the form of the function $f(m)$ in the large m limit:

- **1:** $f(m)$ decays faster than exponential. In this case, the integrals in (2.41) converge and every value of μ in the range $[-\infty, \infty]$ is allowed. This means that for each value of ρ a suitable choice for μ can be made so that Eq. (2.41) holds and there is no condensation.
- **2:** $f(m)$ decays slower than m^{-2}. In this case, a convergence of the integrals in (2.41) is only granted for values of μ in the range $[0, \infty]$. As in the previous case for any given ρ a value for μ can be found so that Eq. (2.41) holds and there is no condensation.
- **3:** $f(m)$ decays slower than exponential but faster than m^{-2}. In this case the allowed range of μ is $[0, \infty]$. In contrast to case **2** the value of $\rho(0)$ is finite. This value also sets the critical density $\rho_c = \rho(0)$ since for $\rho < \rho_c$ a positive μ satisfying (2.41) can be found. However, a condensation transition takes place for $\rho > \rho_c$ since no real solution can be found in this case. The extra mass $(\rho - \rho_c)L$ accumulates at one site and forms a condensate.

We have to note here that the single-site probability distribution $p(m)$ is given by

$$p(m) = f(m)\mathrm{e}^{-\mu m} \quad \text{for} \quad \rho < \rho_c. \tag{2.42}$$

This result of the grand-canonical approach does not hold for $\rho > \rho_c$ where the grand canonical approach fails.

In the following we will discuss some special cases of mass transport models, the zero range and the asymmetric random average process, that were extensively studied in the last years.

2.3.1. Zero Range Process. The Zero-Range Process (ZRP) serves as a model of transportation between sites which are occupied by single mass units or particles which hop to neighboring sites and was introduced by Spitzer in [**59**]. Each lattice may thus contain an integer number of particles leading to the special case of $m_i \in \mathbb{N}$ for all sites of the system $i \in \{1, ..., L\}$. So we say that the number of particles on site l is equal to

n_l and we consider configurations $\{n_1, ..., n_L\}$ which are hereby elements of $\mathbb{N}^L$. The total number of particles

$$N = \sum_{i=0}^{L} n_i \tag{2.43}$$

is conserved by the dynamics. It can be shown [**42, 43**] that for this class of models a factorized steady state can be found for both types of update dynamics, parallel and random sequential.

For parallel dynamics we consider discrete time-steps. At each time-step from all sites containing masses that are above zero a unit mass is chipped off and transported to next site (we consider here totally asymmetric dynamics) with a probability $\tilde{u}(n)$ where n is the mass at the site. For this simple model we have $\phi_{\ell,n} = 0$ for all $\ell > 1$ and thus we see that there exists only one cross ratio, namely, for $\ell = 0$,

$$R(0, n) = \frac{\tilde{u}(n+2)[1 - \tilde{u}(n)]}{\tilde{u}(n+1)[1 - \tilde{u}(n+1)]}. \tag{2.44}$$

Consequently the ZRP admits a factorized steady state since R is independent from ℓ. By inserting now this expression for R in Eq. (2.40) we get [**59**]

$$f_n = \begin{cases} \frac{(f_1\tilde{u}(1))^n}{1-\tilde{u}(n)} \left[\prod_{m=1}^{n} \frac{1-\tilde{u}(m)}{\tilde{u}(m)} \right] & \text{for } n > 0 \\ 1 & \text{for } n = 0. \end{cases} \tag{2.45}$$

The same result was derived in [**46, 15**] by using the more complicated transfer matrix method. We continue now by considering the random sequential dynamics. This is easily obtained by letting $f_1\tilde{u}(1) = \mathrm{d}t$ and $\tilde{u}(m) = u(m)\mathrm{d}t$ where $u(m)$ describes the departure rate of a particle sitting at a site with m particles. Taking now the limit $\mathrm{d}t \to 0$ yields

$$f_n = \prod_{m=1}^{n} \frac{1}{u(m)} \quad \text{for } n \geq 1. \tag{2.46}$$

This simple relation can also be found by considering the master equation for the steady state

$$0 = \sum_{l=1}^{L} \left[u(n_{l-1}+1) P\left(..., n_{l-1}+1, n_l - 1, ...\right) - u(n_l) P\left(..., n_{l-1}, n_l, ...\right) \right] \Theta\left(n_l\right). \tag{2.47}$$

Here we use the notation Θ in order to characterize the Heaviside function. Insertion of the factorization property

$$P\left(n_i, n_2, ..., n_L\right) = \frac{1}{Z_{L,N}} \prod_{i=1}^{L} f(n_i) \delta\left(\sum_{i=1}^{L} n_i - N \right) \tag{2.48}$$

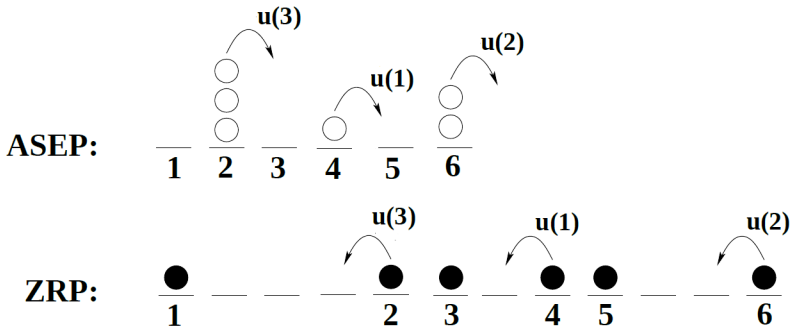

FIGURE 2.1. Diagrammatic representation of the mapping between the ASEP and the ZRP.

where $Z_{L,N}$ is the normalization

$$Z_{L,N} = \sum_{\{n_i\}} \prod_{i=1}^{L} f(n_i)\delta\left(\sum_{i=1}^{L} n_i - N\right) \tag{2.49}$$

leads then to the relations

$$u(n_{l-1}+1)f(n_{l-1}+1)f(n_l-1) = u(n_l)f(n_{l-1})f(n_l) \tag{2.50}$$

$$\Leftrightarrow \quad u(n_{l-1}+1)\frac{f(n_{l-1}+1)}{f(n_{l-1})} = u(n_l)\frac{f(n_l)}{f(n_l-1)} \stackrel{!}{=} \text{constant}, \tag{2.51}$$

for all values of l. The constant can now be set equal to unity without loss of generality so that the iteration

$$f(n_l) = \frac{f(n_l-1)}{u(n_l)} \tag{2.52}$$

is obtained. Now again without loss of generality we can set $f(0) = 1$ and derive the above expression for the terms $f(n)$

$$f(n) = \prod_{i=1}^{n} \frac{1}{u(i)} \quad \text{for} \quad n > 0. \tag{2.53}$$

The Zero-Range process possesses two rather interesting properties. First, there is the existence of a mapping to the asymmetric exclusion process (ASEP). This mapping procedure relies on one side in the replacement of the particles in the ZRP through vacancies in the exclusion process and the replacement of the sites in the ZRP through occupied sites in the exclusion process on the other side. A diagrammatic representation is shown in the Figure 2.1 above.

Second, the zero range process proves to be an excellent case study for the analysis of the condensation phenomenon. The condensation taking place in the ZRP is closely related to the Bose-Einstein condensation. One has to note hereby that while Bose-Einstein condensation takes place in the state space the condensation of the zero range process is a real space

condensation. Another important difference is that in contrast to the Bose-Einstein condensation the grand-canonical analysis breaks down for the ZRP (as we have seen above).

We have also seen in the last subsection how the analysis of the condensation phenomenon for factorized steady states can be performed by analyzing the properties of the function $\rho(\mu)$. Here we will show how a similar approach can be used for the case of models evolving in discrete configuration space.

We start from the definition of the grand canonical partition function in a discrete setting

$$\mathcal{Z}_L(z) = \sum_{n=0}^{\infty} z^n Z_{L,n}, \tag{2.54}$$

where the fugacity z is used to determine the density ρ through

$$\rho = \frac{z}{L} \frac{\partial \ln \mathcal{Z}_L(z)}{\partial z}. \tag{2.55}$$

By inserting the previous expression of the partition function (2.49) we get

$$\mathcal{Z}_L(z) = \sum_{\{m_l=0\}}^{\infty} z^{\sum_l m_l} \prod_{l=1}^{L} f(m_l) = [F(z)]^L \tag{2.56}$$

where

$$F(z) = \sum_{m=0}^{\infty} z^m f(m) \tag{2.57}$$

and

$$\rho = z \frac{F'(z)}{F(z)}. \tag{2.58}$$

The critical density is then easily derived if we observe that the right hand site of the equation above is an increasing function of z. But this increase of the density with increasing values of z is limited by the convergence radius of the function $F(z)$, which we set now to be $z = \beta$. We thus have a critical density of

$$\rho_c = \beta \frac{F'(\beta)}{F(\beta)}. \tag{2.59}$$

Now there exist two possibilities either ρ_c is infinite which would lead to the existence of a solution for all values of ρ. On the other side if ρ_c is finite for values of ρ above this value the relation may not hold and we have the condensation of the excess mass of particles $L(\rho - \rho_c)$.

Now if know the hop rate $u(n)$ we can determine the critical density for this system. Our condition for condensation is here related to the existence of a convergence radius for the infinite series $zF'(z) = \sum_{n=1}^{\infty} n z^n f(n)$. We can consider hereto the ratio of successive terms which reads

$$\frac{(n-1)f(n-1)}{znf(n)} = \frac{u(n)}{z}\left(1 - \frac{1}{n}\right). \tag{2.60}$$

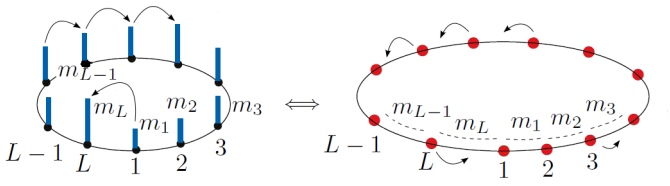

FIGURE 2.2. Mapping between the particles on a circle and mass exchange between different sites picture for the asymmetric random average process

From the ratio test it follows that this ratio should decay more slowly than $1 + 1/n$ which leads to the requirement

$$u(n) > \beta \frac{n+1}{n-1} \simeq \beta \left(1 + \frac{2}{n} + \mathcal{O}\left(\frac{1}{n^2}\right)\right). \tag{2.61}$$

This method may be applied as example in order to see that for the generalized hopping rate

$$u(n) \simeq \beta \left(1 + \frac{a}{n^\lambda}\right) \tag{2.62}$$

a condensation occurs when $0 < \lambda < 1$, and for $a > 2$ when $\lambda = 1$, in which case the critical density

$$\rho_c = \frac{1}{a-2} \tag{2.63}$$

can be found exactly [**15**].

2.3.2. Asymmetric Random Average Process. The asymmetric random average process (ARAP) is a stochastic mass transport model in which each site contains a continuous amount of mass, meaning that we consider here the case of $m \in \mathbb{R}_+$. Processes taking place in a continuous phase space setting have served as a basic model for a variety of physical systems and therefore have been the object of a large number of studies in the last years [**20, 22, 21**]. They are also in general more complicated that discrete mass models since the characterization of the steady is not an easy task in a continuous state space. Furthermore the dynamics of condensation in a continuous phase space setting cannot be easily understood.

We start again by considering parallel update and totally asymmetric dynamics. At each update a random proportion $r = \mu/m \in [0, 1]$ of the continuous mass of each site is transported to the neighboring site

$$m_i(t+1) = (1 - r_i(t))m_i(t) + r_{i+1}(t)m_{i+1}(t). \tag{2.64}$$

Like in the zero range process we can use an equivalent picture of particles moving on a ring as shown in Figure 2.2 above.

In this picture we can imagine L particles which move on a line. Let $x_i \in \mathbb{R}_+/\rho L$ describe the position of the i-th particle. Then one can think of m_i as the distance between the $i+1$-th and the i-th particle, $m_i = x_{i+1} - x_i$.

Hereby we imply periodic boundary conditions by setting $x_{L+1} = x_1$ with $m_L = x_1 - x_L$. The positions of the particles are updated after each time-step simultaneously according to the rules given by Eq. (2.64). We can imagine each particle making a jump of the length $\mu_{i,t} \leq x_{i+1,t} - x_{i,t}$ forward

$$x_i(t+1) = x_i(t) + r_i(t)(x_{i+1}(t) - x_i(t)). \tag{2.65}$$

These simple dynamics are generally described by a chipping kernel of the form

$$\phi(\mu|m) = \frac{\chi(\mu/m)}{m}. \tag{2.66}$$

As before we can test the factorization for this general form by differentiating twice

$$\frac{\partial}{\partial\mu}\bigg|_\sigma \frac{\partial}{\partial\sigma}\bigg|_\mu \ln\phi\left(\mu|\mu+\sigma\right) = -\frac{r(1-r)}{m^2}\frac{\mathrm{d}}{\mathrm{d}r}\frac{1}{\chi(r)}\frac{\mathrm{d}\chi(r)}{\mathrm{d}r} - \frac{1-2r}{m^2}\frac{1}{\chi(r)}\frac{\mathrm{d}\chi(r)}{\mathrm{d}r} + \frac{1}{m^2}. \tag{2.67}$$

If we claim now that this expression depends only on m we come to the conclusion that

$$\frac{\mathrm{d}}{\mathrm{d}r}\left[r(1-r)\frac{\mathrm{d}}{\mathrm{d}r}\frac{1}{\chi(r)}\frac{\mathrm{d}\chi(r)}{\mathrm{d}r}\right] = \text{constant}. \tag{2.68}$$

The solution to this equation is given by

$$\chi_{a,b}(r) = \frac{1}{B(a,b)} r^{a-1}(1-r)^{b-1} \tag{2.69}$$

with $a, b \in \mathbb{R}_+$, where the normalization constant is given by the Beta function

$$B(a,b) = \int_0^1 \mathrm{d}r\, r^{a-1}(1-r)^{b-1}. \tag{2.70}$$

We see also that the steady state mass distribution factorizes if the chipping kernels are Beta densities. This general result was first suggested in [**21**] and later proven in [**22**]. It could be also shown that in this case the single-site mass distribution is described by the Gamma densities

$$p_\lambda(m) = \frac{\lambda^\lambda}{\Gamma(\lambda)}\frac{1}{\rho}\left(\frac{m}{\rho}\right)^{\lambda-1} \mathrm{e}^{-\lambda m/\rho}, \tag{2.71}$$

where the parameter λ is given by $\lambda = a + b$.

The simplest version of the asymmetric random average process (ARAP) is given for the choice of $a = b = 1$ leading to the fraction density $\chi(r) = 1$. This process is often referred to as free ARAP since no restriction (except the conservation of the total mass, $M = \sum_i m_i(t) = \rho L$) is applied. In this case we have $\lambda = 2$ which leads to

$$P(m) = \frac{4m}{\rho^2}\mathrm{e}^{-2m/\rho}. \tag{2.72}$$

This expression was first derived in [**16**] where the force fluctuations in bead packs were analyzed. One has to note that the product measure Ansatz $P(m_1, ...) = \prod_i P(m_i)$ is exact for parallel update rules [**17, 18**].

As in the case of the zero range process it is interesting to consider the application of random sequential update rules for the asymmetric random average process. One just has to consider that at each time-step the chipped-off mass is transported to the neighboring site only with a probability p while in the complementary case, appearing with a probability $(1 - p)$, the mass returns to the original site, leading to

$$\chi(r) = (1 - p)\delta(r) + p. \tag{2.73}$$

Let us say that the difference between two time-steps is equal to $\mathrm{d}t$, then by setting $p = \mathrm{d}t$ and taking the limit $\mathrm{d}t \to 0$ we arrive at a continuous time model. This model is best approximated by a random sequential update mechanism. In this case the product measure ansatz delivers for the single-site mass distribution

$$P(m) = \frac{1}{\sqrt{2\pi\rho m}} \mathrm{e}^{-m/(2\rho)} \tag{2.74}$$

which is not exact as was shown in [**17, 18**].

2.4. Truncated processes

In the past several rigorous results for state-independent functions, $\chi(r)$, have been derived [**23, 24, 25, 26, 27, 28, 29, 30, 31**]. While these models can be easily analyzed and find applications in a large range of fields their state-independent nature also imposes several limits on the nature of the possible discussed systems. It is namely so that in many systems a reduction of the flux is not only explained by the interaction between the different particles but also due to the limited transport properties of the system. In stochastic mass transport models such an effect is often described as a bottleneck [**32**]. As example, data transport between different servers is not only limited by the capacities of the servers but also depends on the capability of the connection between them. In order to describe this feature in terms of the random average process a truncation mechanism proves useful.

We have to note here that truncation models also provide an interesting challenge since in contrast to the ZRP or the ARAP the existence of a unique stationary measure is not necessarily given [**59, 33, 34**] allowing us thus to study systems with a broken ergodicity property [**36, 37**]. Furthermore the metastability and phase transition properties related to the condensation phenomenon which became recently an object of scientific interest [**38, 39, 40, 41**] are easily implemented in the setting of truncation dynamics.

Here, as in the next chapter, we use parallel update rules and consider totally asymmetric dynamics. The evolution of the system is thus described

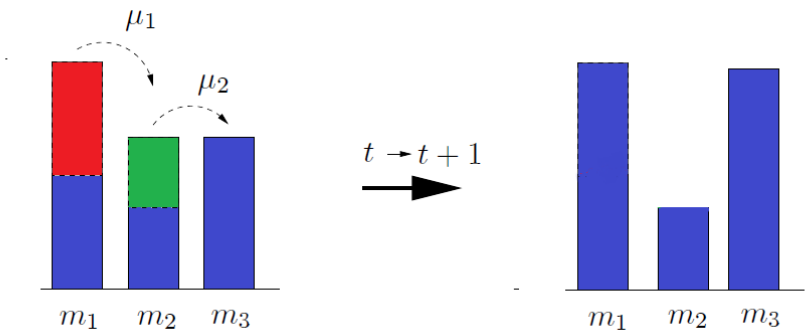

FIGURE 2.3. Characteristic representation of the dynamics of the TARAP. The mass fraction μ_1 cannot be transported to site 2 since $\mu_1 > \Delta$. On the other side the transport from site 2 to site 3 takes place since $\mu_2 < \Delta$.

by the equation

$$m_i(t+1) = m_i(t) - \mu_i(t) + \mu_{i-1}(t). \tag{2.75}$$

The terms μ describe a noise process where each term is given by the probability density function $\phi(\mu|m)$. The stochastic mass transport models discussed in this chapter do not fulfill the factorization condition. An analytical approach to questions regarding the condensation transition and the nature of the condensate is thus difficult and proves even impossible for the truncation models discussed here.

In order to define the truncation dynamics we use a cutoff parameter Δ. A simple example is the truncated asymmetric random average process [**36**] for which at each time-step a random fraction of the mass from each site is chosen and transported to the neighboring site only if the chosen amount is smaller than the cutoff Δ. The fraction density of this process has correspondingly the form

$$\phi(\mu|m) = \frac{1 - R'(m)}{m}\delta(\mu) + \frac{\Theta\left(R'(m) - \mu\right)}{m} \tag{2.76}$$

where Θ is the Heaviside step-function and

$$R'(m) = \min\left(m, \Delta\right) \tag{2.77}$$

represents the maximum possible amount.

In the following we choose to set $\Delta = 1$. This does not lead to a loss of generality since the dynamics of the process and specifically the occurrence of a condensate are fully specified by the ratio Δ/ρ and the length of the system L.

For the analysis of truncation dynamics two parameters are useful. The first one is the flux in the system at a specific time-point t:

$$J(t) = \frac{\sum_{i=1}^{L} \mu_i(t)}{L}. \tag{2.78}$$

We can namely claim that for truncation processes the ensemble average of the flux at a specific time-point is always below that of the corresponding free ARAP

$$\langle J(t) \rangle \leq 0.5\rho. \tag{2.79}$$

One has to note that for the models presented here the free ARAP case can be restored by choosing $\Delta = \infty$.

Another important characteristic of truncated processes is the largest mass in the system at a specific time-point. We consider also in the following the order statistics of the masses in the system. We characterize hereto the k-largest mass in the system at the time-point t by $\ell_k(t)$. Hence we use the notation $\ell_k(t)$ with

$$\ell_L(t) < \ell_{L-1}(t) < ... < \ell_1(t) = \max_{1 \leq i \leq L} m_i(t). \tag{2.80}$$

It can be shown that in the free ARAP case following equation for the largest mass in the system is fulfilled (see Appendix B)

$$\langle \ell_1 \rangle = 0.54\rho \ln(8.63L + 1). \tag{2.81}$$

The brackets refer again to the ensemble average and we ignored the indication of time since this expression holds for all time-points. In the following we will consider only systems with $L = 100$. This makes the comparison between the different models easier. Now if we set $L = 100$ then we can derive

$$\langle \ell_1 \rangle = 3.65\rho = 100\rho\ell^*. \tag{2.82}$$

This value $\left(\ell^* = 3.65 \cdot 10^{-2}\right)$ will serve as reference in the following discussion.

We start now with the analysis of truncation processes with a finite system length. We have seen that for the ZRP the grand canonical approach provides a description of the critical density. Furthermore the canonical approach that will be introduced in the next chapter allows us to analyze the nature of the condensate for mass transport models with factorized steady states. Since both of these approaches cannot be used here we rely on a different method.

An inquiry of the condensation transition for truncated models would require us to consider next to the probability for a condensate to appear in the system also the stability of those condensates. Unfortunately an analysis of this property proves to be difficult, if not impossible. In order to avoid this problem we decided to introduce a parameter γ which allows us to control the persistence of a condensate in the system. The effect of this parameter can be read from the corresponding probability density function $\phi(\mu|m)$ presented in the following three subsections.

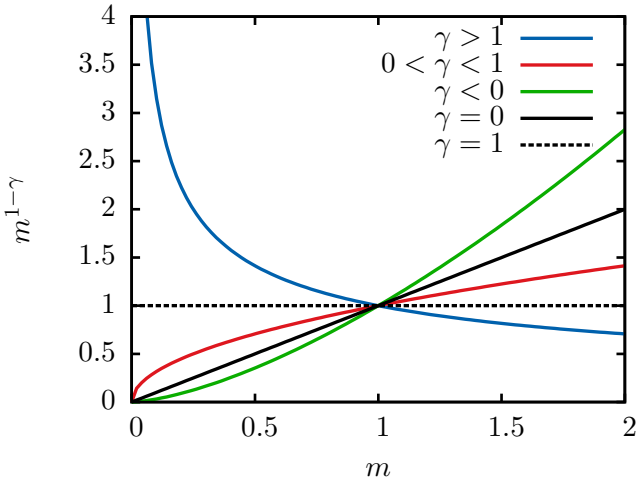

FIGURE 2.4. Characteristic representation of the function $m^{1-\gamma}$ for different values of the parameter γ. This representation helps us evaluate the function $R(m) = \min\{m, m^{1-\gamma}\}$ used extensively in the next sections.

2.4.1. TARAP. We start with a generalization of the truncated random average process (TARAP) by introducing the fraction density

$$\phi(\mu|m) = \frac{m - R(m)}{m}\delta(\mu) + \frac{\Theta\left(R(m) - \mu\right)}{m}, \tag{2.83}$$

where Θ is the Heaviside step-function and

$$R(m) = \min\left\{m, m^{1-\gamma}\right\} \tag{2.84}$$

represents the maximum possible amount. This fraction density describes a process that prohibits each transport between two sites where the transported amount of mass μ is above the cutoff $m^{1-\gamma}$. If we choose to set $\gamma = 1$ then the expression of the original TARAP for $\Delta = 1$ is restored (see Fig. 2.4). On the other side if we set $\gamma = 0$ then we can restore the free ARAP model. The moments of the transported mass per site and time-step, $\langle r^k m^k \rangle = \langle \mu^k \rangle$, are given by the equation

$$\langle r^k m^k \rangle = \int_0^m \mathrm{d}\mu\, \mu^k \phi(\mu|m) = \frac{R^{k+1}(m)}{(k+1)m}. \tag{2.85}$$

By using Monte Carlo simulations one can observe three different states as represented in Figure 2.5. We characterize these states by the time averaged values of the parameters $\langle \ell_1(T)\rangle \rho^{-1} L^{-1}$ and $\langle J(T)\rangle$ averaged also over 10^5 realizations in the stationary regime. We have to note here that since it is impossible to define analytically the time necessary for the distribution to become stationary, a numerical method becomes indispensable. For most

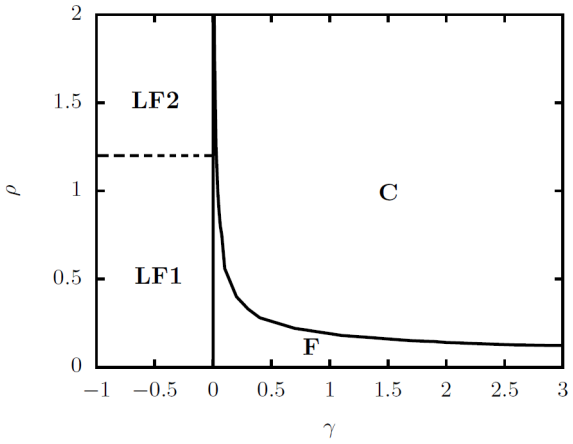

FIGURE 2.5. Schematic diagram for the TARAP model in the ρ-γ plane for $L = 100$. The dashed line describes the crossover between **LF1**-**LF2**. The characteristics of these corresponding states are described by the same dynamics and thus we choose a distinct way of displaying the crossover line between them.

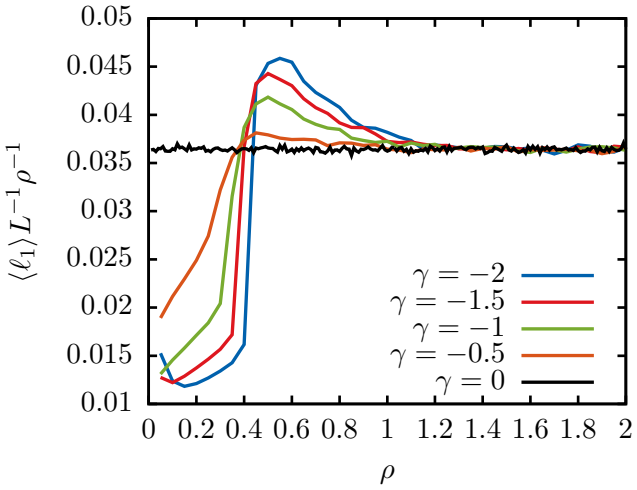

FIGURE 2.6. Mean largest value of the TARAP in the stationary limit for $L = 100$ and different values of γ.

of the parameter sets $\{\rho, \gamma\}$ and $L = 100$ the steady state is achieved after approximately $T = 10^5$ time-steps. The time averaged quantities are also calculated by taking 10^5 time-steps into account.

For $\gamma < 0$ we see that the flux of the system is below the free ARAP expectations and the overall variance of the single site mass distribution is

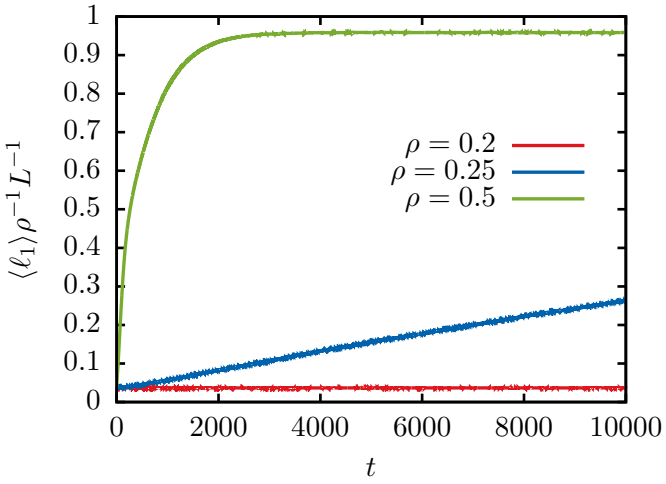

FIGURE 2.7. Time evolution of the largest mass for the TARAP for $L = 100$, $\gamma = 1$ and different densities.

also minimal. We therefore characterize this state as low-flow state (**LF**). In this state for small densities the mean largest value of the system is below ℓ^*. This changes completely for higher densities ($\rho \approx 0.4$ for $\gamma = -1$), where we observe values of ℓ_1 well above the free ARAP expectation ℓ^*. We see that in this case the truncation has a significant effect on the distribution of the largest value (**LF1**).

For increasing densities ($\rho > 1.2$) the value of ℓ_1 shows no difference to the free ARAP case as shown in Figure 2.6. For such high densities more than half of the sites have a mass above 1 and the effect of the truncation in the distribution of the largest value becomes negligible. At the same time this state is completely distinguishable from the free ARAP state since the flux in the system is well below $\rho/2$ (**LF2**).

For $\gamma > 0$ we can observe two different states. For small values of γ the differences to the free ARAP system are minimal. This state is characterized, due to the high flow in the system, as fluid phase (**F**). The probability of condensation as well as the lifetime of the corresponding condensates are small and consequently no deviation of $\langle \ell_1 \rangle$ from ℓ^* could be observed in our simulation.

For high densities and values of γ several condensates form (**C**). This is expressed through a steady increase of the largest value for high values of ρ (Figure 2.7). Due to the conservation of mass we have also a competition of the different condensates and with evolution of time only one condensate may survive.

The evolution of the system is characterized by the stability of the condensate. We can say that the fluctuations observed early in the system diminish for $\ell_1 > 0.9\rho L$ but never disappear and in rare cases may lead to

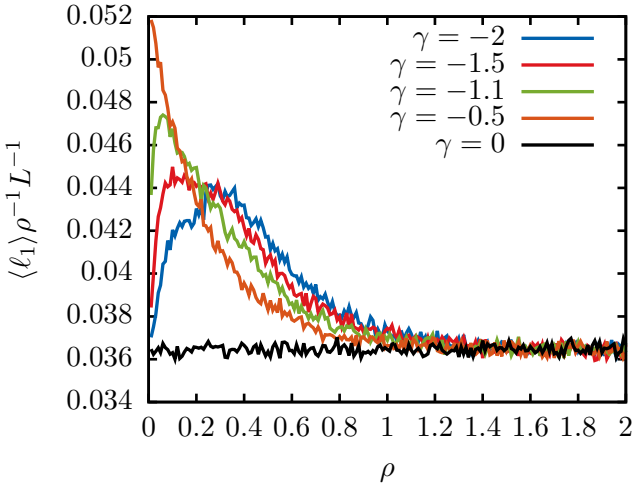

FIGURE 2.8. Mean largest value of the ZRRAP in the stationary limit for different values of γ.

the destruction of the condensate which is characterized by a drop of the largest mass in the system and the following change in the position of the condensate. Finally we have to note that all of these dynamics observed in the condensate state are accelerated for lower densities.

We summarize the characteristics of these three states in the next table.

	$\langle \ell_1 (T) \rangle$	$\langle J (T) \rangle$
C	$> \ell^*$	~ 0
F	$\sim \ell^*$	$\sim \rho/2$
LF1	strong fluctuations	$< \rho/2$
LF2	$\sim \ell^*$	$< \rho/2$

TABLE 1. Characterization of the different characteristic regimes of the TARAP.

2.4.2. ZRRAP. The truncation of the TARAP analyzed in the last subsection manifests itself in two different ways: the prohibition of transport expressed through the term $m^{-1}(m - R(m))\,\delta(\mu)$ and the reduction of the transported fraction as dictated by the term $\Theta(R(m) - \mu)$. In order to understand the relevance of these two distinct effects for the condensation mechanics we decided to study two different processes designed according to these terms.

By starting with the first term we arrive at a process which can be regarded as the continuum state space analogue of the zero range process (since only the prohibition of the transported mass is considered). We will

therefore call this process zero-range random average process (ZRRAP). The fraction density of this process is given by

$$\phi(\mu|m) = \frac{m - R(m)}{m}\delta(\mu) + \frac{R(m)}{m^2}\Theta(m - \mu) \tag{2.86}$$

where we use for $R(m)$ the same expression as defined above by Eq. (2.84). For the moments of this density we get the expression

$$\langle r^k m^k \rangle = \int_0^m \mathrm{d}\mu\, \mu^k \phi(\mu|m) = \frac{m^{k-1}}{k+1} R(m). \tag{2.87}$$

This fraction density describes a process for which with a state-dependent probability the transported fraction $\mu_i(t)$ of a certain site i at the time point t will be set to 0. This event occurs with a probability equal to $(m-R(m))/m$. Alternatively the fraction $\mu_i(t)$ is randomly distributed with equal probability in the interval $[0, m]$. This property is the big difference between the ZRRAP and the TARAP, introduced in the last subsection 2.3.1, where the transported mass per site and time-step had an upper bound of $R(m)$, as seen by Eq. (2.83).

For the ZRRAP three characteristic regimes can be defined. By choosing $\gamma < 0$ we can see that the mean largest value shows a very interesting behavior, whereas the expected value is always bigger than ℓ^* for $\rho < 1.2$ (**LF1**). This fact can be observed in Figure 2.8. Initially a spatial concentration of masses with $m_i > 1$ takes place, which travels through the system unhindered. At the same time the rest of the mass in the system contributes only marginally to the overall flow leading thus to ($\langle J \rangle < 0.5\rho$). This local concentration of mass leads to a stationary mean largest value with $\langle \ell_1(\infty) \rangle > \ell^*$. For higher densities ($\rho > 1.2$ with $\gamma < 0$) this effect disappears and the free ARAP-like case is restored (**LF2**).

By studying the system for $\gamma > 0$ we can observe again a fluid and condensate regime as for the TARAP (see Figure 2.9). There is in general a striking similarity between the two diagrams, which proves the relevance of the constraint on the transition (δ-term in Eq. (2.83)) for the condensation effect. The dynamics of condensation is in general similar to the one for the TARAP. The main difference lies in the speed with which the condensate builds up in the system. The concurrence between different condensates resolves faster in the ZRRAP in comparison to the TARAP. This is also reflected in the fact that for the same values of γ a smaller ρ is necessary for a condensate to appear in the system. Fluctuations persist for all parameter values and decrease for increasing values of γ and decreasing densities allowing therefore for a smooth crossover to the stable high flow phase (**F**).

These numerical results are summarized by the following tabular representation.

2.4.3. SRAP. In the last two subsections we investigated the effect of truncation for fraction densities with a non-zero probability for the event

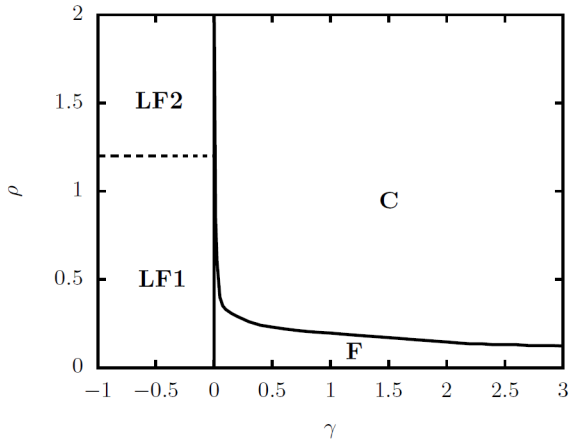

FIGURE 2.9. Schematic diagram for the ZRRAP model in the ρ-γ plane for $L = 100$. The dashed line describes the crossover between **LF1**-**LF2**. The characteristics of these two states are described by the same dynamics and thus we choose a distinct way of displaying the crossover line between them.

	$\langle \ell_1 (T) \rangle$	$\langle J (T) \rangle$
C	$> \ell^*$	~ 0
F	$\sim \ell^*$	$\sim \rho/2$
LF1	$> \ell^*$	$< \rho/2$
LF2	$\sim \ell^*$	$< \rho/2$

TABLE 2. Characterization of the different characteristic regimes of the ZRRAP.

$\{r_i(t) = 0\}$. In this subsection we will show that even for transport processes for which $\{r_i(t) > 0 \ \ \forall i, t\}$ holds, a condensate phase appears in the $\rho - \gamma$ plane.

We introduce hereto the function

$$\phi(\mu|m) = \frac{1}{R(m)} \Theta \left(R(m) - \mu \right) \tag{2.88}$$

where $\Theta(x_0 - x)$ is again the Heaviside function and $R(m)$ defined as in Eq. (2.84). For this class of models the truncation can only lead to a reduction of the transported mass but not to the prohibition of transport as in the two previous cases. It is clear that for $\gamma = 0$ the free ARAP model is restored. As before the introduction of the parameter γ allows us to study systems

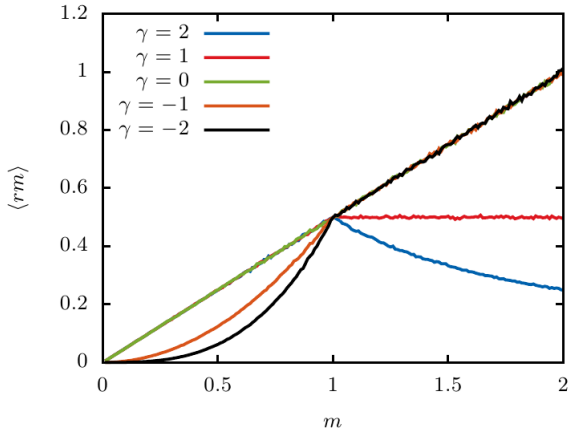

FIGURE 2.10. Mean transported mass per time-step for a site with mass m for the ZRRAP and the SRAP and different parameters γ. We can see that for these two models the first moment μ_1 is described by the same function (Eq. (2.87) and (2.89)).

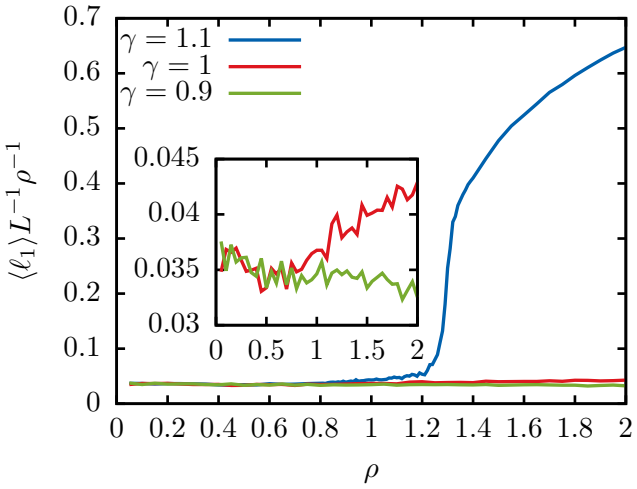

FIGURE 2.11. Mean largest value of the SRAP in the stationary limit for different values of γ.

with a large range of moments

$$\langle r^k m^k \rangle = \int_0^1 \mathrm{d}\mu \, \mu^k \phi(\mu|m) = \frac{R(m)^k}{k+1}. \tag{2.89}$$

In Figure 2.10 we can see the first moment of the transported mass μ_1 as function of the mass. We will see later that although the first moments for

the transported mass of the two models (SRAP and ZRRAP) are equal, the corresponding diagrams have a completely different structure. We can see that the condensate/fluid separation appears in the system only for $\gamma > 1$. For the fluid case we again observe that the largest value in the system remains constant around the expected value of ℓ^* with small fluctuations. The same holds for the flux which fluctuates around 0.5ρ.

In the condensate phase this no longer holds. We can clearly see that $\langle \ell_1(T) \rangle > \ell^*$ and $\langle J(T) \rangle < 0.5\rho$. It is especially interesting that in this regime the spatially extended condensate performs a drift through the system. For high values of γ ($\gamma > 1$) the position of the condensate stabilizes and the largest value in the system rises up to a stationary value which is given by the equation

$$\ell_1^{1-\gamma}(T) = \rho - \frac{\ell_1(T)}{L}. \tag{2.90}$$

This equation agrees well with our numerical results and follows from following simple argument. Let us assume that at the time-point t there exists only one condensate in the system, then we know that the evolution of this condensate is described by the differential equation

$$\frac{\partial}{\partial t}\ell_1(t) = -\xi\ell_1(t) + \xi^* \left(\rho - \frac{\ell_1(t)}{L}\right). \tag{2.91}$$

The terms ξ, ξ^* describe noise processes with the mean value $\langle \xi \rangle_{\text{Ens}} = \langle \xi * \rangle_{\text{Ens}} = 0.5$. By taking now the ensemble average we can clearly see that the steady state condition

$$\left\langle \frac{\partial}{\partial t}\ell_1(t) \right\rangle_{\text{Ens}} = 0 \tag{2.92}$$

is equivalent to Eq. (2.90).

Fluctuations are present even after the formation of the condensate, but this value remains stationary when integrated over long time-intervals ($T = 10^3$).

For $0 < \gamma < 1$ the flow of the system is below $\rho/2$ while at the same time we can observe a homogeneous mass distribution. We therefore characterize this phase as homogeneous low flow state (**HLF**). Surprisingly we found that for $\rho > 0.9$ as shown in Figure 2.11 the mean largest value in the system decreases with increasing densities (**HLF2**). This discovery is explained by the slowdown of the mass drift for sites with $m > 1$ due to the truncation effect. Correspondingly we get an equilibration of the mass distribution and thus a lower mean largest value. This effect does not arise for lower densities and we regain the expected mean largest value of ℓ^* (**HLF1**).

The diagram for this process is quite more complicated than the previous models. But as seen in the table above a clear distinction between the different phases can be made. We have to note here that although for the **HLF1** and the **LF2** the truncation seems to have no effect on the mean largest value distribution the two states have completely different characteristics. In the one case (**LF2**) we have collective dynamics while in the

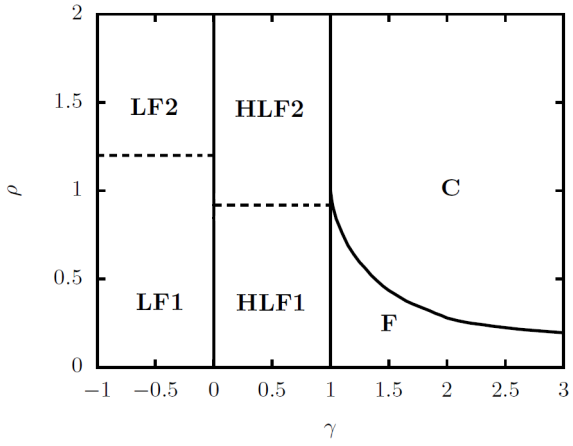

FIGURE 2.12. Schematic diagram for the SRAP model in the ρ-γ plane for $L = 100$. The dashed lines do describe the crossover between **LF1**-**LF2** and **HLF1**-**HLF2** correspondingly.

other (**HLF1**) the mean largest value distribution is solely defined by single site mass deviations. This is the reason why these two states appear on completely different ranges of the density parameter.

Regarding the $\gamma < 0$ case we have the same structure as described above for the TARAP. For $\rho < 1.2$ we see again a strong fluctuation of the mean largest value with respect to the density. Like in the former processes these fluctuations disappear for $\rho > 1.2$. It becomes clear that the dynamics of condensation for the TARAP and therefore the transition from fluid to the condensate phase are controlled by single site fluctuations and consequently by the prohibition of transport ($\delta -$ term). At the same time the nature of the phases for $\gamma < 0$ is controlled by collective dynamics and the reduction of the mass transport ($\Theta -$ term).

2.5. Discussion and Conclusions

We introduced and studied three different truncated random average processes. We started with the analysis of finite size systems which could be approached only by numerical methods. A convenient choice for the characteristic variables of this system are the largest single-site mass and the flow in the system. The introduction of the parameter γ allowed us to control effectively the dynamics of the system and hereby the stability of the condensates that appear in the evolution of the system. The impact of this parameter on the condensation transition was studied by determining numerically the evolution of the system. This allowed us to characterize several states in the $\rho - \gamma$ plane. By comparing the different diagrams we could also clarify the relevance of the different processes like prohibition of

	$\langle \ell_1(T) \rangle$	$\langle J(T) \rangle$
C	$> \ell^*$	~ 0
F	$\sim \ell^*$	$\sim \rho/2$
LF1	strong fluctuations	$< \rho/2$
LF2	$\sim \ell^*$	$< \rho/2$
HLF1	$\sim \ell^*$	$< \rho/2$
HLF2	$\leq \ell^*$	$< \rho/2$

TABLE 3. Characterization of the different characteristic regimes of the SRAP. No difference between the **HLF2** and **LF2** state can be determined if we observe only the parameters $\ell(\infty)$ and $J(\infty)$.

transport (δ - term) or reduction of the fraction (Θ - term) for the nature of the condensates.

Interesting generalizations of the presented model may arise. As example one could consider the transport properties of the same model with open boundary conditions. Another question that arose during this work and was inspiration for chapter 3 is the behavior of systems with $\gamma = -\infty$. In this case an absorbing stationary state exists in the system and the relation to similar non-equilibrium processes is at hand. Surprisingly, as we will show in the next chapter, it is possible to determine the single site mass distribution for this absorbing state analytically.

CHAPTER 3

Continuous Mass Transport Models with $\gamma = -\infty$

3.1. Introduction

In the last chapter we have studied systems with factorized steady states and discussed the condensation phenomenon occurring for stochastic mass transport models with truncation dynamics. We could see that in the latter case analytical results are rather cumbersome. This problem arises out of the fact that the steady state is non-factorizable. Nevertheless the introduction of the parameter γ and its strong influence on the dynamics of condensation helped us gaining a better understanding of some aspects of the condensation process.

In the last chapter we have chosen γ to be a real number. For negative values of γ a condensation is excluded but at the same time a large range of other interesting phenomena arise. As a first step in the analysis of these phenomena we decided to consider the simple case of $\gamma = -\infty$. This choice leads to a quite simple stochastic transport model which could be interesting for a series of applications for example traffic systems or transport along one-dimensional DNA sequences [**4**]. Surprisingly several properties of this model can be determined analytically. As example the steady state occurring for $\rho < 1$ can be exactly calculated using the canonical ensemble approach.

Characterizing the non-equilibrium steady state of an interacting many-particle system has always been a fundamental problem [**49, 50**]. Although these systems appear in a variety of situations and have a potentially richer behavior than equilibrium systems, mainly due to the lack of a detailed balance condition, a general approach to this problem is still missing. The biggest challenge lies in the fact that in contrary to equilibrium systems the stationary state cannot be described by a Boltzmann distribution. In the past there have been several attempts to provide a relative broad framework inside of which questions with regard to the nature of non-equilibrium steady states could be addressed [**51**]. The additivity property has proven extremely useful in that regard when dealing with the special case of stochastic mass transport models where chipping, diffusion and coalescence of neighboring masses is considered [**27, 28**].

The application of the canonical ensemble formalism for non-equilibrium systems is made possible inside the mathematical framework of Large Deviation Theory. So before we go over to the details of our model it is surely helpful to provide a brief introduction to Large Deviation Theory [**52**]. Then

we will discuss the canonical ensemble formalism for stochastic mass transport models. In section 3.4 we will apply this formalism to the special case of restricted processes. Following that in section 3.5 and 3.6 we will see some generalizations of the presented models. At the end of this chapter some concluding remarks will be made.

3.2. Large Deviation Theory

Large deviation theory is the mathematical theory concerned with the exponential decay of probabilities of large fluctuations (or rare events) of random systems. The concept of weights with an exponential form is established in physics since the work of Boltzmann and Gibbs. We can namely find several equilibrium systems, where the probabilities of a certain observational state can be expressed in terms of exponential functions with exponents mostly proportional to the entropy or free energy function. Large Deviation Theory provides a rigorous mathematical formulation of this property. Furthermore the introduction of more technical terms like the rate function and the scaled cumulant generating function allows for the generalization of Einstein's fluctuation theory. This lead to the increase of the popularity of this theory in the last years in the field of both equilibrium and non-equilibrium statistical mechanics.

Our goal in this chapter is to provide the essential elements of the large deviation theory and show the close connection between large deviation theory and statistical mechanics. We follow hereby the great introduction provided by Touchette in [**56, 57**].

3.2.1. Basic Elements of Large Deviation Theory. In order to get a better idea about the basic approach and methods we start by considering the simple example of the average S_N of N real independent and identically distributed (i.i.d.) random variables X_k

$$S_N = \frac{1}{N} \sum_{k=0}^{N} X_k. \tag{3.1}$$

The probability distribution function (pdf) of the sum S_N which we denote by $P_{S_n}(s)$ [1] can be determined by the corresponding joint pdf of $X_1, ..., X_n$ which in the case of i.i.d. RVs may be written in the factorized form

$$P_{\{X_1,...,X_N\}}(x_1, ..., x_N) = \prod_{k=0}^{N} P_{X_k}(x_k). \tag{3.2}$$

We can calculate the pdf associated with the event $S_N = s$ by taking into account all possible realizations $(x_1, ..., x_N) \in \mathbb{R}^N$ of $X_1, ..., X_N$ that respect

[1] We will denote in this section the pdf of a RV X as $P_X(x)$. Correspondingly the pdf for a set of RVs $\{X_1, ..., X_N\}$ is characterized by $P_{\{X_1,...,X_N\}}(x_1, ..., x_N)$.

the condition $S_N = s$. This is easily expressed in a mathematical way by using the Dirac δ function and writing

$$P_{S_N}(s) = \int_{\mathbb{R}} \mathrm{d}x_1 \cdots \int_{\mathbb{R}} \mathrm{d}x_N \, \delta\left(\sum_{k=1}^{N} x_k - Ns\right) P_{\{X_1,\ldots,X_N\}}(x_1,\ldots,x_N)\,. \quad (3.3)$$

This equation can be solved by using the method of generating functions or by calculating the Laplace transform and use the saddle point approximation as will be shown in the next section.

Independent of the chosen method we come to the realization that in the case of i.i.d. RVs X_k with Gaussian densities

$$P_{X_k}(x) = \frac{1}{\sqrt{2\pi\sigma^2}} \mathrm{e}^{-(x-\mu)^2/(2\sigma^2)}, \quad x \in \mathbb{R} \quad (3.4)$$

the general form

$$P_{S_N}(s) \approx \mathrm{e}^{-NI(s)} \quad (3.5)$$

with

$$I(s) = \frac{(s-\mu)^2}{2\sigma^2} \quad (3.6)$$

is obtained.

We have to note that the general exponential form $\mathrm{e}^{-NI(s)}$ can be replicated for numerous choices of the pdf $P_{X_k}(x)$. This result is the cornerstone of large deviation theory and referred to as the Large Deviation Principle (LDP).

In general we say that the pdf of a random variable S_N satisfies the large deviation principle if the following limit exists:

$$\lim_{N\to\infty} \left(-\frac{1}{N} \ln P_{S_N}(s)\right) = I(s). \quad (3.7)$$

The function $I(s)$ is the so-called Cramér or rate function. For simplicity we assume that this function is analytic and not everywhere zero.

An equivalent formulation of the LDP is expressed in terms of the equation

$$P_{S_N}(s) = \mathrm{e}^{-NI(s)+o(N)} \quad (3.8)$$

where $o(N)$ describes any correction that is sub-linear in N. This equivalence illustrates the close connection between the LDP and the exponential decay of large fluctuations. This last property is of course relevant for a wide range of applications and shows the great importance of the LDP. This led to the development of the Large Deviation Theory which can be considered as a collection of methods devised for attacking two problems: first showing that a LDP exists for a given RV and second provide the expression of the corresponding rate function.

Both of these problems can be addressed directly, indirectly or through the contraction method. The direct method consists in calculating the pdf $P_{S_N}(s)$ and show that the limit (3.7) holds. This approach can in general be very difficult, especially when dealing with continuous RVs.

The indirect method on the other side is far more general and relies on a fundamental result of LDT known as Gärtner-Ellis Theorem (GE Theorem). In the following we present a simplified version of this theorem.

We start from the definition of the scaled cumulant generating function

$$\lambda(k) = \lim_{N\to\infty} \frac{1}{N} \ln \mathbb{E}\left[\mathrm{e}^{kNS_N}\right]. \tag{3.9}$$

According to the GE Theorem, if $\lambda(k)$ is differentiable for all $k \in \mathbb{R}$, then S_N satisfies an LDP and the rate function is the Legendre-Fenchel transform of $\lambda(k)$:

$$I(s) = \sup_{k\in\mathbb{R}} \{ks - \lambda(k)\}. \tag{3.10}$$

We will not provide here a rigorous proof of the GE Theorem as it would be beyond the scope of this short introduction. For readers interested in the technical details we would like to recommend the textbooks of Varadhan [**53**], Ellis [**54**] or Dembo and Zeitouni [**55**]. Although we cannot provide a proof we would like to give some insight by providing a simple proof of the second part of the theorem namely showing that Eq. (3.10) holds if we assume that a LDP holds for S_N.

We start from the functional

$$\mathbb{E}\left[\mathrm{e}^{NkS_N}\right] = \int \mathrm{d}s\, P_{S_N}(s)\mathrm{e}^{Nks}. \tag{3.11}$$

The assumption that S_N satisfies an LDP with rate function $I(s)$ leads to the expression

$$\mathbb{E}\left[\mathrm{e}^{NkS_N}\right] \approx \int_{\mathbb{R}} \mathrm{d}s\, \mathrm{e}^{N[ks-I(s)]}. \tag{3.12}$$

Now this form is reminiscent of the Laplace integral and it thus allows us to replace the integral by the approximation

$$\mathbb{E}\left[\mathrm{e}^{NkS_N}\right] \approx \mathrm{e}^{N\sup_s\{f(s)-I(s)\}}. \tag{3.13}$$

This approximation is called Laplace approximation or saddle-point approximation and is justified in the large deviation theory since all correction terms are subexponential in N. Now by returning to the definition of the scaled cumulant generating function, we can see that

$$\lambda(k) = \lim_{N\to\infty} \frac{1}{N} \ln \mathbb{E}\left[\mathrm{e}^{NkS_N}\right] = \sup_s \{ks - I(s)\}. \tag{3.14}$$

Since the the function $\lambda(k)$ is everywhere differentiable, the Legendre-Fenchel transform is self-inverse, so that

$$I(s) = \sup_s \{f(s) - \lambda(k)\}. \tag{3.15}$$

This short calculation is quite important since it shows that the knowledge of the scaled cumulant generating function provides automatically an expression for the rate function.

A generalization of the result above for a large class of RVs, random vectors and random functions was provided by Varadhan who used the generalized version of the SCGF, corresponding to the functional $\lambda[f]$, and showed that

$$\lambda\left[f\right] = \lim_{N\to\infty} \frac{1}{N} \ln \mathbb{E}\left[\mathrm{e}^{Nf(S_N)}\right] = \sup_{s\in\mathbb{R}} \left\{f(s) - \lambda(k)\right\} \tag{3.16}$$

holds for an arbitrary continuous function f of S_N.

The clear connection between the GE and the Varadhan Theorem is demonstrated by considering the case of $f(s) = ks$ which then leads to the formula derived above (3.15). It is also worthy to note here that Legendre-Fenchel transform appears in this theory as natural consequence of Laplace's approximation.

Another way to derive the LDP is given by the contraction method. Let therefore A_N be a random variable for which an LDP with a rate function $I_A(a)$ holds and let B_N be a second random variable with $f(A_N) = B_N$. Naturally then the question arises, if this condition is sufficient for the validity of an LDP also for the RV B_N. Furthermore, is it possible to derive the corresponding rate function?

The answer to these questions is given by expressing the pdf of B_N in terms of the pdf of A_N

$$P_{B_N}(b) = \int_{\{a:f(a)=b\}} \mathrm{d}a\, P_{A_N}(a) \approx \int_{\{a:f(a)=b\}} \mathrm{d}a\, \mathrm{e}^{-NI_A(a)}. \tag{3.17}$$

This integral can be approximated according to the Laplace principle by the maximum value which corresponds to the minimum of $I_A(a)$ for a such that $b = f(a)$. It follows therefore immediately that an LDP of the form

$$P_{B_N}(b) \approx \exp^{-N \inf\limits_{a:f(a)=b}\{I_A(a)\}} \tag{3.18}$$

for B_N can be found. The corresponding rate function is simply given by

$$I_B(b) = \inf_{a:f(a)=b} I_A(a). \tag{3.19}$$

This principle is called contraction principle and can be used in order to derive the maximum entropy from the minimum free energy principle and vice versa. These in turn were essential for the determination of equilibrium states in the microcanonical and canonical ensemble respectively.

Lastly we will show that large deviation theory contains the Central Limit Theorem. This seems logical if we consider that the LDP implies some form of a Law of Large Numbers (LLN) since in the large N limit the pdf $p\left(S_N\right)$ concentrates around the typical values of S_N. These typical values correspond of course to the minimal values of the rate function $I(s)$. Next to this information with regard to the mean value one can also evaluate the likelihood of small deviations from the typical value of S_N. We consider here that we have only one such typical value and use a Taylor series expansion

of the rate function around this typical value s^*:

$$I(s) = I(s^*) + I'(s^*)(s - s^*) + I''(s^*)\frac{(s - s^*)^2}{2} + \mathcal{O}(s^3). \tag{3.20}$$

Since s^* corresponds to a minimum of $I(s)$ the first derivative vanishes. Now from the two remaining terms we need to consider only the second order term. The first term contributes only with a term of $\mathrm{e}^{-I(s^*)}$ to the pdf which can be considered just as a normalization factor. This leads us to the prediction that the pdf around the typical value takes a Gaussian form:

$$P_{S_N}(s) \approx \mathrm{e}^{-NI''(s^*)(s-s^*)^2/2}. \tag{3.21}$$

We see also that large deviation theory can be considered as extension of the central limit theorem since it provides us with estimates not only of small deviations but also of large deviations far away from the typical values.

3.2.2. Connection to the Boltzmann Formalism. Now we will see how the formalism presented in the previous subsection is connected to the Boltzmann formalism used in equilibrium statistical mechanics.

We consider now a statistical ensemble consisting of N trials in which each random variable X_I may take only a finite set of n different values $\{x_1, ..., x_n\}$. Each experiment then is described by the set $\{N_1, ..., N_n\}$ with

$$\sum_{k=1}^{n} N_n = N. \tag{3.22}$$

The natural numbers N_1, N_2,.... describe the number of samples with the outcome x_1, x_2 and so on. Alternatively one could consider the relative frequencies

$$f_i = N_i/N, \qquad i = 1, ..., n. \tag{3.23}$$

Now the probability to measure the set $\{f_1, ..., f_n\}$ in such an experiment consisting of N trials is given by

$$P(f_1, ..., f_n) = \frac{N!}{(Nf_1)!...\,(Nf_n)!} \prod_{i=1}^{n} [P(x_i)]^{Nf_i}\,, \tag{3.24}$$

where $P(x_i) = p_i$ is the probability for the outcome x_i for a single trial. Using the Stirling formula we find

$$P(f_1, ..., f_n) \simeq \frac{\sqrt{2\pi N}}{\prod_{i=1}^{n}\sqrt{2\pi f_i N}} \mathrm{e}^{-N\sum\limits_{i=1}^{n} f_i(\ln f_i - \ln p_i)} \tag{3.25}$$

We see that the expression

$$H(f_1, ..., f_n) = \sum_{i=1}^{n} f_i \ln \frac{f_i}{p_i} \tag{3.26}$$

serves as rate function. This rate function is called the relative entropy or Kullback-Leibler divergence.

In the absence of constraints other than the normalization condition $\sum_{i=1}^{n} f_i = 1$ and for N large, the frequencies f_i converge towards the values

p_i that maximize $H(f_1, ..., f_n)$. This property arises from the convexity of $H(f_1, ..., f_n)$ and is an expression of the law of large numbers.

Our present formalism allows us to go beyond the LLN and consider the possibility of a fluctuation for the set $\{f_1, ..., f_n\}$. We consider hereto the deviation from the mean value

$$\sum_{i=1}^{n} f_i x_i - \sum_{i=1}^{n} p_i x_i = \hat{x}. \tag{3.27}$$

If we make now the observation $x = \sum_{i=1}^{n} f_i x_i$ we can apply an additional condition. The frequencies in this case are those that minimize the function

$$H(f_1, ..., f_n) + \lambda_1 \left(\sum_{i=1}^{n} f_i - 1 \right) + \lambda_2 \left(\sum_{i=1}^{n} f_i x_i - x \right), \tag{3.28}$$

where λ_1 and λ_2 are the two corresponding Lagrange parameters.

The corresponding expressions for f_i are then given by [**58**]

$$f_i = p_i \frac{\mathrm{e}^{-\lambda_2 x_i}}{Z(\lambda_2)} \tag{3.29}$$

where $Z(\lambda_2)$ is the normalization factor

$$Z(\lambda_2) = \sum_{i=1}^{n} p_i \mathrm{e}^{-\lambda_2 x_i}. \tag{3.30}$$

The existence of a deviation leads to a corresponding modification of the empirical frequencies, which is reminiscent of the Boltzmann formalism. This can be seen by renaming the second Langrange parameter λ_2 as β [2]. These parameters are namely determined by the equation

$$\frac{\partial}{\partial \beta} \ln Z(\beta) = x = \sum_{i=1}^{n} f_i x_i. \tag{3.31}$$

This strong similarity is not surprising if we consider that the canonical ensemble approach in equilibrium physics (as introduced in most textbooks) also originated from the consideration of large fluctuations of the energy made possible by the contact of the system with a reservoir. Lastly we have to note that if we assume $\hat{x} = 0$ then $f_i = p_i$ is recovered in the asymptotic limit since then $\beta = 0$.

In the next section we will return to stochastic mass transport models and see how the implementation of additional conditions creates a deviation between the weight functions and the single site mass distribution. This inquiry will allow us to provide another example for the relevance of the "canonical ensemble" approach for non-equilibrium systems.

[2] This notation is often used in statistical mechanics in order to characterize the intensive thermodynamic parameter which is proportional to the inverse temperature of the system, $\beta = (k_B T)^{-1}$.

3.3. Canonical Ensemble Approach for Mass Transport Systems

We have seen in the previous chapter that for the ZRP and the ARAP the chipping kernel $\phi(\mu|m)$ determining the dynamics of transport can be written in the form

$$\phi(\mu|m) \propto u(\mu)w(m-\mu), \tag{3.32}$$

where $u(z)$ and $v(z)$ are arbitrary non-negative functions. We also claimed that for chipping kernels of this form the steady state probability takes a factorized form

$$P(m_1, ...m_L) = \frac{1}{Z_L(M)} \prod_{k=1}^{L} f(m_k)\delta\left(\sum_{i=1}^{L} m_i - M\right) \tag{3.33}$$

where $Z_L(M)$ is the normalization constant, $f(m_i)$ is the single-site weight and the δ function ensures the conservation of mass in the system. The single site weight is given by

$$f(m) = \int_0^m \mathrm{d}\mu\, u(\mu)w(m-\mu). \tag{3.34}$$

Furthermore the grand canonical ensemble framework analysis was introduced in the last chapter which allowed us to determine the conditions for condensation in general mass transport models. This analysis proved to be easy and useful but granted us no insight into the condensed phase itself. For this reason a canonical ensemble formalism was established in the past [**44, 45**] which concentrates on the analysis of the single-site mass probability distribution function

$$p(m) \stackrel{!}{=} \int ... \int \mathrm{d}m_2 ... \mathrm{d}m_L\, P(m, m_2, ..., m_L)\, \delta\left(\sum_{i=2}^{L} m_i + m - \rho L\right) \tag{3.35}$$

in a finite system size of size L. It is now clear that due to the factorization property

$$p(m) = f(m)\frac{Z(M-m, L-1)}{Z(M, L)}. \tag{3.36}$$

One hast to note here that there is a striking similarity between this equation and Eq. (3.29) derived in the last section. In the work of Evans, Majumdar and Zia [**44, 45**] this approach was used in order to analyze $p(m)$ in the special case of

$$f(m) \approx Cm^{-\gamma} \quad \text{with} \quad \gamma > 2. \tag{3.37}$$

The constant C is an arbitrary constant defined by the normalization condition. We can choose now without loss of generality to set $\int \mathrm{d}m\, f(m) = 1$.

One easy argument to see that the choice $\gamma > 2$ leads to a condensation is considering that for normalized weight functions $f(m)$ the product $\prod_{i=1}^{L} f(m_i)$ corresponds to the probability that L i.i.d. positive RVs, each

drawn from the distribution $f(m)$, take the values $m_1, m_2, ...m_L$. Under the assumption that the first moment

$$\langle m \rangle = \int \mathrm{d}m\, m f(m) \tag{3.38}$$

exists we can consider two distinct cases. In the first case we have the relation $L\langle m \rangle > M$ which correspondingly leads to the conclusion that the ensemble is dominated by configurations with $m_i = \mathcal{O}(1)$ for all i. On the other hand we could have the relation $L\langle m \rangle < M$. In this second case the ensemble is dominated by configurations where $L-1$ masses are of the order $\mathcal{O}(1)$ and one of $\mathcal{O}(M)$. The choice of $f(m) \sim m^{-\gamma}$ is therefore a good candidate for studying systems with a condensation at a critical density $\rho_c = \langle m \rangle$.

In contrast to these works we will use here this approach not in order to study the condensation transition but to derive an exact expression for the factorizable steady state for a relatively broad class of stochastic mass transport system that have not been studied yet. This is an exciting result since in general for non-equilibrium systems where stochastic dynamical rules have such an important effect the steady state distributions are not a priori known. Especially not if the dynamics are specified by a state-dependent kernel as for the process treated here.

3.3.1. Model and general approach. We start this section by describing the dynamics of the mass transport process studied. The studied dynamics are rather similar to that of the asymmetric random average process (ARAP). We assume that the transport takes place on a lattice consisting of L sites with periodic boundary conditions. As in the case of the random average process each site $i \in \{1, ..., L\}$ carries a positive mass $m_i \in \mathbb{R}_+$. At each time-step a fraction of the mass $\mu_i \leq m_i$ is transported to a neighboring site, only and only if, the mass at the departure site is bigger than 1. We consider in this section only totally asymmetric dynamics ($i-1 \to i$). In the next section we will also consider partially asymmetric dynamics. The total mass in the system $M = \rho L$ is conserved by these dynamics.

The dynamics of this stochastic process are described by the evolution equation of the mass $m_i(t) = m_{i,t}$ at a site i:

$$m_{i,t+1} = m_{i,t} - \mu_{i,t} + \mu_{i-1,t} \tag{3.39}$$

whereas the random variables $\mu_{i,t} \leq m_{i,t}$ are white noise processes derived from the probability density function

$$\phi(\mu|m) = \begin{cases} \delta(\mu) & \text{if } m < 1 \\ \varphi(\mu) & \text{if } m \geq 1. \end{cases} \tag{3.40}$$

In the following we will assume that the distributions are non-degenerate and $\varphi(\mu) > 0$ holds for all $\mu \in [0, 1]$.

Let us focus now on the case of an exponential distribution for the initial configuration of the mass (gap) statistics

$$f_0(m) = \rho^{-1} e^{-\frac{m}{\rho}}. \tag{3.41}$$

This choice is easily implemented by creating an interval of length ρL and choosing $L-1$ i.i.d. RVs X_i with uniform distribution in the interval $[0, \rho L]$. We go now over to the order statistics of these RVs X_i characterized by Y_i with

$$Y_L < Y_{L-1} < ... < Y_1 = \max_{1 \leq i \leq L} X_i. \tag{3.42}$$

By setting $m_i = Y_{i+1} - Y_i$ with $m_L = \rho L - Y_{L-1}$ and $m_1 = Y_1$ one gains a configuration of masses $\{m_1, ..., m_L\}$ with $\sum\limits_{i=1}^{L} m_i = \rho L$. Each of these RVs m_i is now identically and independently distributed with a probability density function given by (3.41).

We will see in the next section that for mass chipping models like the one introduced here a factorizable steady state is achieved in the limit of $(t \to \infty, L \to \infty)$. For $\rho = \sum_{i=1}^{L} m_i / L < 1$ there exists a stationary state which is an absorbing state i.e. a configuration that can be reached by the dynamics but cannot be left [**60**]. This absorbing state is defined by the following two properties. First due to the conservation of mass by the dynamics the sum of all masses in the absorbing state have to be equal to $M = \rho L$. Second a configuration $\{m_1, ..., m_L\}$ is an absorbing state if and only if, $m_i < 1$ for all sites i in the system.

As in [**61, 62**] the corresponding factorized steady state is described by an expression over the large deviations of a sum of random variables. Furthermore as we will see the introduction of a truncation effect does not lead to the loss of the additivity property and a Gamma-like distribution is restored for the single site mass distribution in the stationary case.

We start also by the assumption that the probability of observing a configuration of masses $\{m_i\}$ is given by

$$P(m_1, ..., m_L) = \frac{\prod_{k=1}^{L} f(m_k)}{Z_L(M)} \delta\left(\sum_{k=1}^{L} m_k - M\right) \Theta(1 - m_k) \tag{3.43}$$

where $Z_L(M)$ is just the normalization

$$Z_L(M) = \prod_{k=1}^{L} \int \mathrm{d}m_k \, f(m_k) \, \delta\left(\sum_{k=1}^{L} m_k - M\right) \Theta(1 - m_k). \tag{3.44}$$

We have to note here that $P(m_1, ..., m_L)$ is equivalent to the probability of picking L independent and identically distributed random variables (i.i.d.RVs) with a common probability density $f(m)$, conditioned on the fixed value of their total sum and the fact that each random variable has to be smaller than 1. In that context the partition function $Z_L(M)$ itself becomes a probability distribution for the sum of L independent and identically distributed random variables.

By using now this equation we can determine the stationary distribution of the system by calculating the Laplace transform of (3.44):

$$\int \mathrm{d}M\, Z_L\,(M)\, e^{-sM} = [g(s)]^L \tag{3.45}$$

where

$$g(s) = \int_0^1 \mathrm{d}m\, f(m) e^{-sm}. \tag{3.46}$$

We use here the approach described in detail in [**44, 45**] in order to derive the inverse of Eq. (3.45). We rely also on the Bromwich formula but in contrast to the case of $f(m) \sim m^{-\gamma}$ we do not have any singularities for finite values of s.

It is not hard to see that a saddle point approximation is applicable whereas the partition function takes the form

$$Z_L(M) \simeq \frac{\exp\left[Lh(s_0)\right]}{\sqrt{2\pi L h''(s_0)}}. \tag{3.47}$$

Substituting (3.47) in (3.44) we get $p(m) \simeq f(m)e^{-s_0 m}$, whereas the saddle point s_0 is determined by the minimum of the function $h(s) = \rho s + \ln g(s)$.

In order to proceed it is necessary for us to know the exact form of the weight functions $f(m)$. This would allow us to specify $g(s)$ and thus the saddle point in the equation above. We could see that for fraction densities of the form $\phi(\mu|m) = u(\mu)w(m-\mu)$ the weight functions can be easily determined. Unfortunately this is not the case here and we have to determine $f(m)$ exactly by analyzing the dynamics of the system. In the next section we will show how this can be done for the relatively broad class of the so-called "restricted" processes.

3.4. Restricted Processes

In the following we will consider processes for which the total transported mass per site and time-point is bounded from above, $\mu_{i,t} < 1$, $\forall i, t \in \mathbb{N}$. We use the terminology "restricted" for this large class of processes.

As in many non-equilibrium systems the exact calculation of the mass distribution during the relaxation process is a rather cumbersome and even impossible undertaking. But in the steady state this is rather easy if we consider that the absorbing state is achieved when all masses in our system are below 1. Up to this stationary limit we have a more or less constant inflow and outflow of masses at each site. These increments and decreases are hereby i.i.d. random variables given by the fraction density, $\phi(\mu|m)$. Let us now use the concept of stopping time which can be defined as the time at which a given stochastic process exhibits a certain behavior of interest. Here we define as stopping time τ_i for a site i the time

$$\tau_i = \inf\left\{t' \in \mathbb{N} : m_{i,t'} = m_{i,t} \quad \forall t > t'\right\}. \tag{3.48}$$

Furthermore let us define the overall stopping time

$$\tau = \max\{\tau_1, .., \tau_L\}. \tag{3.49}$$

From the definition of the stopping time τ it follows the mass at each single site in the stationary state is given by the following equation

$$m_{i,\tau} = m_{i,0} + \xi_i^+ - \xi_i^- < 1. \tag{3.50}$$

With $m_{i,0}$ being the initial mass at site i derived from the initial mass distribution. On the other hand, the terms ξ_i^+ and ξ_i^- describe the sum of increments and decreases.

These inflows and outflows are independent from each other and we use the white noise process ξ_n given by the probability density function $\varphi(\xi)$ for the representation:

$$\xi_i^+ = \sum_{n=1}^{\tau} \mu_{i-1,n} = \sum_{n=1}^{q_i} \xi_n \quad \text{and} \quad \xi_i^- = \sum_{n=1}^{\tau} \mu_{i,n} = \sum_{n=1}^{r_i} \xi_n. \tag{3.51}$$

We used the term q_i in order to describe the number of the increments during the evolution of the system and r_i for the number of decreases for the respective site i. This number differs greatly from site to site and we are in no position to derive these numbers here analytically. From the above expression it clearly follows that $q_i, r_i \leq \tau$ for all $i \in \{1, ..., L\}$.

In the following we omit the indices from τ_i, q_i, r_i since our arguments are independent from the respective site. This relies on the fact that the distribution of m_τ converges to a steady distribution for increasing values of q. One has to take into account that the random variable $m_0 + \xi^+$ is a Gaussian random variable for high values of q which becomes independent from the initial value. On the other hand, the number r is solely defined by the requirement $m_\tau < 1$.

In other words if we denote the distribution of the mass m_τ with q increments by $P_{m_\tau,q}(m)$ then there exists for each density function $\varphi(\xi)$ a natural number q^* so that

$$P_{m_\tau,q_1}(m) = P_{m_\tau,q_2}(m) \quad \forall q_1, q_2 > q^* \quad \text{and} \quad \forall m \in [0,1]. \tag{3.52}$$

This is to be expected since for increasing number of exchanges the information regarding the initial distribution gets lost and the final distribution is defined solely by the dynamics of the exchanges. This fact is shown by a numerical simulation in Figure 3.1.

Due to this property we can now determine the weight functions for a series of truncated processes. We need therefore only to consider the probability density function of the random variable m_τ, which is characterized by the following properties $m_\tau < 1$ and $m_\tau + \xi = m_{\tau-1}$ with $\xi \sim \varphi(\xi)$ and $m_{\tau-1} > 1$. So if we ask ourselves how probable the event $\{m_\tau = x\}$ is, we get the expression

$$\begin{aligned} &\mathbb{P}\left[m_\tau = x | m_\tau < 1, m_{\tau-1} > 1, m_\tau + \xi = m_{\tau-1}\right] = \\ &\quad \mathbb{P}\left[m_{\tau-1} - m_\tau = \xi > 1 - x\right] \propto \int_{1-x}^{1} \mathrm{d}\xi\, \varphi(\xi) \end{aligned} \tag{3.53}$$

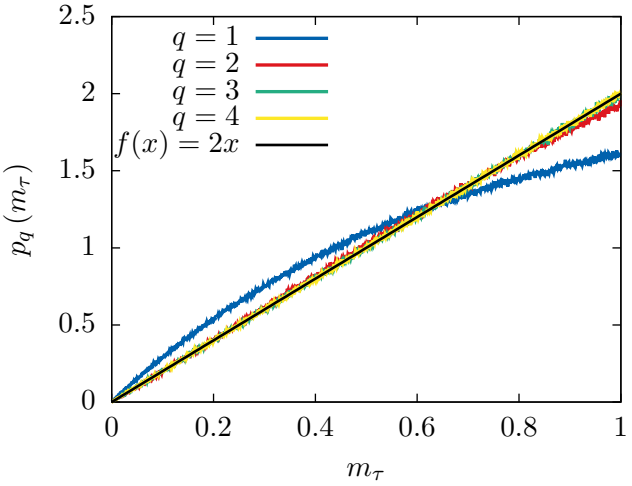

FIGURE 3.1. Numerical evaluation of the probability density function for a random process described by the equation (3.50) for different $q's$ and $\xi_i \sim \varphi(\xi)$ with $\varphi(\xi) = \Theta(1-\xi)$. As we can see for increasing values of q we have a convergence to the expected weight function.

Here we have used the fact that no information with regard to the value of $m_{\tau-1}$ except to $m_{\tau-1} \geq 1$ is necessary. In order to illustrate this fact we can consider the position of $m_{\tau-1}$ for which

$$\mathbb{P}\left[m_{\tau-1} = y\right] = \mathbb{P}\left[y - \xi < 1\right] \propto \int_{y-1}^{1} \mathrm{d}\xi\, \varphi(\xi) \tag{3.54}$$

holds. Now we can use a symmetry argument in order to determine the pdf of m_τ. We expect the measure to remain invariant under the transformation $y - 1 = 1 - x$, which leads us to Eq. (3.53).

Let us now characterize with $P_{m_\tau}(x)$ the probability density function of the random variable m_τ under the assumption that the number of increments is above q^* then

$$\mathbb{P}\left[m_\tau \in (x + \mathrm{d}x)\right] = P_{m_\tau}(x)\mathrm{d}x. \tag{3.55}$$

By taking into account the normalization

$$\int_0^1 \mathrm{d}x\, P_{m_\tau}(x) = 1 \tag{3.56}$$

we can easily see that when the number of increments per site exceeds the fraction density specific value of q^*, then the stationary state is described by the normalized weight function

$$P_{m_\tau}(m) = f(m) = \frac{\int_{1-m}^{1} \mathrm{d}x\, \varphi(x)}{\int_0^1 \mathrm{d}x \int_{1-x}^{1} \mathrm{d}y\, \varphi(y)}. \tag{3.57}$$

Now one can thus use these results in order to determine numerically the partition function for a set of random variables constrained from their fixed sum and independently distributed according to a large range of monotone increasing density functions $f(m)$ fulfilling the equations

$$\frac{df(m)}{dm} = -\varphi(1-m) \tag{3.58}$$

with $f(0) = 0$. On the other side one can invert these equations and determine analytically the stationary absorbing state for any given analytic fraction density $\phi(\mu|m)$.

Now let us return to the applicability of our results. The requirement described above with regard to the number of increments surely does not hold for all ranges of parameters ρ, L but as we will show shortly a sufficient condition for the existence of a unique stationary measure for this class of processes can be derived. In general we can say that as long as the condition

$$\int \mathrm{d}m\, m f(m) < \rho \tag{3.59}$$

is fulfilled, then a unique stationary measure described by Eq. (3.57) exists in the thermodynamic limit ($M, L \to \infty, \rho = M/L = \text{const.}$).

Let us start with our numerical observation (see Figure 3.2) that for increasing lengths for systems with $\rho > \int \mathrm{d}m\, m f(m)$ we can observe that the condition $q > q^*$ is fulfilled for all sites in the system. In order to understand this property we introduce the following algorithm. Instead of creating a system with L sites which are evolved by parallel dynamics we can just consider the system consisting by a collection of subsystems with increasing length $L_\nu = \nu$ where each of these subsystems is evolved by a sequential procedure.

Now at the beginning we create a subsystem of length ℓ where the mass distribution for each site is given by the function $f_0(m) = \rho^{-1} e^{-\rho^{-1} m}$. We evolve all sites of this subsystem according to the described dynamics (totally asymmetric with transport in the direction $i \to i+1$) while we forbid any kind of inflow to this subsystem. The mass that flows out of the system is characterized as the excess mass m_1^{exc} of this first update step. After all sites of the subsystem have frozen out ($m_n < 1, \forall n \in [1, \ell]$) we expand our subsystem to the size 2ℓ by adding ℓ sites to the right side of the old system. All new sites carry a mass distributed according to the function $f_0(m)$. Before we can start with the evolution of this new subsystem we have to add the excess mass of the previous update step to the first site of the new addition, $m_{\ell+1}$. We repeat this algorithm several times and analyze hereby the time series of m_ν^{exc} where ν corresponds to the number of updates. For simplicity we will set now $\ell = 1$.

The process of the excess mass is given by a random walk in a random environment for $m_n^{exc} < q^*$ while a positive drift is present for $m_n^{exc} > q^*$. This positive drift comes from the fact that after each time step and while $m_\nu^{exc} > q^*$ new masses are created through the update mechanism which

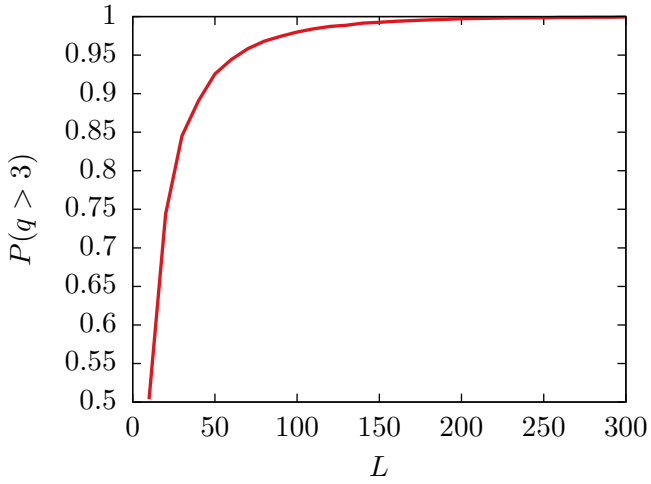

FIGURE 3.2. Rate of sites with more than three updates for the uniform density function $\varphi(\mu) = 1$ for a periodic boundary system with $\rho = 0.7$.

follow the probability density function $f(m)$. Correspondingly they have the mean value $\int \mathrm{d}m\, mf(m)$ whereas their previous mean value was equal to ρ. This leads to a mean increase of the excess mass after each time step

$$\langle m_{\nu+1}^{exc} - m_{\nu}^{exc} \rangle = \rho - \int \mathrm{d}m\, mf(m) \quad \text{for} \quad m_{\nu}^{exc} > q^*. \tag{3.60}$$

We see also that the condition $\int \mathrm{d}m\, mf(m) < \rho$ proves sufficient for us to have a system where for increasing lengths the number of increments rises to a satisfying level.

Due to the positive drift we can develop following hypothesis: let T_ν^* be the time of the last ruin [3]

$$T_\nu^* = \sup \{\nu^* \leq \nu : m_{\nu^*}^{exc} < q^*\} \tag{3.61}$$

then for all $q^* < \infty$ there exists a $\nu < \infty$ so that $m_\nu^{exc} > T_\nu^* + q^*$.

In order to prove this hypothesis we just need to show that the survival probability

$$\mathbb{P}\left[m_{T_\nu^*+1}^{exc} > q^*, m_{T_\nu^*+2}^{exc} > q^*, ..., m_{T_\nu^*+n}^{exc} > q^*\right] \tag{3.62}$$

[3]We adopt here the notation from the famous ruin problem in stochastic analysis. In the traditional ruin problem the term ruin was used in order to describe the event $S_n = 0$, where S_n is a symmetric random walk. Here we use it in order to characterize the event $m_{\nu^*}^{exc} < q^*$.

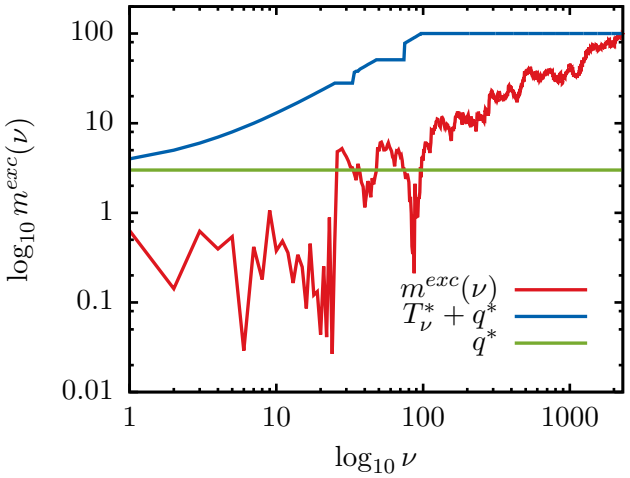

FIGURE 3.3. Single site excess mass (in logarithmic scale) as function of the number of the update steps (also in logarithmic scale) for the algorithm described in detail in the text. The presented results were derived for a system with $\varphi(\mu|m) = 1$ and $\rho = 0.7$.

for finite n is always bigger than zero. This is shown rather easily by using the fact that

$$\mathbb{P}\left[m^{exc}_{T^*_\nu+1} > q^*, m^{exc}_{T^*_\nu+2} > q^*, ..., m^{exc}_{T^*_\nu+n} > q^*\right] = \mathbb{P}\left[m^{exc}_{T^*_\nu+n} > q^* | m^{exc}_{T^*_\nu+n-1} > q^*\right] ... \mathbb{P}\left[m^{exc}_{T^*_\nu+2} > q^* | m^{exc}_{T^*_\nu+1} > q^*\right] \times \times \mathbb{P}\left[m^{exc}_{T^*_\nu+1} > q^*\right]. \tag{3.63}$$

Now due to the drift for processes with $m^{exc}_\nu > q^*$ we get for all $k \in \mathbb{N}$

$$\mathbb{P}\left[m^{exc}_k > q^* | m^{exc}_{k-1} > q^*\right] > \frac{1}{2}, \tag{3.64}$$

leading us to the result

$$\mathbb{P}\left[m^{exc}_{T^*_\nu+1} > q^*, m^{exc}_{T^*_\nu+2} > q^*, ..., m^{exc}_{T^*_\nu+n} > q^*\right] = \frac{\mathbb{P}\left[m^{exc}_{T^*_\nu+1} > q^*\right]}{2^{n-1}} \tag{3.65}$$

which is strictly positive for all finite values of $n \in \mathbb{N}$, since

$$\int_{q^*+1}^{\infty} \mathrm{d}m\, \rho^{-1} e^{-\rho^{-1} m} > 0 \Rightarrow \mathbb{P}\left[m^{exc}_{T^*_\nu+1} > q^*\right] > 0. \tag{3.66}$$

Now due to this fact we can claim that in a long series of renewal processes[4] there exists at least one which can survive for long enough times so that the law of large numbers applies. We characterize here such a process with $X_n = m^{exc}_{T^*_\nu+n}$, namely a process such that $X_k > q^*, \forall 1 \leq k \leq n$ with n sufficiently large. We know that for this process $\langle X_n \rangle = n\mu + q^*$ holds, whereas $\mu = \rho - \int \mathrm{d}m\, mf(m) > 0$.

Now according to the law of large numbers, if $\epsilon < \mu$ is fixed and η is an arbitrary small number then for n sufficiently large [**63**]

$$\mathbb{P}\left[\left|\frac{X_n}{n} - \mu\right| < \varepsilon, \left|\frac{X_{n+1}}{n+1} - \mu\right| < \varepsilon, ...\right] > 1 - \eta \Rightarrow$$

$$\mathbb{P}\left[X_n > n(\mu - \varepsilon), X_{n+1} > (n+1)(\mu - \varepsilon), ...\right] > 1 - \eta. \tag{3.67}$$

By choosing now a n big enough so that $n(\mu - \varepsilon) > q^*$ we can prove our hypothesis. Explicitly we have proven that if the mean step is positive, then after a sufficiently large number of steps the process will remain beyond any arbitrarily chosen point in the positive direction with probability as close to unity as we please. It is therefore given that the condition $m^{exc}_\nu > T^*_\nu + q^*$ can be satisfied in finite number of steps ν.

Before we continue we have to make following remarks. We did not make any statement about the behavior of the random walk in the range $[0, q^*]$. This proved to be unnecessary since the only relevant property of this random walk is the fact that a jump to values above q^* is always possible. We will return to this problem in the conclusion since it is closely related to the expansion of the present work for different initial conditions.

Now if the condition $m^{exc}_\nu > T^*_\nu + q^*$ is fulfilled then we can create a link between the last site of the system created by this algorithm and its first site system and gain a closed boundary system where all sites in the system will have more than q^* increments for each site. If the number of necessary steps ν is big enough then due to the law of large numbers we will get a system where the total mass in the system is really close to the expected value of ρL. But we can of course insert some more sites between the first and last one so that the total mass in the system will be exactly equal to ρL.

It is clear that, although the time scale of the proposed algorithm follows different rules than the one initially presented by us, the dynamics of the system were not changed so that the derived distribution of the expected increments as well as the stationary distribution is the same as the one derived by our traditional approach. We can claim that the steady state distribution is invariant under a change from parallel update rules to ordered sequential ones. This statement is strongly supported by numerical results. Although the presented algorithm does not lead to qualitatively new

[4] We consider each jump of the excess mass above the value of q^* as a renewal. The term refers to the fact that the process "starts afresh" after each jump above the value of q^* [**72**].

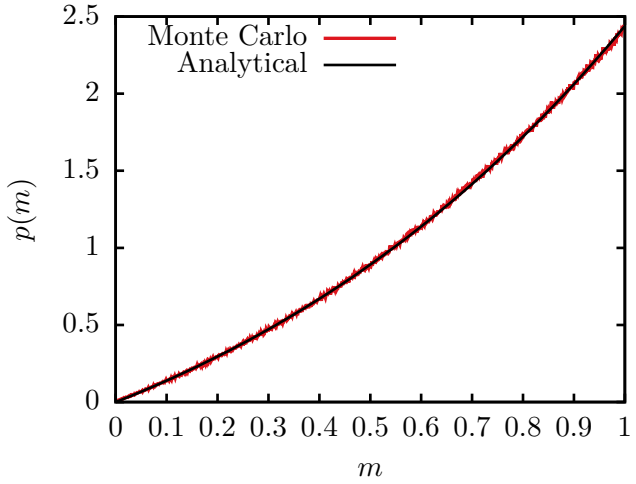

FIGURE 3.4. Single site mass distribution for a system with $L = 100, \rho = 0.7$ and a uniform distribution of the transported masses. The results of the Monte Carlo simulation rely on 10^6 realizations and each trial showed excellent agreement to our analytical result of $p(m) \simeq 1.3m \exp(0.627m)$.

results we thought that its introduction would be meaningful since it helps us illustrate why increasing lengths lead to the desired distribution

3.4.1. Examples. In this subsection we will consider the specific case of three different probability density functions φ and calculate analytically as well as numerically the stationary single site mass distribution.

Uniform distribution. At first we consider the fraction density

$$\phi(\mu|m) = \begin{cases} \Theta(1-\mu) & \text{if } m \geq 1 \\ \delta(\mu) & \text{if } m < 1. \end{cases} \tag{3.68}$$

So we have the case of a uniform probability density function of the random variables μ in the interval $[0, 1]$. For this function we will get the normalized weight function

$$f(m) = 2m. \tag{3.69}$$

In general for systems with $f(m) = m^\delta$ we have to study densities in the range of

$$\frac{\int \mathrm{d}m\, m f(m)}{\int \mathrm{d}m\, f(m)} = \frac{\delta+1}{\delta+2} < \rho < 1. \tag{3.70}$$

For $f(m) = 2m$ we have correspondingly $\rho_c = \frac{2}{3}$. By knowing now the exact weight function we can return to the method described above and use the Laplace transform of the norm $Z(\rho, L)$ as well as the inversion of the Bromwich formula to derive the formula $p(m) = f(m)e^{-s_0 m}$ whereas the

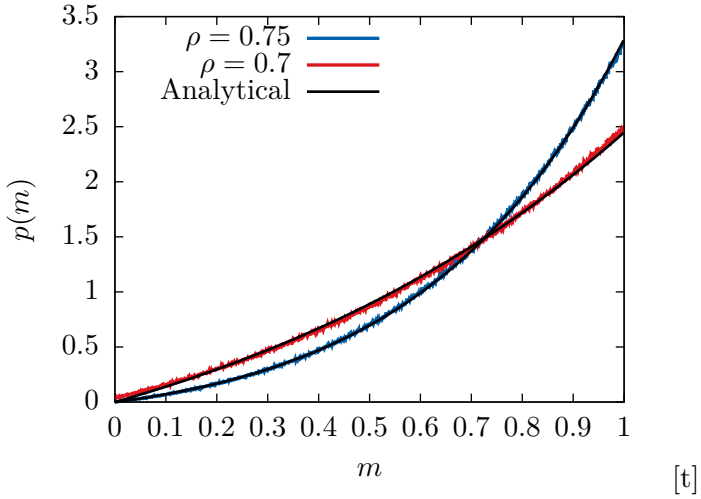

FIGURE 3.5. Analytical and numerical description of the single site mass distribution for a system with $L = 100$. The fraction density is given by $\varphi(\mu) = \exp(-\mu)$ and we consider two different densities. For the derived weight function we have a critical density of $\rho_c = 0.6961$. As we can see the described analytical method shows an excellent agreement to the Monte Carlo simulation for values of ρ well above the critical regime, while a deviation can be observed for $\rho = 0.7$. We considered in both cases 10^6 realizations.

exponent s_0 is determined by the minimum of the function

$$h(s) = \rho s - 2\ln s + \ln(1 - e^{-s} + se^{-s}). \tag{3.71}$$

Our analytical results have an excellent agreement to the numerical results as shown in Figure 3.4.

Exponential distribution. In the following we will present the results of our calculation for the special case of

$$\varphi(\mu) = \frac{e^{-\mu}}{1 - e^{-1}}. \tag{3.72}$$

By using the Formula (3.57) one can easily see that

$$f(m) = \frac{e^{m-1} - e^{-1}}{1 - 2e^{-1}}. \tag{3.73}$$

We make now again a saddle point approximation $p(m) = f(m)e^{-s_0 m}$ where the saddle point is here determined for two different densities

$$s_0 = \begin{cases} -0.076282 & \text{for } \rho = 0.7 \\ -1.15892 & \text{for } \rho = 0.75. \end{cases} \tag{3.74}$$

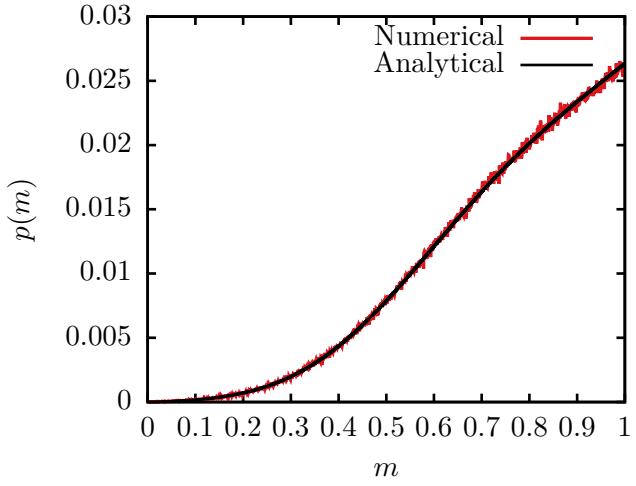

FIGURE 3.6. Single site mass distribution for the Gaussian-like probability density functions. The numerical results were derived by a Monte Carlo simulation over 10^4 samples where the dynamics of periodic systems with $L = 100$ were simulated. We have chosen here to set $\sigma = 0.2$ and $\rho = 0.75$. For these parameters we have the critical value $\rho_c = 0.73$ and $s_0 = -1.3$.

In Figure 3.5 one can see that our derived results show a relatively good agreement to the numerical results. The small discrepancies observed for values of ρ close to the critical density disappear for increased lengths.

Normal distribution. We consider now the case where the transported mass is given by a Gaussian function

$$g(x) = \frac{1}{\sigma\sqrt{2\pi}} e^{-\frac{(x-0.5)^2}{2\sigma^2}}. \tag{3.75}$$

Due to the condition $0 < \mu < 1$ we have the actual density function

$$\varphi(\mu) = \frac{e^{-\frac{(\mu-0.5)^2}{2\sigma^2}}}{\int_0^1 \mathrm{d}\mu\, e^{-\frac{(\mu-0.5)^2}{2\sigma^2}}}. \tag{3.76}$$

We can calculate the weight function as described above

$$f(m) = \frac{\operatorname{erf}\left(\frac{0.5}{\sqrt{2\pi\sigma^2}}\right) - \operatorname{erf}\left(\frac{0.5-\mu}{\sqrt{2\pi\sigma^2}}\right)}{\operatorname{erf}\left(\frac{0.5}{\sqrt{2\pi\sigma^2}}\right) - \int \mathrm{d}\mu \operatorname{erf}\left(\frac{0.5-\mu}{\sqrt{2\pi\sigma^2}}\right)}. \tag{3.77}$$

One can see that this complicated expression provides indeed the expected distribution by comparing it to a numerical simulation as we did in Figure 3.6. We see also that our method delivers good results for a variety of density functions $\varphi(\mu)$.

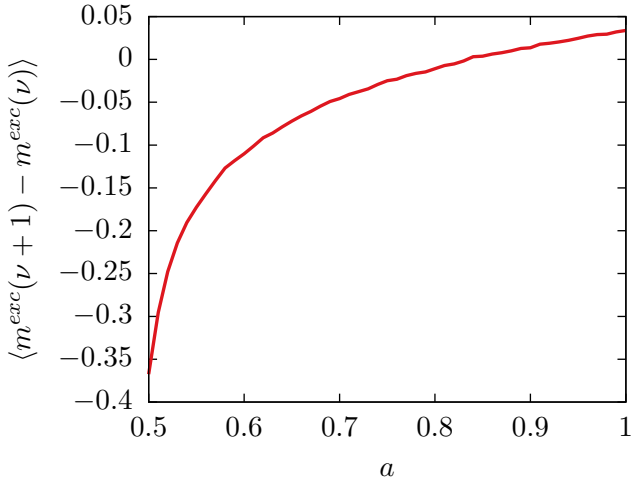

FIGURE 3.7. The mean increment of the excess mass for a system with a uniform distribution $\varphi(\mu) = 1$ and $\rho = 0.7$. We can see that for decreasing asymmetry coefficients the mean value decreases to the point where the increament is negative. This means that for specific values of ρ and a no unique stationary value for the single site distribution can be achieved even if we choose to set $L \to \infty$.

3.5. Partial Asymmetric Case

In the last section we have analyzed the single site mass distribution of the steady state only for totally asymmetric dynamics. Here we would like to test if our results can be expanded for the case of partially asymmetric processes. In the following we consider also processes which in general can be described by the equation

$$m_{i,t+1} = m_{i,t} - \alpha_{i,t}\mu_{i,t} + \alpha_{i-1,t}\mu_{i-1,t}. \tag{3.78}$$

Where $\alpha_{i,t}$ is a white noise process described by the following probability density function

$$f(x) = a\delta(x-1) + (1-a)\delta(x). \tag{3.79}$$

This process is especially interesting since it cannot be analyzed by a mean-field approach as shown in [**17**].

We have studied numerically several such processes with a variety of parameters a. In general we could see that a sufficient number of update steps could not be achieved. In order to study this behavior we decided to use a variation of the excess mass algorithm as it was presented in the previous Section **3.4** where we take into account the effect of the asymmetry coefficient a.

We create again a subsystem of size $\ell = 3$ which is then evolved until $m_i < 1$ for all $i \in \mathbb{N}$ with $i \leq \ell$ is fulfilled. After this step we create either

one or two new sites. The difference to the previous approach is namely that although we always add a new site to the right side of the old system this adding process may also take place to the left side. A necessary condition herefore is that the site which is further to the left carries a mass that is bigger than the cutoff value of 1. Again the excess mass is gathered on either side and then added to the new sites of the system which initially carries a mass defined by the initial probability density function $f_0(m)$.

By evaluating this algorithm numerically we can see that the mean increment of the excess mass per step of the algorithm may become negative when a is sufficiently small. We show in Figure 3.7 how this mean value changes as function of the different asymmetry coefficients for a system with a uniform probability density function.

If we have $\rho = 0.7$ then we can see a change in the sign for $a = 0.83$. The expected minimum of the mean increase of the excess mass is of course expected when $a \to 0.5$.

In general we can also say that for a range of asymmetry coefficients we are not in the position to arrive at a unique stationary state if we choose to send L to ∞. We could also see that there exists a critical asymmetry coefficient for which a unique stationary state cannot be found. Depending on the dynamics on the system as well as the density we have different dependencies of the value $\langle m_\nu^{exc} - m_{\nu-1}^{exc} \rangle$ as function of the asymmetry coefficient. We are also in no position to give a general function. Nevertheless it is possbile calculate the specific curve for each given set of parameters.

The unique stationary state calculated for systems with $a > a_c(\rho, \varphi)$ and $\rho > \rho_c$ is of course independent of the asymmetry coefficient and the results of the last section still hold.

3.6. Unbounded Transport

In the past sections we have shown explicitly how to create a set of independent random variables fulfilling several constraints. We have implemented several restrictions on the transported masses leading to random variables which were bounded from above as well as from below. This of course had the consequence of monotonically increasing weight functions with $f(0) = 0$.

Now we can ask if analytical results can be derived if we overcome this restrictions. In general this is not the case but there exist such examples and we think that it is interesting to discuss at least one.

In the following we consider the uniform distribution presented above where the truncation effect is lifted:

$$\phi(\mu|m) = \begin{cases} \delta(\mu) & \text{if } m < 1 \\ m^{-1} & \text{if } m \geq 1. \end{cases} \tag{3.80}$$

Explicitly we consider here the case where $m > \mu > 1$ is allowed.

We expect for this process the weight function $f(m) = 1$. This result may seem trivial but is explained in detail in the following. Let us return

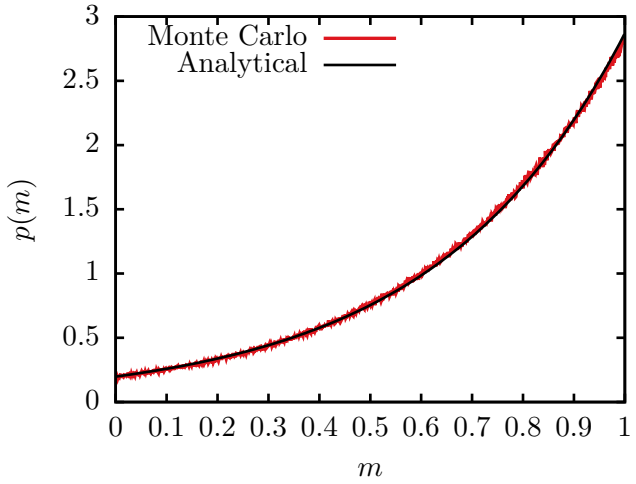

FIGURE 3.8. Single site mass distribution for a system with $L = 50$ and $\rho = 0.7$. The results of Monte Carlo simulation rely on 10^6 realizations and show excellent agreement to our analytical result of $p(m) \simeq 0.2 \exp(2.647m)$.

to the time series described by Equation (3.50) and consider the transition probability, $g(x, t; x_0; t-1)$, describing the likelihood of the crossover from state $(x_0, t-1)$ to the state (x, t). Then we know from our fraction density that $g(x_1, \tau; x_0, \tau - 1) = g(x_2, \tau; x_0, \tau - 1)$ for all $x_1, x_2 < x_0$. Correspondingly it follows that $p(m_\tau) = 1$ for all $0 \leq m_\tau \leq 1$ and hence we get the weight function $f(m) = 1$. Based on this result we can calculate the single site mass distribution for a large range of densities. As we can see from Figure 3.8 we have an excellent agreement with the Monte Carlo simulation leading us to the conclusion that the canonical ensemble approach still holds even for this class of processes.

For the total asymmetric process we get very good results which could even be improved by considering larger systems increasing good results for higher lengths. We can see that in this case a good agreement with the numerical simulations can be gained also for systems with a length $L = 50$. This is not surprising since a sufficient condition for getting this weight function lies just in a single jump of the single-site mass to values above 1, or equivalently $q^* = 1$.

For this generalized case we also investigated the partial symmetric dynamics by means of Monte-Carlo simulation. We could see that for such systems our analytical approach is still useful for a relatively wide range of values of a. Of course this range also depends on the density. So one can see that for $\rho = 0.7$ our approach fails for $a < 0.57$ while the threshold of $a \sim 0.96$ is at hand when considering the density $\rho = 0.51$. Unfortunately we are not in the position to provide a generalized approach for this class

of processes. The algorithm described by us in a previous section 3.3 can also not be applied here since a change from parallel to ordered sequential update rules would lead to a different steady state.

3.7. Discussion and Conclusions

We have analyzed the partition function for a set of i.i.d. random variables where next to the constraint fixing their total sum another one determining the threshold of largest value was implied. We could see that the sought configuration could be easily realized as the absorbing state of a truncated stochastic mass transport model, allowing us to determine the single site mass distribution for several fraction densities by a canonical ensemble approach. This result shows that a factorizable steady state is possible even if the dynamics of the system is state-dependent. Furthermore we determined the conditions under which our approach becomes exact in the thermodynamic limit. Next to the exactness of our approach in the thermodynamic limit we could also show that the method can be useful when studying finite size systems. We have initially studied a system with total asymmetry but through numerical simulations we could show that our results are suited for a wide range of partially asymmetric processes. In the last section we could see that our method is applicable even in the case of a generalized version where no constraints on the transported mass were implied.

We treated here the problem of state-dependent fraction densities only for the case of $\rho < 1$. For higher densities ($\rho > 1$) we expect that a non-equilibrium steady state exists. The analysis of such system proved rather difficult but has shown some very interesting characteristics, like the condensation of masses with $m > 1$ around a single non-stationary site. We think that the present work will help us understand the different features of these complicated systems. An interesting Ansatz lies in the possibility of separating the system in two subsystems, one where masses are in a frozen state and one where an active exchange takes place. The work of Bertin *et al.* [**70**] has shown that a factorization for both subsystems and the conservation of the total mass make the existence of an associated intensive thermodynamic parameter possible. The definition of such an intensive parameter would greatly improve our understanding of stochastic mass transport models in general.

The presented good agreement between analytical and numerical results raises the question with regard to the expansion of the present method for a larger range of densities. We have to note that the implied restrictions on the fraction density distributions are not intuitive and our goal should be to expand our model to a larger class of weight functions. The results of the last section prove hereby that an expansion of the presented method to processes with weight functions that are not strictly increasing can be fruitful.

Another interesting question that arose during this work and has been gathered attention in the past years is related to the relation of mass transport to the linear statistics of sums of i.i.d random variables. As mentioned in the introduction partition functions with similar constraints have been analyzed in the past [**61, 62**]. We hope that the presented results prove the efficacy of large deviation theory and will serve as inspiration for further studies in this interesting field.

Lastly we have to note that it is possible to apply the presented methods to systems with initial distributions that are not exponential. Based on the results of our excess mass algorithm we tend to believe that for each initial distribution function which is heavy tailed the unique stationary state will be achieved. This raises naturally the question with regard to the existence and uniqueness of the absorbing state for initial distributions which are light tailed.

CHAPTER 4

Diffusion with Resetting in Bounded Domains

4.1. Introduction

In this and the next chapter we focus on the properties of stochastic search processes [**94**]. In the last years an increasing number of works concerned with the efficiency of stochastic search models has been published. The general interest in problems of this kind is explained by the fact that they find applications in a wide range of fields such as chemical or biochemical reactions [**73, 74, 75**], cell biology [**76**], zoology [**77**], risk management [**108**] up to astrophysics [**78**].

Usually stochastic search models are described in terms of a first passage problem [**94**]. In these problems we ask ourselves when did a specific event took place for the first time. Let us imagine therefore that we have a stochastic process X_t that can assume a specific value x_A, then the first passage time (FPT) is the time-point at which the event $\{X_t = x_A\}$ occurred for the first time.

When we define a stochastic search model we often use the term 'searcher' in order to describe the process X_t. In the following we will often use the specific term Brownian searcher which describes in this chapter a simple one-dimensional Brownian motion. On the other hand the term 'target' is used in order to describe the value x_A. We consider also here the case of a stationary target.

The event $\{X_t = x_A\}$ is considered as a necessary condition for the absorption of the searcher. This absorption is usually presented as the annihilation of the searcher and leads to the termination of the search process. The mean time to absorption (MTA) corresponds to the average of this termination time over many trials.

If the first passage time is equal to the termination time for all trials then we have perfect absorption. In this case the event $\{X_t = x_A\}$ is not only a necessary but also a sufficient condition for the absorption of the searcher. This corresponds to the assumption that a first meeting between target and searcher must have an intermediate effect on the studied system. Realistic examples for such situations from neural and financial sciences respectively are the firing of a neuron when a voltage fluctuation is high enough and the execution of buy/sell order when a certain stock price reaches a specific value.

On the other side for certain experimental applications this assumption is rarely true, e.g. two ions in a chemical solution do not necessarily recombine when they encounter [**131, 91**]. This fact makes the introduction of the concept of the partial absorption process, where the time to absorption does not correspond to the first passage time, necessary. In this chapter we will focus on the solution of a master equation describing the time evolution of a partial absorption diffusion process under the effect of a resetting potential [**115**].

4.1.1. Background and Motivation. The term reset describes in general the restart of an ongoing process. In physics literature resetting and especially stochastic processes with resetting have been investigated recently. One the first scientific works on this topic is the paper by Manrubia and Zanette [**111**] that analyzes a stochastic multiplicative process with reset events. A similar model was analyzed 14 years later by Montero and Villarroel [**112**], who derived the stationary distribution and exit time of a continuous time random walk with reset.

The work of Evans and Majumdar who first discussed the case of a one-dimensional Brownian motion modified by a resetting mechanism [**113**] has a great impact on this field. Inspiration for this process was the fact that many searches in real-life situations are interrupted by resettings, as example searching for the car keys while often returning to the point where one remembers last seeing them. This situation is easily modeled by considering a perfectly absorbing target at the origin that is searched by an one-dimensional Brownian particle. The evolution of the process is then interrupted by resetting events forcing the particle back to its initial position.

The mean first passage time, T, becomes a function of the resetting rate r. If the process has the diffusion constant D and starts from the initial position $X_0 = x$, then the first passage time for the event $\{X_t = 0\}$ is given in this case by the formula

$$T(x) = \frac{1}{r}\left(\exp\left(\sqrt{\frac{r}{D}}x\right) - 1\right). \tag{4.1}$$

By performing a Taylor expansion we can easily see that $T \sim r^{-1/2}$ holds in the limit $r \to 0$. Consequently, we recover the well-known result that the mean first passage time for a diffusive particle in a semi-infinite interval is infinite [**94**]. Also T diverges for $r \to \infty$ since in this limiting case a diffusion of the particle away from its initial position becomes impossible and the particle appears to be trapped at the initial position. The divergence of T in both limits $r \to 0$ and $r \to \infty$ is an indication for the existence of a minimum for T with respect to r in the interval $r \in (0, \infty)$. In [**113**] the existence of such a positive optimal resetting rate was shown and furthermore its exact value for a diffusion in the semi-infinite interval was calculated.

This model of Majumdar and Evans has shown the possible beneficial effect of a resetting mechanism on the distribution of search times and thus

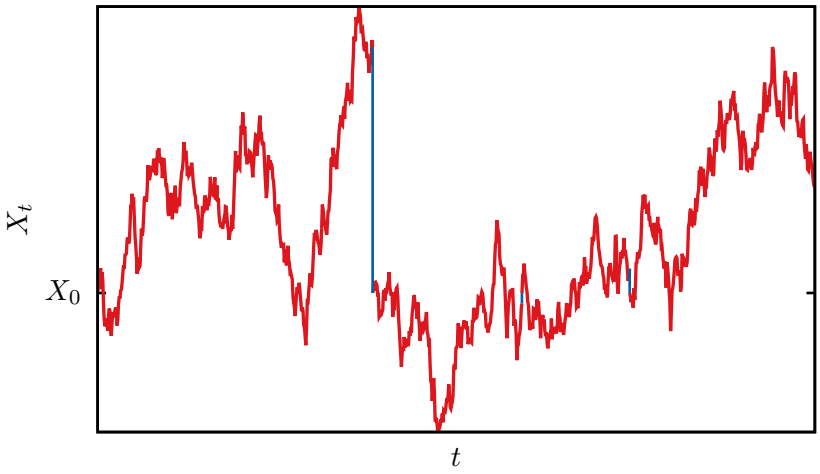

FIGURE 4.1. Characteristic path of a diffusion process X_t with resetting. The red lines correspond to the path of the stochastic process while the blue lines indicate the jumps performed due to the resetting to the initial position X_0.

triggered the study of the dynamics of similar processes. A first generalization of this problem was provided in terms of space-depending resetting rates in [**114**]. In the same work also different conditions with regard to the position at which resetting may take place and with regard to the position of the searcher after the resetting have been considered. An expansion of the presented formalism for higher dimensional cases is also possible and was provided in a later work [**79**].

In the last years one can observe an ongoing interest in stochastic processes with resetting [**138, 139, 140, 126, 127**]. This interest is on the one hand explained by their importance in computer science and network theory where resetting proves to be a useful strategy when trying to optimize search algorithms in combinatorial problems [**80, 82, 81, 83**]. On the other hand, processes with random resettings do not only find application in artificial systems but also in various natural systems. For example foraging animals improve their search strategy by returning to previously visited sites [**119**]. Another important aspect is the fact that diffusion with resetting has similar features to intermittent search processes that are very important in the description of biochemical reactions in microbiological systems [**109, 85, 86, 87**].

Another interesting feature of stochastic processes with resetting is the nature of their stationary states. The implementation of a resetting mechanism leads to non-vanishing probability currents and hence allows the study of interesting non-equilibrium steady states [**132, 133**]. In the work of Pal *et. al.* [**117**] the non-equilibrium steady state of a diffusion inside a potential

landscape was analyzed. Other examples of stochastic processes with interesting stationary states are the surface growth process described by a KPZ equation with resetting which shows non-Gaussian interface fluctuations in the stationary limit [**121, 124**] and the coagulation-diffusion process with a stochastic reset [**88**]. Here, we will derive the stationary distribution of a diffusion process taking place in one-dimension with reflecting boundary conditions.

Our main goal in this chapter is to reevaluate the importance of resetting for a process that takes place in a bounded domain. One has to consider hereby that boundary conditions have a great and mostly erratic influence on the search properties of realistic stochastic processes [**90**]. As example the expression $\lim_{r\to 0} T = \infty$, presented above for a diffusive search process in a semi-infinite interval, does in general not hold for a stochastic process evolving in a bounded domain. This leads us to question the existence of an optimal resetting rate for this kind of processes.

This chapter has following structure: In section 4.2 we describe the main characteristics of our model and show how the forward equation for diffusion processes with resetting and partial absorption can be formulated. We proceed by calculating the stationary solution of the derived differential equation (section 4.3). The targeting properties of our model will be discussed in section 4.4. This will be done by determining the survival probability of a single random walker. Several special cases with regard to the resetting and absorbing potential are discussed in detail. One of these special cases can also be evaluated in terms of a Monte Carlo simulation. This circumstance also allows us to test the validity of our analytical findings. Some concluding remarks are reserved for the final section.

4.2. Model

We start our analysis by showing a way to derive the master equation for a diffusion process with resetting in a bounded domain. Alternative strategies that do not follow this approach and do not require the derivation of a differential equation can also be successful and have been used in the past [**112**]. This alternative way of proceeding may be easy but it is not promising for the general problems with of space-dependent resetting rates. In this case the determination of the resetting event dispersion has to be undertaken and this is a rather difficult undertaking. Furthermore the master equation approach is suited for a wide class of random walks with resetting.

In this section we focus on a random walk taking place in a one-dimensional domain with two reflecting walls. A resetting event can be represented mathematically in terms of 'gain' and 'sink' potentials in the master equation. These 'gain' and 'sink' terms describe the disppearance and simultaneous reappearance of the random walker in different regions of the system. We characterize in the following these potentials by the probability density functions $p_S(x)$ and $p_G(x)$, respectively. The complete disappearance of random

walkers from the system due to the partial absorption is described by the function $p_A(x)$.

The probability distribution function of a random walker starting from the position y is characterized by $\psi(x, y; t)$[1]. We can derive a differential equation that describes the time evolution of this propagator $\psi(x, y; t)$ as follows. We consider an ensemble consisting of several diffusing particles. The pdf $\psi(x, y; t)$ corresponds to the concentration function of the set of particles. The derivation of the differential equation describing the evolution for this concentration function starts by regarding the transition probability at a time $t + \Delta t$, with Δt being a small interval of time, as a function of the transition probability at the time t. This can be done by dividing the time interval $[t, t + \Delta t]$ into two intervals: $[t, t + t']$ and $[t + t', t + \Delta t]$, with $0 \leq t' \leq \Delta t$. Three possibilities exist now in this first interval:

1: the particle gets resetted to a new position which will then be the starting position for a diffusive motion in the subsequent interval $[t + t', t + \Delta t]$,
2: the particle gets absorbed,
3: no resetting or absorbing takes place and the particle diffuses to a new position.

The probability of the occurrence of one of these events depends on the time that has elapsed. On the other hand the path of the diffusive walker in correlation to the spatial form of the resetting and absorbing field described correspondingly by the functions $p_S(x), p_A(x) \in \mathcal{L}^1(\mathbb{R})$ must also be taken into account. In case of a resetting event a new position is derived from the probability distribution function $p_G(x)$ and a diffusion starting from that position takes place. This ensuing stochastic exploration is performed in the remaining time interval $\Delta t - t'$. The probability of a jump with length ξ in the time interval $(\Delta t - t')$ is given by the Gaussian law

$$p(\xi, \Delta t - t') = (4\pi D(\Delta t - t'))^{-1/2} \exp\left[-\frac{\xi^2}{4D(\Delta t - t')}\right]. \tag{4.2}$$

The resetting procedure is described by the following two terms

$$-\int_0^{\Delta t} \mathrm{d}t'\, p_S(x')\, \psi(x', x_0; t + t') \tag{4.3}$$

[1]The term $\psi(x, y; t)$ is equal to the term $P(x, t|y, t_0)$ used in chapter 2. The probability to find the diffusive particle at the position x at the time-point t if it was at the time-point t_0 at the position x_0 depends only on the time-difference $t - t_0$. We can also for convenience replace the term $P(x, t|y, t_0)$ by the term $\psi(x, y; t - t_0)$. In the following we set $t_0 = 0$ and hence we use the function $\psi(x, y; t)$ in order to describe the probability distribution function of the position of the particle.

and

$$\int_0^{\Delta t} \mathrm{d}t'\, p_G(x) p(\xi, \Delta t - t') \int \mathrm{d}x'\, p_S(x') \psi(x', x_0; t + t')\,. \tag{4.4}$$

The first term describes the disappearance of a particle due to resetting at a certain position drawn from the pdf $p_S(x)$ and the second one the reappearance of the same particle at a position drawn from the pdf $p_G(x)$ together with the subsequent diffusion from that position.

Lastly we need to take the possibility of an absorption of the particle into account. This event can only take place in domains of $[0, L]$ for which $p_A(x) > 0$ holds. Through this absorption mechanism a reduction of the number of particles takes place. The difference in the number of particles in the time interval $[t, t + \Delta t]$ at a specific point x' in the system due to absorption is given by the formula

$$-\int_0^{\Delta t} \mathrm{d}t'\, p_A(x') \psi(x', x_0; t + t')\,. \tag{4.5}$$

The resemblance between Eq. (4.3) and Eq. (4.5) is obvious.

The third case is the complementary event of the two other events and described by a simple diffusion process. All walkers who do not get resetted or annihilated perform a Brownian motion described by

$$\int \mathrm{d}\xi\, p(\xi, \Delta t) \psi(x, x_0; t). \tag{4.6}$$

By combining all these terms we get

$$\begin{aligned}
\psi(x, x_0; t + \Delta t) = &\int \mathrm{d}\xi\, p(\xi, \Delta t) \psi(x - \xi, x_0; t) + \\
&+ \int_0^{\Delta t} \mathrm{d}t' \int \mathrm{d}\xi\, p(\xi, \Delta t - t') p_G(x - \xi) \int \mathrm{d}x'\, p_s(x') \psi(x', x_0; t + t') - \\
&- \int_0^{\Delta t} \mathrm{d}t' \int \mathrm{d}\xi\, p(\xi, \Delta t - t') p_S(x - \xi) \psi(x - \xi, x_0; t + t') - \\
&- \int_0^{\Delta t} \mathrm{d}t' \int \mathrm{d}\xi\, p(\xi, \Delta t - t') p_A(x - \xi) \psi(x - \xi, x_0; t + t')
\end{aligned} \tag{4.7}$$

Now we consider the limit

$$\lim_{\Delta t \to 0} \frac{\psi(x, x_0; t + \Delta t) - \psi(x, x_0; t)}{\Delta t} \tag{4.8}$$

while taking into account the approximation

$$\int \mathrm{d}t f(t) \approx f(\Delta t)\, \Delta t \tag{4.9}$$

for small time intervals Δt. This way we can derive the differential equation

$$\frac{\partial\psi(x,x_0;t)}{\partial t} = D\frac{\partial^2\psi(x,x_0;t)}{\partial x^2} + p_G(x)\int \mathrm{d}x'\, p_S(x')\psi(x',x_0;t) \\ -p_S(x)\psi(x,x_0;t) - p_A(x)\psi(x,x_0;t). \tag{4.10}$$

In the derivation of Eq. (4.10) we ignored the possibility of a second resetting or the case in which the particle gets absorbed after being reset. These terms are of the order $\mathcal{O}(\Delta t^{1+\varepsilon})$ and in the continuum time limit negligible.

We have chosen here to consider the simple case where the functions p_A, p_G and p_S are time-independent. Of course one could also consider time-dependent functions as shown in [**129**]. The complicated nature of the present model forced us to restrict ourselves to the time-independent case.

The reflecting boundary condition can be expressed with the additional equation

$$\left.\frac{\partial\psi(x,x_0;t)}{\partial x}\right|_{0,L} = 0\,. \tag{4.11}$$

For the special case of a constant resetting field with reset to a specific point and a pointlike target ($p_S(x) = r$, $p_G(x) = \delta(x - x_r)$ and $p_A(x) = \alpha\delta(x - x_B)$) we obtain the equation

$$\frac{\partial\psi(x,x_0;t)}{\partial t} = D\frac{\partial^2\psi(x,x_0;t)}{\partial x^2} + r\delta(x-x_r)\int \mathrm{d}x'\,\psi(x',x_0;t) - \\ - r\psi(x,x_0;t) - \alpha\delta(x-x_B)\psi(x,x_0;t). \tag{4.12}$$

The relations

$$\int \mathrm{d}x'\,\psi(x',x_0;t) = 1$$

and

$$\delta(x-x_B)\psi(x,x_0;t) = \delta(x-x_B)\psi(x_B,x_0;t) \quad \textit{almost surely}$$

lead us to an expression which is the same as Eq. (1) in [**89**]. The terms r and α label the resetting and absorbing rate respectively. They define the probability of absorbing or resetting in an infinitesimal time interval dt which is equal to αdt and rdt respectively. Lastly one should note that Eq. (4.12) could be written alternatively as

$$\left(\frac{\partial}{\partial t} - D\frac{\partial^2}{\partial x^2} + V(x)\right)\psi(x,x_0;t) = r\delta(x-x_r) \tag{4.13}$$

with

$$V(x) = r + \alpha\delta(x-x_B). \tag{4.14}$$

This Schrödinger operator representation can be extremly useful when dealing with general resetting functions [**98**].

4.3. Stationary solution

In this section we will determine the stationary distribution for the diffusion process described by the forward Eq. (4.12) with $\alpha = 0$.

The stationary solution ϕ for this process fulfills the equation

$$\frac{\partial}{\partial t}\phi(x, x_0; t) = 0\,. \tag{4.15}$$

The described diffusion process is ergodic for $r < \infty$. Hence the stationary solution is independent of the initial position x_0. Since the stationary solution is by definition time-independent we use the notation $\phi(x)$. In order to calculate its exact form we start from

$$D\frac{\partial^2}{\partial x^2}\phi(x) - r\phi(x) + r\delta(x - x_r) = 0. \tag{4.16}$$

We follow here the steps presented in [**92**] and represent the eigenfunctions of the operator

$$D\frac{\partial^2}{\partial x^2} - r + r\mathcal{I}_{x_r} \tag{4.17}$$

in terms of the eigenfunctions, $\phi_n(x)$, of the Laplace operator $\partial^2/\partial x^2$. $\mathcal{I}_{x_r}$ is used hereby as the short form of the integral transform

$$\mathcal{I}_{x_r}[\psi](x) = \delta(x - x_r)\int_0^L \mathrm{d}x\,\phi(x) = \delta(x - x_r). \tag{4.18}$$

The Laplace operator in a square well potential with reflecting boundary conditions

$$\phi'(0) = \phi'(L) = 0 \tag{4.19}$$

has eigenvalues $n\pi/L$ for the eigenfunctions

$$\phi_n(x) = \sqrt{2/L}\cos(n\pi x/L), \quad \forall n \in \mathbb{N}^+ \tag{4.20}$$

respectively. We assume now that the stationary solution has a representation of the form

$$\phi(x) = \phi_0 + \sum_{n=1}^{\infty} a_n\phi_n(x). \tag{4.21}$$

The first term on the right hand side of equation (4.21) is given by the probability conservation law

$$\int_0^L \mathrm{d}x\,\phi(x) = \int_0^L \mathrm{d}x\,\phi_0(x) + \sum_{n=1}^{\infty} a_n\int_0^L \mathrm{d}x\,\phi_n(x) = 1 \tag{4.22}$$

leading due to Eq. (4.20) to

$$\phi_0(x) = \frac{1}{L} \quad \forall x \in [0, L]. \tag{4.23}$$

It is obvious from our choice of the orthonormal basis that

$$\frac{\partial^2 \phi_n(x)}{\partial x^2} = \varepsilon_n \phi_n(x) \tag{4.24}$$

with

$$\varepsilon_n = -\frac{n^2 \pi^2}{L^2}\,. \tag{4.25}$$

We can generalize now the presented approach by assuming that there exist N different resetting positions, $\{x_{r_1}, x_{r_2}, ..., x_{r_N}\}$. In this case Eq. (4.16) takes the form

$$D\frac{\partial^2 \phi(x)}{\partial x^2} = r\phi(x) - \frac{r}{N}\sum_{d=1}^{N} \mathcal{I}_{x_{r_d}} \phi(x). \tag{4.26}$$

The combination of (4.24) with (4.26) delivers the equation

$$D\sum_{n=1}^{\infty} a_n \varepsilon_n \phi_n(x) = r\phi(x) - \frac{r}{N}\sum_{d=1}^{N} \delta(x - x_{r_d})\,. \tag{4.27}$$

The prefactors a_n are easily derived by multiplication with the orthonormal vector (in $\mathcal{L}^2$) $\sqrt{2/L}\cos(k\pi x/L)$ and integration over the interval $[0, L]$

$$a_k = \frac{r/N}{r - D\varepsilon_k}\sum_{d=1}^{N} \cos(k\pi x_{r_d}/L)\,. \tag{4.28}$$

Reinserting this formula in (4.21) we get

$$\phi(x) = \phi_0(x) + \sum_{n=1}^{\infty} \frac{2r}{NL(r - D\varepsilon_n)} \cos(n\pi x/L) \sum_{d=1}^{N} \cos(n\pi x_{r_d}/L)\,. \tag{4.29}$$

This formula shows that the stationary solution is continuous in the interval $[0, L]$ while the derivative has singularities at the points $x_{r_d} \in [0, L]$, as expected.

Alternatively one could calculate the stationary distribution by dividing the space into different regimes separated by the resetting positions. Inside these different regimes one can calculate the stationary solution and furthermore derive a general solution by combining these separate equations [**93**].

We see that our stationary solution depends on the resetting positions x_{r_d} and the parameter

$$\ell_0^{-1} = \sqrt{D/r}. \tag{4.30}$$

This term represents the characteristic diffusion length between two resetting events. From now on we will call this length scale the *mean free path length* [**94**]. We rewrite therefore Eq. (4.29) as

$$\phi(x) = \phi_0(x) + \sum_{n=1}^{\infty} \frac{2}{NL(1 - \ell_0^{-2}\varepsilon_k)} \cos(n\pi x/L) \sum_{d=1}^{N} \cos(n\pi x_{r_d}/L). \tag{4.31}$$

It is a clear that the the limit of the pure diffusion is recovered for $\ell_0^{-1} \to \infty$. in this case of course the stationary state $\phi(x) = \phi_0(x)$ is expected.

4.4. Survival Probability

We will now analyze the mean first passage time of the described process. We consider hereto the survival probability $Q(z,t)$ of the diffusive particle to have survived up to time t if it started from the position z. This function is easily derived by the corresponding function $\psi(x,z;t)$ describing the transition probability

$$\int_0^\infty \mathrm{d}x\, \psi(x,z;t) = Q(z,t)\,. \tag{4.32}$$

It is also possible to calculate the survival probability by deriving an explicit form of the backward equation from the corresponding forward equation and provide its solution. This approach will be used in the next chapter where we consider a perfect absorbing target. The fact that we consider here partial absorbing conditions forces us to follow a different way and start from the Laplace-transform of Eq. (4.12)

$$\begin{aligned} 0 =& D\frac{\partial^2\tilde{\psi}(x,z;s)}{\partial x^2} - (r+s)\tilde{\psi}(x,z;s) + \\ &+ r\delta(x-x_r)\int \mathrm{d}x'\,\tilde{\psi}(x',z;s) - \alpha\delta(x-x_B)\tilde{\psi}(x,z;s)\,. \end{aligned} \tag{4.33}$$

We use now the Laplace transform of the free Green's function

$$G_0(x,z;s) = \frac{1}{2}(sD)^{-1/2}\exp\left[-\left(\frac{s}{D}\right)^{1/2}|x-z|\right] \tag{4.34}$$

in order to find the solution of the differential equation (4.33). We start with the solution to the differential equation where we consider only the resetting trigger field

$$0 = D\frac{\partial^2 G(x,z;s)}{\partial x^2} - (r+s)G(x,z;s). \tag{4.35}$$

This equation is solved by the substitution $s \to s+r$ in the free Green's function above. We have also

$$\begin{aligned} G(x,z;s) &= \int \mathrm{d}t\, \exp\left[-(r+s)t\right]\psi(x,z;t) = \\ &= \frac{1}{2}((r+s)D)^{-1/2}\exp\left[-\left(\frac{r+s}{D}\right)^{1/2}|x-z|\right]. \end{aligned} \tag{4.36}$$

We can imply reflecting boundary conditions at $x=0$ and $x=L$ by using the reflexion theorem [**99**]. The propagator takes in this case the form

$$G_r(x,z;s) = \sum_{n=-\infty}^{\infty} G(x,z+2nL;s) + G(x,-z+2nL;s), \quad 0 \le x \le L\,. \tag{4.37}$$

All of these terms can be combined together in order to construct the Green's function $K(x,z;s)$ fulfilling the equation

$$0 = D\frac{\partial^2}{\partial x^2}K(x,z;s) - (r+s)K(x,z;s) + r\delta(x-x_r)\int \mathrm{d}x'\,K(x',z;s) \tag{4.38}$$

together with the boundary conditions

$$\frac{\partial}{\partial x}K(x,z;s)\Big|_{0,L}=0\,. \tag{4.39}$$

The solution to this equation is

$$K(x,z;s)=G_r(x,z;s)+\frac{r}{s}G_r(x,x_r;s). \tag{4.40}$$

From the exact form of $K(x,z;s)$ one can calculate the survival probability for the process described by Eq. (4.33). The formula derived in [**91**] for the special case of a point-like partial absorbing target is rather useful in that regard

$$\tilde{\psi}(x,z;s)=K(x,z;s)-\frac{\alpha K(x,x_B;s)K(x_B,z;s)}{1+\alpha K(x_B,x_B;s)}\,. \tag{4.41}$$

The Laplace transform of the survival probability $Q(z,t)$ is correspondingly given by

$$\tilde{Q}(z,s)=\frac{1}{s}\left(1-\frac{\alpha K(x_B,z;s)}{1+\alpha K(x_B,x_B;s)}\right)\,. \tag{4.42}$$

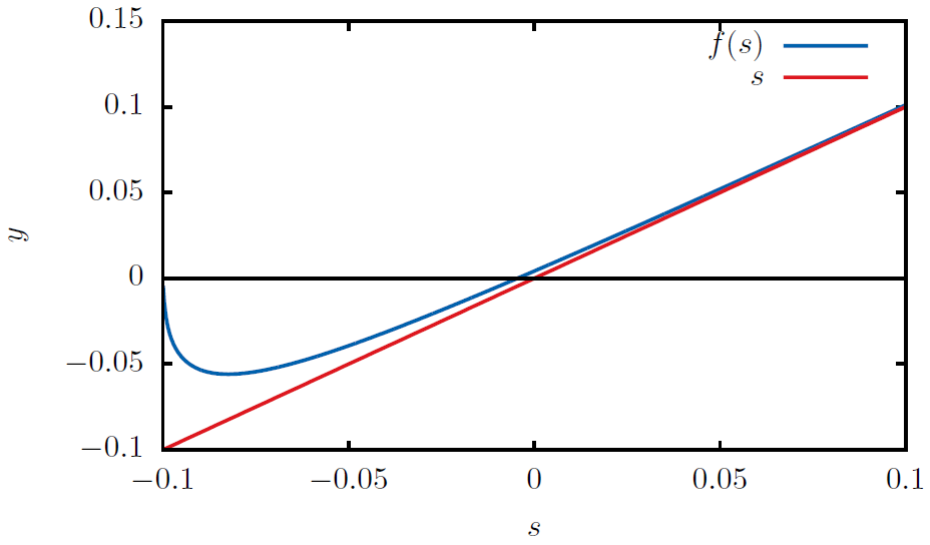

FIGURE 4.2. Plot of $f(s)=s+\frac{r\alpha G_r(x_B,x_r;s)}{1+\alpha G_r(x_B,x_B;s)}$ for $r=0.1$, $D=10^{-4}$, $L=1$, $\alpha=10^7$, $x_B=0.54$ and $x_r=0.44$. In the limit $s\to\infty$ we get $f(s)\to s$, while for $s\to -r$, $f(s)$ approaches negative value proportional to r.

We can derive the survival probability by calculating the inverse Laplace transform of this formula. The function $G_r(x,z;s)$ is strictly decreasing for

increasing s. This leads us to the conclusion that $\tilde{Q}(z,s)$ has a simple pole at $s = s_0$ (see Fig. 4.2), which is defined through

$$s_0 = -\frac{r\alpha G_r(x_B, z; s_0)}{1 + \alpha G_r(x_B, x_B; s_0)}. \tag{4.43}$$

Furthermore due to the positivity of $G_r(x,z;s)$ we can claim that

$$-r < s_0 \leq 0. \tag{4.44}$$

In the complex plane there is a branch point at $s = -r$. The long time behavior of the survival probability is determined by the residue from s_0 which can be determined numerically by the point at which $f(s) = s + \frac{r\alpha G_r(x_B,x_r;s)}{1+\alpha G_r(x_B,x_B;s)}$ crosses the x-axis (see Fig. 4.3).

4.4.1. Existence of the optimal rate. A first indication for the existence of an optimal resetting rate that minimizes the mean time to absorption (MTA) is the existence of a value of r for which s_0 is minimal. This can be seen Fig. 4.3 where s_0 as function of r is plotted. We can investigate this further by studying directly the properties of the MTA, $T(z)$, for a particle which originated at z,

$$T(z) = -\int_0^\infty \mathrm{d}t\, t\frac{\partial Q(z,t)}{\partial t} = \int_0^\infty \mathrm{d}t\, Q(z,t) = \tilde{Q}(z,0)\,. \tag{4.45}$$

$\tilde{Q}(z,s)$ is a continuous function of s and we can set

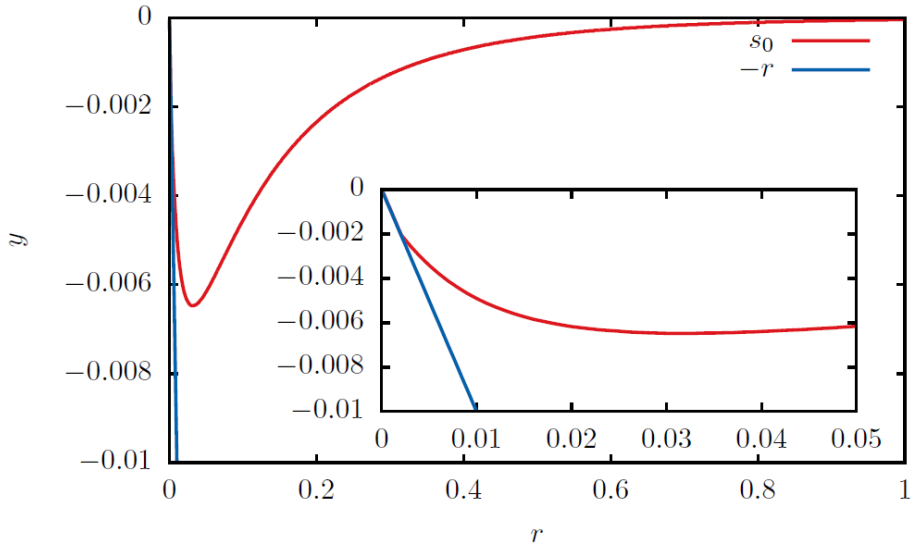

FIGURE 4.3. Plot of s_0 in dependence of r for $\alpha = 10^7$, $L = 1$, $D = 10^{-4}$, $x_B = 0.54$ and $x_r = 0.44$. We see that in the limit $r \to 0$ the behaviour of s_0 approximates that of $-r$. The limit of zero is approached for big resetting rates.

$$T(x_0) = \tilde{Q}(x_0, 0) = \lim_{s\to 0} \frac{1 + \alpha(K(x_B, x_B; s) - K(x_B, x_0; s))}{s + \alpha s K(x_B, x_B; s)}. \tag{4.46}$$

This formula can be further modified by inserting the expression (4.40) for the propagator $K(x_B, x_B; s)$

$$T(x_0) = \frac{1 + \alpha(G_r(x_B, x_B; 0) - G_r(x_B, x_0; 0))}{\alpha r G_r(x_B, x_r; 0)}. \tag{4.47}$$

The optimal resetting rate can no been determined by solving the equation

$$\frac{\partial}{\partial r} T(x_0) = \frac{r\alpha^2 (G_r(x_B, x_B; 0) - G_r(x_B, x_0; 0))' G_r(x_B, x_r; 0)}{\alpha^2 r^2 G_r^2(x_B, x_r; 0)} - \\ - \frac{[1 + \alpha(G_r(x_B, x_B; 0) - G_r(x_B, x_0; 0))](\alpha r G_r(x_B, x_r; 0))'}{\alpha^2 r^2 G_r^2(x_B, x_r; 0)} = 0 \tag{4.48}$$

or equivalently

$$\alpha^2 (r G_r'(x_B, x_B; 0) + G_r(x_B, x_0; 0) - G_r(x_B, x_B; 0) - \alpha^2 r (G_r(x_B, x_B; 0) - \\ - r G_r'(x_B, x_0; 0)) G_r(x_B, x_r; 0) - G_r(x_B, x_0; 0)) G_r'(x_B, x_r; 0) - \\ - \alpha (G_r(x_B, x_r; 0) + r G_r'(x_B, x_r; 0)) = 0\,. \tag{4.49}$$

From Eq. (4.37) follows that each propagator consists of a sum over infinitely many exponential functions. This exponential form allows us to approximate each propagator by a finite sum that can be evaluated numerically. We could see that the deviation between the evaluation of Eq. (4.37) for $n = 10^5$ and $n = 10^6$ is smaller than 10^{-10}. We have set $n = 10^6$ and could calculate this way an optimal resetting rate of $r = 0.026$ for the case presented above in Fig. 4.3.

As stated in our introduction for a stochastic search process in a bounded domain the possibility of a divergent search is excluded. This mean that in this case resetting may be advantageous or disadvantageous and its effect depends on the positions x_0, x_r and x_B. In the following we focus on this matter for the simple case of a resetting mechanism that leads the diffusive searcher back to its original position ($x_0 = x_r$).

Setting $x_0 = x_r$ in Eq. (4.47) we see that depending on the value of $|x_B - x_r|$ the typical behavior of $T(x_0)$ as function of r can described in two distinct ways. If the distance $|x_B - x_r|$ is equal or bigger than half the order the size of the system $T(z)$ is a monotonic increasing function of r:

$$\frac{\partial T(x_0)}{\partial r} > 0 \quad \forall r \in \mathbb{R}_+ \tag{4.50}$$

and

$$\partial T(x_0)/\partial r \to \infty \quad \text{for} \quad r \to \infty. \tag{4.51}$$

On the other hand, for values of $|x_B - x_r|$ that are smaller than $\mathcal{O}(L/2)$, the function $\partial T(x_0)/\partial r$ becomes negative for values of r close to zero. But there exists a value $r^* \in \mathbb{R}_+$ so that $\partial T(x_0)/\partial r > 0$ for all $r > r^*$. This behavior is shown explicitly in Fig. 4.4. Now we can consider several system sizes L and a wide range of values for $|x_B - x_r|$ in order to verify that this

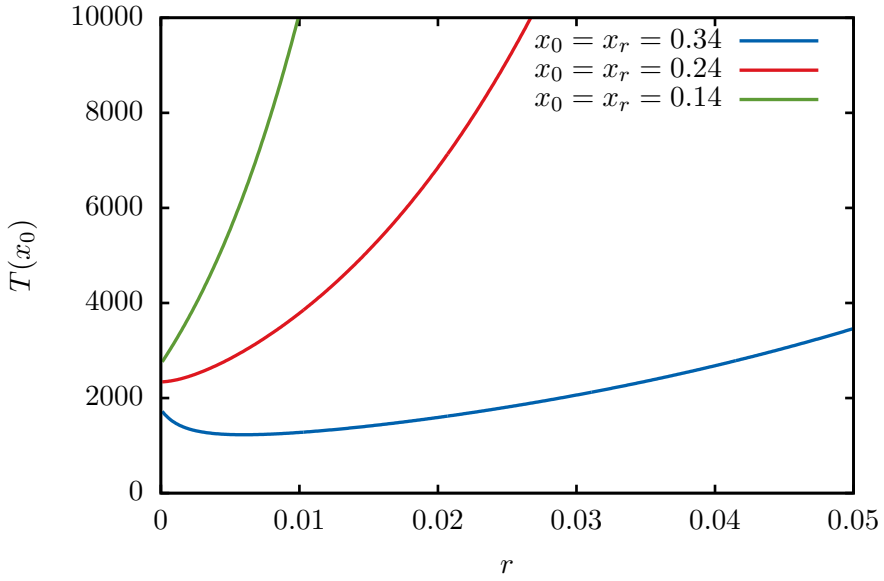

FIGURE 4.4. The MTA as a function of the resetting rate r for different values of $|x_B - x_0|$. We set $x_B = 0.54$, $L = 1$, $D = 10^{-4}$ and $\alpha = 10^7$. We see that the existence of an optimal resetting rate for $T(x_0)$ is evident only for the smallest value of $|x_B - x_0|$.

pattern is universal and described by the linear functions shown in Fig. 4.5. It is clear that the different regimes are separated by lines the slope g_r of which depend on the parameter α.

The dependency of the function $T(x_0)$ on the absorption rate α is reflected in the equation

$$T(x_0) = \frac{1}{\alpha r G_r(x_B, x_r; 0)} + \frac{(G_r(x_B, x_B; 0) - G_r(x_B, x_0; 0))}{r G_r(x_B, x_r; 0)}. \tag{4.52}$$

The first term of this equation is dominant for values of α which are smaller than 10^{-5} while the opposite case, where this term can be ignored, occurs if $\alpha > 0.01$. This fact allows us to produce Fig. 4.6 where g_r is described as function of the absorption rates α.

We can also declare that for reflecting boundary conditions the existence of an optimal resetting rate depends on the distance $|x_B - x_0|$. Furthermore the exact value of this optimal resetting rate is a function of the distance $|x_B - x_0|$ and the absorption rate α. This finding is not surprising since a similar dependency between optimal parameters and initial conditions could be shown also for a Lévy flight process in one dimension [**95**]. In this work the two optimal parameters μ^* and r^*, undergo a discontinuous jump, from nonzero finite values to $r^* = 0$ and $\mu^* = 0$ at a critical value x_0^*. Here we observe a continuous transition as represented in Fig. 4.7.

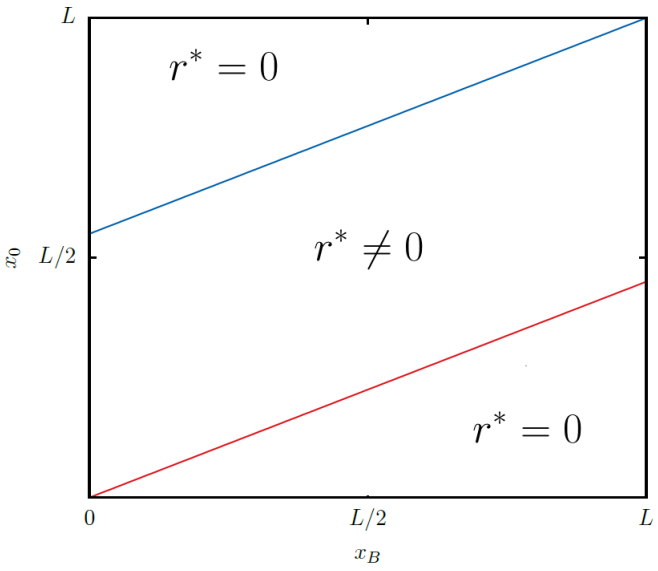

FIGURE 4.5. Phase diagram for the existence of an optimal resetting rate r^* for a random walk taking place in a bounded domain with reflecting walls. In the region between the two lines (blue and red) resetting can be beneficial. The blue line is given by the formula $x_0 = (1 - g_r) + g_r x_B$ and the red line is of the form $x_0 = g_r x_B$.

This continuous nature of the transition is expected. We know that for large values of $x_B - x_0$ the optimal resetting rate r^* is equal to zero and $T_r(x_0)$ a strictly increasing function of r. Now if we decrease the distance of $x_B - x_0$ then at the critical value of $x_0^* \approx g_r x_B$ we observe the disappearance of the derivative $\partial_r T_r(x_0)$ for a large range of values of r around $r = 0$. A numerical evaluation of the optimal value is impossible at that point. Further decrease of the distance $x_B - x_0$ will lead the development of a minimal value for the function $T_r(x_0)$ and hence we have a single optimal value with $r^* > 0$.

4.4.2. Special cases. In the following we consider different special cases that correspond to limiting cases with regard to the resetting or absorbing rates for the survival probability described by Eq. (4.42). The complex structure of the numerator makes an analytical determination of the simple pole impossible. Fortunately qualitative statements are possible in the limiting cases that we will consider in the following. This allows us to test if the derived solutions are consistent with the expected behavior.

Weak Absorption ($\alpha \to 0$). In this limiting case Eq. (4.42) simply transforms to

$$\tilde{Q}(z, s) = \frac{1}{s}. \tag{4.53}$$

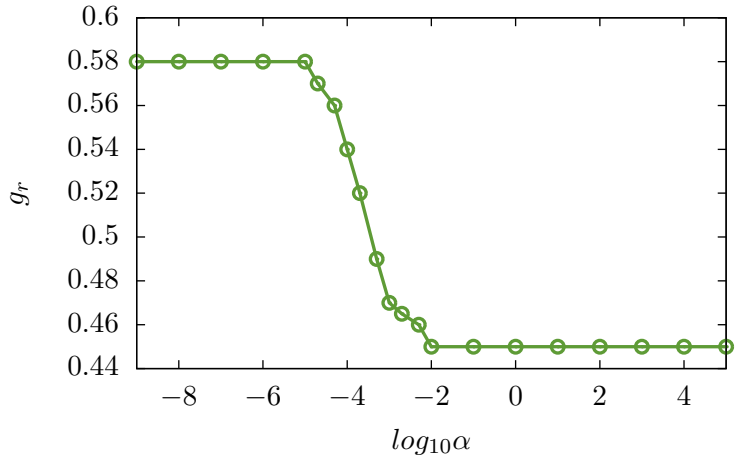

FIGURE 4.6. Proportionality factor g_r introduced in Fig. 4.5 as function of the absorption constant α.

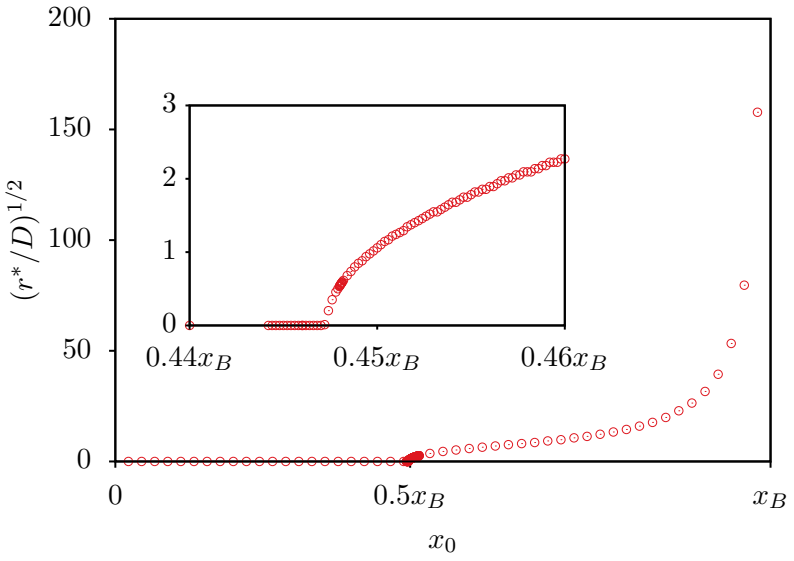

FIGURE 4.7. Optimal resetting rate as a function of the initial position. We show the behavior of the optimal resetting rate for $L = 1$, $x_B = 0.5$, $\alpha = 1$ and $D = 10^{-4}$. Numerical calculations for different combinations of the parameters ($L = 1; 2; 3$, $x_B = 0.5 \cdot L$, $D = 10^{-4}; 4 \cdot 10^{-4}; 9 \cdot 10^{-4}$, $\alpha = 1$) show the same behavior. The critical value is estimated at $x_0^* = (0.448 \pm 0.004) x_B$.

This corresponds to an infinite $T(z)$, which is natural since no absorption can take place.

Weak Resetting ($r \to 0$). In the limit of $r \to 0$ we can replace the function $K(x, y; s)$ by the term

$$H(x, y; s) = \sum_{n=-\infty}^{\infty} G_0(x, y + 2nL; s) + G_0(x, y - 2nL; s)\,. \tag{4.54}$$

The expression $H(x, y; s)$ corresponds to a simple diffusion process in a bounded domain $[0, 1]$ with reflecting boundary conditions at $x = 0$ and $x = 1$. The Laplace transform of the survival probability reads as

$$\tilde{Q}(z, s) = \frac{1}{s}\left(1 - \frac{\alpha H(x_B, z, s)}{1 + \alpha H(x_B, x_B; s)}\right)\,. \tag{4.55}$$

We notice now that $\lim_{s\to 0} H(x, y; s) \to \infty$ for all $x, y \in \mathbb{R}$ and come hence to the conclusion that

$$\lim_{r\to 0} T(x_0) \sim const. \tag{4.56}$$

This constant value depends solely on the parameters α, L and $|x_B - x_0|$.

Strong Resetting ($r \to \infty$). In the limiting case of strong resetting we expect a situation similiar to the one of weak absorption. We have namely

$$K(x, y; s) \sim rG_r(x, x_r; s) \sim r^{1/2} \exp\left[-\left(\frac{r+s}{D}\right)^{1/2} |x - x_r|\right] \sim 0 \tag{4.57}$$

leading to

$$\tilde{Q}(z, s) \sim \frac{1}{s}. \tag{4.58}$$

This expression is equivalent to the one derived for $\alpha = 0$. In the limit of $r \to \infty$ the random walker has not the opportunity to travel away from its initial position since it gets constantly resetted to its initial position. Absorption has correspondingly no effect on the evolution of the process.

Strong Absorption ($\alpha \to \infty$). It is easy to see that in the limitng case of ($\alpha \to \infty$) the Laplace transform of the survival probability can be replaced by the expression

$$\tilde{Q}(x_0; s) = \frac{K(x_B, x_B; s) - K(x_B, x_0; s)}{sK(x_B, x_B; s)}. \tag{4.59}$$

We can now use the explicit expression (4.40) for the function $K(x, y; s)$ which leads us to

$$T(x_0) = \frac{G_r(x_B, x_B; 0) - G_r(x_B, x_0; 0)}{rG_r(x_B, x_r; 0)}\,. \tag{4.60}$$

The same problem could be considered in terms of one absorbing

$$q(x_B, y; t) = 0 \tag{4.61}$$

and one reflecting boundary condition

$$\left.\frac{\partial q(x,y;t)}{\partial x}\right|_0 = 0\,. \tag{4.62}$$

It is therefore no surprise that no explicit dependence of $T(x_0)$ on the absorbing rate exists.

Furthermore we can claim that in this case the propagator $G_r(x,y;s)$ can be replaced by the Laplace transform

$$\tilde{q}(x,y;s) = \frac{1}{2}\left[(r+s)D\right]^{-1/2} \times \\ \times \left\{\exp\left[-\left(\frac{r+s}{D}\right)^{1/2}|x-y|\right] + \exp\left[-\left(\frac{r+s}{D}\right)^{1/2}|x+y|\right]\right\}. \tag{4.63}$$

This easily proven by a numerical calculation of the propagator $G_r(x,y;0)$ for $L=1$ by taking up to 10^6 elements into consideration

$$\frac{G_r(x,y;0)}{G_r(x,z;0)} \approx \frac{\sum\limits_{n=-10^6}^{10^6} G(x,\pm y+2nL;0)}{\sum\limits_{n=-10^6}^{10^6} G(x,\pm z+2nL;0)} \approx \\ \approx \frac{\exp(-\sqrt{r/D}|x-y|)+\exp(-\sqrt{r/D}|x+y|)}{\exp(-\sqrt{r/D}|x-z|)+\exp(-\sqrt{r/D}|x+z|)} = \frac{\tilde{q}(x,y;0)}{\tilde{q}(x,z;0)}. \tag{4.64}$$

Hence a replacement of Eq. (4.60) by

$$T(x_0) = \frac{\tilde{q}(x_B,x_B;0)-\tilde{q}(x_B,x_0;0)}{r\tilde{q}(x_B,x_r;0)} \tag{4.65}$$

is justified.

4.4.3. Numerical Results. For the special case of a perfect absorption ($\alpha\to\infty$) we can easily test our theoretical predictions by a numerical simulation. A stochastic search process with a perfectly absorbing target correspons to a first passage problem that is easily evaluated by a Montecarlo simulation. In Figs. 4.8 and 4.9 the analytical predictions (blue lines) derived from Eq. (4.60) are compared with the results of Monte Carlo simulations. The calculated average search time is quite well described by our equations. Of course a discrepancy is observed for very small values of the mean free path length. This deviation is explained by the different nature between a continuous time process like the Brownian motion described by our analytical approach and the simulated discrete time random walk. Similar deviations have been observed by Gelenbe in simulations of a two-dimensional random walk in an infinite lattice [**83**].

Our Monte Carlo simulation is based on a random walk $S_n = \sum_{k=0}^{n} X_k$ taking place in a one-dimensional lattice. We have chosen here a lattice

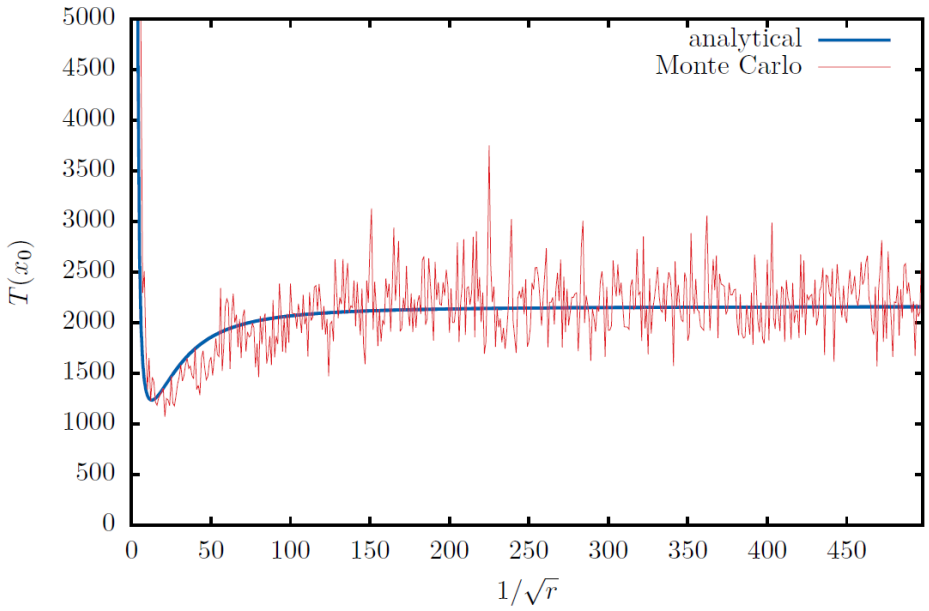

FIGURE 4.8. MTA in dependence of the mean free path $1/\sqrt{r}$. For this simulation we set $x_0 = x_r = 44$ and $x_B = 64$. The numerical results are calculated based on the values of 100 different random walks.

consisting of x_B sites. At the beginning we set the random walker in its initial position $x_0 \in \mathbb{N}$ with $1 \leq x_0 \leq x_B$. At each time step the random walker makes a jump either to the left or the right with equal probability. The left boundary of the system which correspond to the position $x = 0$ is reflective. This mean that a walker at the position $x = 1$ will necessarily perform a jump to the right. After each such step a resetting of the walker to its initial position x_0 may occur with a probability $0 \leq r_n \leq 1$. The mean time between two reset events is therefore equal to $(1 - r_n)/r_n$ and the corresponding mean free path is $\sqrt{(1 - r_n)/r_n}$.

The walk is terminated as soon as the particle arrives at the absorbing position x_B. The effect of the reflecting boundary conditions on the MTA is best observed in the behavior of the function $T(x_0)$ for large values of $\sqrt{(1 - r_n)/r_n} = \sqrt{2D/r}$. In that regime the function $T(x_0)$ appears to be almost constant. The reason being that due to the confinement of the process at a certain domain, the increase of the mean free path length can only have a minimal effect on the search process.

4.5. Discussion and Conclusions

In this chapter we considered the effect of reflecting boundary conditions on a diffusion process in one dimension under the effect of a resetting and an absorbing potential. We asked ourselves how the existence of the boundary

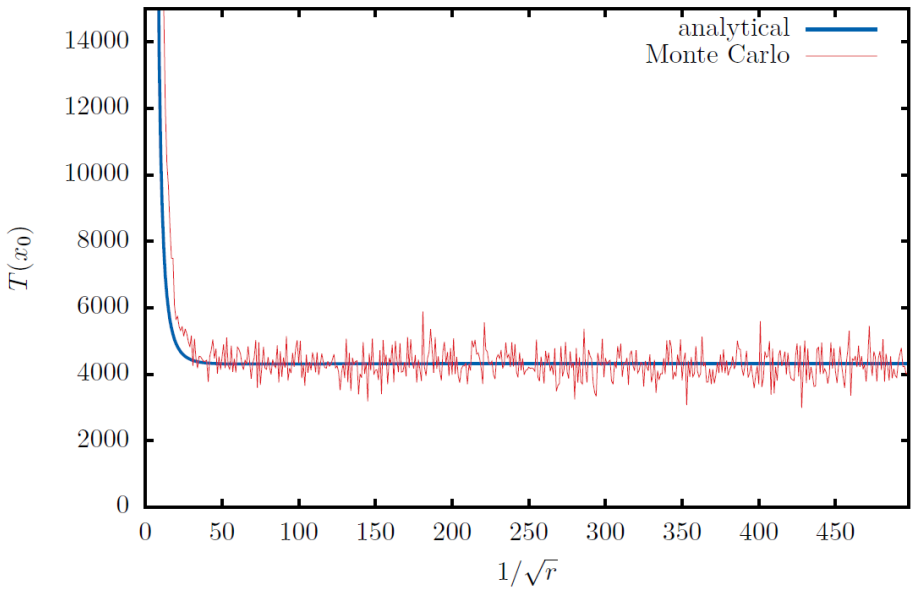

FIGURE 4.9. MTA as a function of the mean free path $1/\sqrt{r}$. For this simulation we set $x_0 = x_r = 34$ and $x_B = 74$. The numerical results are calculated based on the values of 100 different random walks.

conditions will influence the properties of a stochastic search process with resetting. We did that by determining the mean time to absoprtion of the described process. Our approach consisted in expressing the solution to the Laplace transformed forward equation in terms of the free Brownian propagator. From the exact form of the propagator we derived the Laplace transform of the survival probability. A careful analysis of this function showed that the existence of an optimal resetting rate is not granted for this class of processes. Numerical calculations helped us determine exact regions of the initial position for which a positive resettign rate can be found. Furthermore it was possible to determine the exact value of the optimal resetting rate for different cases and a large set of parameters.

For the special case of a perfect absorbing target we used numerical simulations in order to verify our results. The predicted behavior of the MTA as function of the resetting rate was in good agreement with the Monte Carlo simulation. Of course several limitations arose when approaching small values of ℓ_0^{-1} due to the different scaling properties of Brownian motion and discrete time step processes.

The presented model can be extended in several ways. For instance, the problem of a search process with more than one partial absorbing potential is rather interesting. Similarly one could consider the case where the Brownian particle does not necessarily gets reset to its initial position but to a random

previously visited position. Processes that include this kind of memory effect have been the subject of scientific research in the last years [**118, 119**] and were inspired by animal behavior. It would be surely interesting to evaluate the properties of such a process in a bounded domain. The question with regard to the existence of an optimal resetting rate for a process with more than one searcher also arises naturally.

Finally the present framework is suited the study of general integrable resetting and absorbing potentials. Therefore a discussion of the same problem for different resetting mechanisms, relying as example on a Gaussian or an exponential distribution function is possible and probably interesting for several applications. Especially the existence and properties of several regimes in such systems would be an attractive and promising problem.

CHAPTER 5

Diffusion with Resetting inside a two-dimensional Circle

5.1. Introduction

In the last chapter we focused on the properties of an one-dimensional stochastic search process with resetting in a bounded domain. We considered hereto a diffusion process with a partial absorbing target inside an interval bounded by reflecting boundary conditions. In this chapter we will integrate new features to this previous model and consider a stochastic search process with resetting evolving inside a simple two-dimensional confining geometry while also having the property to switch between two different modes of diffusion.

In detail we imagine that we have a circle of radius R inside of which a diffusion process takes place. The Brownian particle is in search of a stationary target that lies on the boundary of the circle. The stochastic searcher performs a two-dimensional Brownian motion with the diffusion constant D_2 until it arrives at the boundary of the circle. The searcher then sticks to the boundary reducing the dimensionality of its motion and undergoing from now on a one-dimensional diffusion with diffusion constant D_1 along the boundary. This whole process may get interrupted by a resetting event appearing with a constant rate r which forces the searching particle to return to its initial position. From this point on a two-dimensional diffusion takes place until the arrival at the boundary and so on. The process is terminated by the first meeting between searcher and target. We will also evaluate in the following the first passage time of this process. By assuming here that the target has no dimension (point target) we can guarantee that a termination of the target is possible only during the one-dimensional diffusion phase. This assumption allows for an exact analytical calculation of the MTA.

A well studied class of stochastic search processes that combine two phases of motion like the one described above are intermittent search processes. They are characterized by a combination of phases of slow motion during which detection of the target is possible and phases of long jumps allowing the searcher to cross over large regions of the system. This very efficient strategy can be observed at different scales (microscopic and macroscopic) and in various fields [**84**].

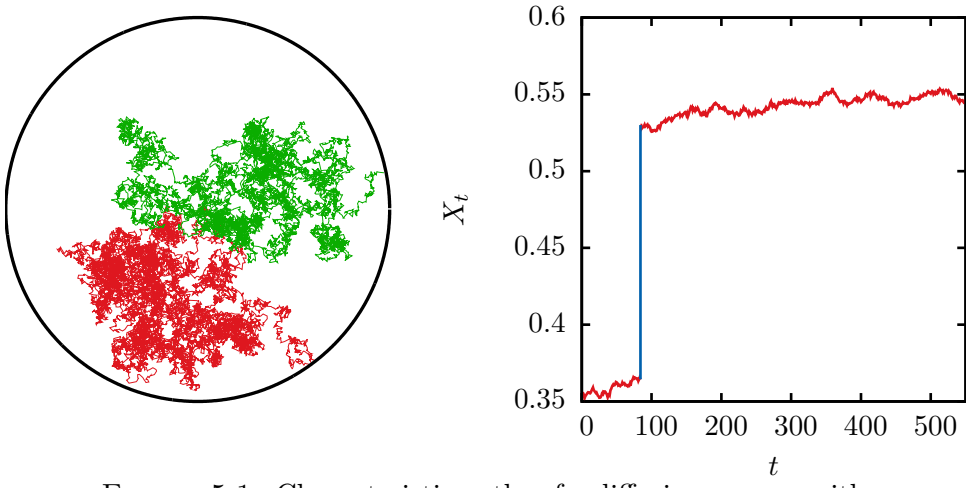

FIGURE 5.1. Characteristic paths of a diffusion process with resetting inside a circle with $R = (2\pi)^{-1}$. The red line on the left figure correspond to the first excursion of the Brownian particle starting from the center of the circle and diffusing inside the circle. Upon arriving on the boundary an one-dimensional stochastic process starts that gets interrupted by stochastic resets. Directly after this resetting a new diffusive excursion from the center of the circle starts (indicated by the green line in the left figure) which ends again at the boundary. As in the last chapter we represent these resetting effects on the boundary by blue lines. Starting an one-dimensional excursion at the position $x = 0/1$ would require a two-dimensional path ending at the position $\vec{R} = \left((2\pi)^{-1}, \pi\right)$.

Although the process studied in this section also has the property that detection of the target is only possible during a certain phase of its evolution the characterization as intermittent search process would be incongruous. The reason for this is the fact that the different nature of the two phases of motion (one-dimensional and two-dimensional process) does not allow for a characterization of a 'slow'- and a 'fast'-moving phase.

A much more fitting characterization for the dynamics studied in this section is surface mediated diffusion. This class of diffusion processes describes search processes that terminate on the surface of a confining domain and is therefore very important for the analysis of chemical reactions in bounded domains [**116, 109, 86, 87**]. A great inspiration for the present chapter was the work of Bénichou *et al.* [**107**] on the "Optimal Reaction Time for Surface-Mediated Diffusion". They considered a Brownian particle

inside a circular domain with alternates between phases of bulk and surface diffusion. The transition from bulk to surface diffusion is initiated as in our model by the arrival of the particle at the surface. The transition from surface to bulk diffusion on the other hand corresponds to a jump of the particle from the surface in a direction perpendicular to the surface and towards the center of the circle. At each desorption event the particle is radially ejected at a distance a from the boundary. We will see here how a replacement of the desorption mechanism through a resetting event would influence the properties of the process.

One has to note here that although for such microbiological systems a resetting mechanism cannot be constructed [1] a vast number of applications can be found in different fields such as computational sciences or zoology. One characteristic example is animal foraging where revisiting previous positions has proven to be an effective strategy [**118, 122**]. When searching for foods animals may also be forced to reduce their dimensionality by different ecological characteristics, as example hunting along a shore. At the same time reduction of dimensionality can be considered as fulfillment of a constraint in terms of a randomized search algorithm which in general profit from a restart mechanism [**137, 141**].

In this chapter we will consider different initial conditions as well as different conditions under which a resetting may occur. We have chosen hereto following structure: We start by showing how one can calculate the mean first passage time for a diffusion process by calculating the Laplace Transform of the survival probability. We will then apply the provided method for the simple case of a diffusion process starting at the boundary of the circle. In section 5.3 we treat the case of the initial position being the center of the circle and prove the validity of our approach by comparing our results to previous works in an intermittent setting [**123**]. In section 5.5 we generalize our approach by considering random initial conditions. This forces us to derive an expression for the gain potential first. In doing so, we can derive the master equation of the process. The solution delivers then the desired MTA. Furthermore, the provided expression allows us to characterize the different regions with a positive resetting rate. Of course in this case the parameters D_2 and D_1 have to be specified. In section 5.6 we follow the same approach as in the preceding section in order to analyze the properties of the generalized process where resetting may even occur during the two-dimensional diffusion. Finally, our last section is reserved for the discussion of our results.

5.1.1. General Approach. Although we consider in the following systems with diverse resetting behavior the establishment of a general approach

[1] Resetting would require the searcher to have some kind of memory with regard to previously visited positions (at least with regard to its initial position). At microbiological level this kind of memory cannot be implemented experimentally.

in analyzing these problems is still possible. Two conditions are hereby crucial. First, we consider a constant resetting rate. Second, the target has no dimension and hence the process is terminated during the one-dimensional diffusion phase. Under these two conditions the MTA is simply given by the addition of the mean times for each of the two different modes consisting purely of one- and two-dimensional diffusion. We characterize the mean time the particle spends during its one-dimensional diffusion by T_1 and by T_2 the mean time for the two-dimensional path. The total mean time to absorption is then given by,

$$T = T_1 + T_2. \tag{5.1}$$

It is important to note here that the mean time of the one-dimensional diffusion T_1 can be calculated analytically, while T_2 can be expressed in terms of T_1 and the mean time of the first two-dimensional excursion, τ_2. We can claim now that due to the stationarity of the diffusion process each two-dimensional excursion starting after a reset from the boundary to the initial position has the same mean duration as the first two-dimensional excursion. Correspondingly we use now the general term "mean time to boundary" (MTB) in order to describe τ_2. The mean time T_2 is then given by the formula

$$T_2 = (c_r + 1)\tau_2 \tag{5.2}$$

where c_r describes the mean number of resets from the boundary.

This new term c_r can also be expressed in terms of the resetting rate r and the mean time of the one-dimensional diffusion T_1. The time interval between two resets follows a Poisson distribution with rate r. Hence the mean time interval is given by $\tau_r = r^{-1}$. Consequently we get

$$c_r = \frac{T_1}{\tau_r} = rT_1. \tag{5.3}$$

Implementing this simple expression in Eq. (5.2) leads to the reformulation of Eq. (5.1)

$$T = rT_1\tau_2 + T_1 + \tau_2. \tag{5.4}$$

Therefore our only task consists in the following in the determination of the two quantities T_1 and τ_2.

5.2. Diffusion with Resetting in one-dimensional periodic domain

We start our analysis by attacking the simple problem of an initial position on the boundary of the circle. Two-dimensional diffusion does not need to be considered in this case as the random searcher can only move on the boundary of the circle. Correspondingly we deal here with an one-dimensional diffusion process with resetting in a periodic domain of length $L = 2\pi R$.

In the last chapter we have seen how a diffusion process with resetting can be described by a Fokker-Planck equation formalism

$$\frac{\partial\psi(x,x_0;t)}{\partial t} = D\frac{\partial^2\psi(x,x_0;t)}{\partial x^2} + p_G(x)\int \mathrm{d}x'\, p_S(x')\psi(x',x_0;t) \\ -p_S(x)\psi(x,x_0;t) - p_A(x)\psi(x,x_0;t). \tag{5.5}$$

The different cases presented in the following sections are easily implemented by defining the corresponding different distribution functions $p_S(X), p_G(x)$ and $p_A(x)$ which describe the dynamics of the resetting and absorption process. We will assume that resetting is possible from any point on the boundary. The possibility of resetting should hereby be independent of the position of the diffusing particle. These features are represented by a resetting potential of the form $p_S(x) = r$. This potential is in turn complemented by the gain potential $p_G(x) = \delta(x - x_r)$, which describes the resetting of the diffusing particle at the position x_r. We start here with a generalized approach and set later on $x_r = x_0$, forcing herewith the particle to return to its initial position at the boundary. Finally since we consider here perfectly absorbing targets we can set $\mathcal{P}_A(x) = \alpha\delta(x - x_A)$ with $\alpha \to \infty$.

The evolution of the probability density function $\psi(x,t;x_0)$ for a process starting from the position x_0 at the time-point $t = 0$, is hence given by the master equation

$$\frac{\partial\psi(x,t;x_0)}{\partial t} = D_1\frac{\partial^2\psi(x,t;x_0)}{\partial x^2} + \delta(x - x_0)\int \mathrm{d}x'\, r\psi(x',t;x_0) - \\ -r\psi(x,t;x_0) - \alpha\delta(x - x_A)\psi(x,t;x_0). \tag{5.6}$$

Now without loss of generality we can choose $x_A = L$. This allows us to replace the annihilation potential $\mathcal{P}_A$ by the boundary conditions

$$\psi(0,t;x_0) = \psi\left(L,t;x_0\right) = 0 \tag{5.7}$$

for the problems studied here. The Fokker-Planck equation (5.6) describes the evolution of our process but is not suited for the determination of the first passage time. Therefore one can rely on the backward master equation fulfilled by the survival probability $Q(x_0,t)$,

$$Q(x_0,t) = \int \mathrm{d}x\, \psi(x,t;x_0). \tag{5.8}$$

The function $Q(x_0,t)$ describes the probability for a process to have survived up to the time-point t if it started from the position x_0.

Integration of the Fokker Planck equation (5.6) leads to the following equation

$$\frac{\partial Q(x,t)}{\partial t} = D_1\frac{\partial^2 Q(x,t)}{\partial x^2} - rQ(x,t) + rQ(x_0,t) \tag{5.9}$$

with

$$Q(0,t) = Q(L,t) = 0. \tag{5.10}$$

This differential equation is easily solved by using the Laplace-Transform

$$\tilde{q}(x,s) = \int_0^\infty \mathrm{d}t\, Q(x,t)e^{-st} \tag{5.11}$$

leading to

$$D_1 \frac{\partial^2 \tilde{q}(x,s)}{\partial x^2} - (r+s)\tilde{q}(x,s) + 1 + r\tilde{q}(x_r,s) = 0. \tag{5.12}$$

which yields [**79**]

$$\tilde{q}(x,s) = Ae^{\sqrt{\frac{r+s}{D_1}}x} + Be^{-\sqrt{\frac{r+s}{D_1}}x} + \frac{1+r\tilde{q}(x_r,s)}{r+s}. \tag{5.13}$$

The mean time to absorption is derived now by setting $s = 0$

$$T(x) = -\int_0^\infty \mathrm{d}t\, t\frac{\partial Q(x,t)}{\partial t} = \tilde{q}(x,0) \tag{5.14}$$

for which the expression

$$T(x) = Ae^{\ell^{-1}x} + Be^{-\ell^{-1}x} + \frac{1+rT(x_r)}{r} \tag{5.15}$$

with $T(0) = T(L) = 0$ holds. We used hereby the notation

$$\ell = \sqrt{\frac{D_1}{r}} \tag{5.16}$$

as in the previous chapter in order to characterize the mean free path length between two resets.

From the symmetry of the system follows

$$\frac{\partial}{\partial x}T(x)|_{x=L/2} = 0 \tag{5.17}$$

which together with the two boundary conditions gives us the solution

$$T(x) = \frac{1+rT(x_r)}{r}\left(1 - \frac{\cosh \ell^{-1}(x-L/2)}{\cosh \ell^{-1}L/2}\right) \tag{5.18}$$

For the special case of $x_r = x$, namely the case where the particle resets to its initial position, our solution takes the form

$$T(x) = -\frac{\ell^2}{D_1}\left(1 - \frac{\sinh \ell^{-1}L}{\sinh \ell^{-1}x + \sinh \ell^{-1}(L-x)}\right). \tag{5.19}$$

We can now evaluate the dependence of this mean time to absorption on the initial position by analyzing the optimal free path length, ℓ^*, which is simply the value of ℓ for which

$$\frac{\partial}{\partial \ell}T(x)|_{\ell=\ell^*} = 0 \tag{5.20}$$

holds. In Fig. 5.2 we can see that a decrease in the distance between the starting position and one of the boundaries leads to a crossover of the optimal mean free path length from an infinite value to a finite one.

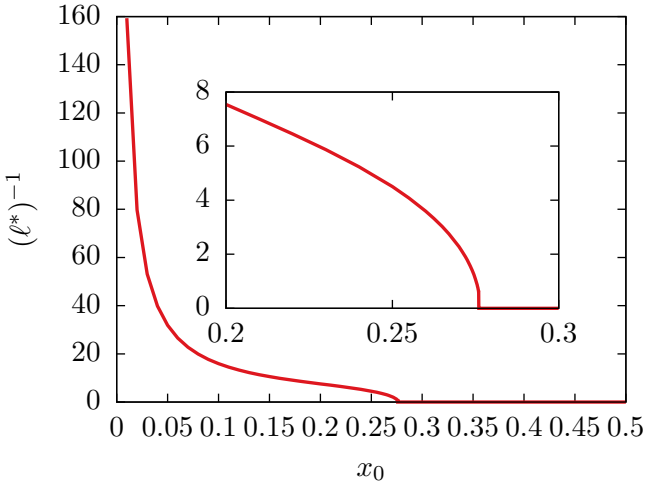

FIGURE 5.2. Inverse of the optimal mean free path length vs the starting position of the searcher for a system of length $L = 1$. We can see that for $0.276L < x_0 < 0.724L$ the optimal mean free path length is equal to ∞. This fact changes if we consider a starting position which is closer to the boundaries and thus a finite value for the mean free path length tends to be optimal.

This explained by the fact that for initial positions close to the boundaries, a finite traveling distance between two resets efficient. A specific choice of r with $r > 0$ is hence optimal. This situation changes if the particle starts at a position between the crossover points $(0.276L, 0.724L)$, as shown in Fig. 5.2. In this case restriction of the mean free path length is unfavorable. So the optimal choice is an infinite time interval between resets and thus pure diffusive motion given for $r = 0$ is preferred.

5.3. Hard Resetting

In this section we consider the case of the initial position being at the center of the circle. A fitting characterization of this process would be *hard reset process*. It can be treated as a special case of the general process presented in the next section. We start with this special case here since it allows us to test our method through the comparison of the derived results to previous findings of works [**107, 110**] concerned with processes that exhibit intermittent dynamics. Furthermore the simple nature of the problem at hand provides a good introduction to our general approach.

The MTB for a Brownian particle starting at the center of a circle with radius R is given by [**94**]

$$\tau_2(R) = \frac{R^2}{4D_2}. \tag{5.21}$$

Now if we consider the one-dimensional excursion we have to note that, since the particle finds itself in the center of the circle after each reset, the subsequent two-dimensional excursion will end due to the radial symmetric nature of the system at an arbitrary point on the circle. This means that each one-dimensional excursion starts at an arbitrary point on the boundary. The gain term in Eq. (5.5) has correspondingly the form a uniform probability distribution function $p_G(x) = L^{-1} = (2\pi R)^{-1}$ for $x \in [0, 2\pi R]$.

The MTA T_1 is also easily calculated by solving the differential equation

$$-1 = D_1 \frac{\partial^2}{\partial x^2} T_1(x) - \frac{r}{L} T_1(x) + \frac{r}{L} \int \mathrm{d}z\, T(z) \tag{5.22}$$

with the boundary conditions

$$T(0) = T(L) = 0. \tag{5.23}$$

In the previous section we could see that the solution takes the form

$$T(x) = -A \frac{\cosh \ell^{-1}(x - L/2)}{r \cosh L\,(2\ell)^{-1}} + \frac{L}{r} + F(0, L). \tag{5.24}$$

where the notation $F(0, L) = \int_0^L \mathrm{d}z\, T(z)$ has been used. From the boundary conditions we can determine the constant A as,

$$A = rF(0, L) + L. \tag{5.25}$$

The above expression can now be reinserted in the general form described in (5.24) and gives us

$$F(0, L) = \left(\frac{L}{r} + F(0, L) \right) \left(1 - 2\ell \tanh L\,(2\ell)^{-1} \right)$$

from which we obtain

$$F(0, L) = \frac{L}{r} \left((2\ell)^{-1} \coth L\,(2\ell)^{-1} - 1 \right). \tag{5.26}$$

Finally we have

$$T(x) = \frac{L \coth L\,(2\ell)^{-1}}{2\ell r} \left(1 - \frac{\cosh \ell^{-1}(x - L/2)}{\cosh L\,(2\ell)^{-1}} \right). \tag{5.27}$$

One interesting property of Eq. (5.27) is the fact that the MTA is vanishing for $\ell \to 0$. The behaviour of the derived formula is shown in Fig. 5.3. This is a quite surprising result since a vanishing mean free path length corresponds to a restriction of the diffusive searcher in a very small region of the system. We would normally expect a slight increase of the mean search time though this narrowing of the diffusive paths. This contradiction is explained by the property of the resetting mechanism in this specific context to accelerate the visit of infinitely many different positions on the circle. The limit $r \to \infty$ leads namely to an infinite-speed sampling which outweighs the restriction of the mean free path length and optimizes the search process.

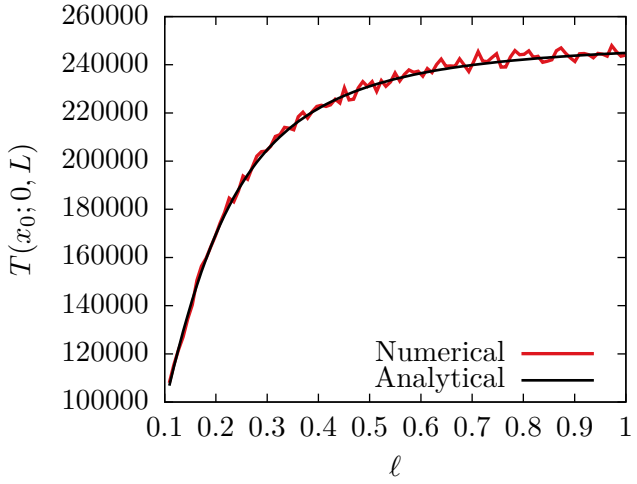

FIGURE 5.3. Numerical evaluation of the formula (5.27) for $x_0 = 0.5$ with $L = 1$. We have chosen here, as before, $D_1 = 5 \cdot 10^{-7}$.

In order to illustrate this feature we introduce the following variation of the original problem. We consider the probability density function for the gain term

$$p_G(x) = \begin{cases} \frac{1}{1-2\varepsilon} & \text{if } \varepsilon < x < 1-\varepsilon \\ 0 & \text{else} \end{cases} \tag{5.28}$$

which is identical to the original uniform function in the limit $\varepsilon \to 0$. For the process described by Eq. (5.28) and $L = 1$ we get the mean time

$$T(x) = \frac{(1-2\varepsilon)\left(\cosh(2\ell)^{-1} - \cosh\ell^{-1}(x-1/2)\right)}{2r\ell\sinh\ell^{-1}(1/2-\varepsilon)}. \tag{5.29}$$

For small values of ℓ and $x \in [0,1]$ we have

$$\left(1 - \frac{\cosh\ell^{-1}(x-1/2)}{\cosh(2\ell)^{-1}}\right) \simeq 1. \tag{5.30}$$

This allows us to replace Eq. (5.29) above with the expression

$$T(x) = \frac{\sigma^{-2}2(1-2\varepsilon)\ell}{\tanh(2\ell)^{-1} - \cosh\ell^{-1}\varepsilon - \sinh\ell^{-1}\varepsilon}.$$

Now by using

$$\tanh\left(\frac{\ell^{-1}}{2}\right) \simeq 1, \tag{5.31}$$

for small values of ε our formula simplifies to

$$T(x) = \varepsilon\sigma^{-2}(1-2\varepsilon)\frac{e^{\ell^{-1}\varepsilon}}{\ell^{-1}\varepsilon}. \tag{5.32}$$

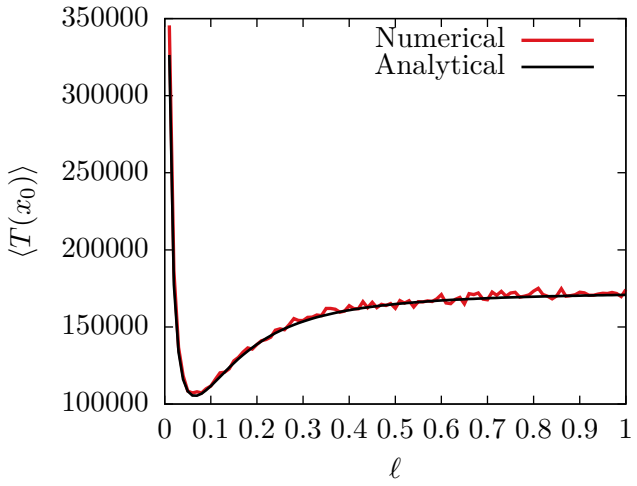

FIGURE 5.4. MTA for the hard resetting problem in the special case of $D_2/D_1 = 2$ for $R = (2\pi)^{-1}$ and $D_1 = 5 \cdot 10^{-7}$.

It is noticeable that the MTA becomes independent of the initial position for high values of the resetting rate, since due to the frequent resetting, the information with regard to the initial position will eventually get lost for increasing times.

Now we proceed in our analysis by considering that the function $x^{-1}e^x$ has a minimum for $x = 1$. Accordingly, the optimal resetting rate for this variation of the one-dimensional problem is achieved when $\ell^{-1} = \varepsilon^{-1}$. In the limit of ε approximating zero, where the original problem is regained, the optimal resetting rate goes correspondingly to infinity.

We see also through the previous calculation that if we consider only the one-dimensional excursion the optimal resetting rate is infinite. This cannot be true if we also take into account the two-dimensional excursion of the particle since each reset adds a term of τ_2 to the mean time. We evaluate therefore Eq. (5.4) by implementing Eq. (5.21) and Eq. (5.27) and integrating over the interval $[0, L]$ leading to

$$T = \frac{R^2}{4D_2} + \frac{L\coth L\,(2\ell)^{-1} - 2\ell}{2r\ell}\left(\frac{rR^2}{4D_2} + 1\right). \tag{5.33}$$

This expression is in perfect agreement with Eq. (2.23) of [**110**]. We can see by a series expansion of the hyperbolic cotangent which transforms the expression above to

$$T = \frac{R^2}{4D_2} + \frac{2}{D_1}\left(1 + \frac{r}{D_2}\right)\sum_{k=0}^{\infty}\frac{L^{-1}}{\left(\frac{2\pi k}{L}\right)^2 + \frac{r}{D_1}}. \tag{5.34}$$

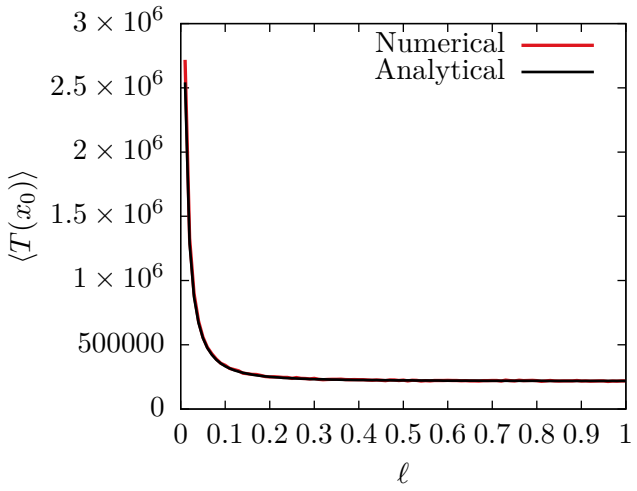

FIGURE 5.5. MTA for the hard resetting problem in the special case of $D_2/D_1 = 0.25$ for $R = (2\pi)^{-1}$ and $D_1 = 5 \cdot 10^{-7}$.

This formula allows us to state that an optimal resetting rate can be found only if $D_2/D_1 \geq 0.38$. In Figs. 5.4 and 5.5 the diverse behavior of the MTA for different values of ℓ is shown.

5.4. Partial Resetting

Now we consider the general case where the initial position is a random position inside the circle and not necessary the center. We again consider only the possibility of resetting taking place only from the boundary of the domain. We will characterize this process from now on as *partial reset process*. In the next section we will generalize the present problem by introducing a persistent resetting field that allows for resetting to take place from any position inside the circle, irrespective of whether the particle is undergoing one-dimensional or two-dimensional diffusion.

It is useful now to consider polar coordinates. The initial position of our particle is given by the set $\vec{x} = (R_0, \theta_0)$, where R_0 is the distance from the center and θ_0 is the angle between the line connecting the initial position to the center of the circle with the vertical.

As before we start with the two-dimensional excursion of the particle. The MTB is given by

$$\tau_2(R, R_0) = \frac{R^2 - R_0^2}{4D_2}. \tag{5.35}$$

Now next to the time needed we have also to calculate the likelihood of crossing the boundary at a specific angle as function of the parameters R_0 and θ_0. This simple step is sufficient to provide us with the probability distribution function of the starting position for the subsequent one-dimensional diffusion phase. The probability distribution function of the hitting angle is

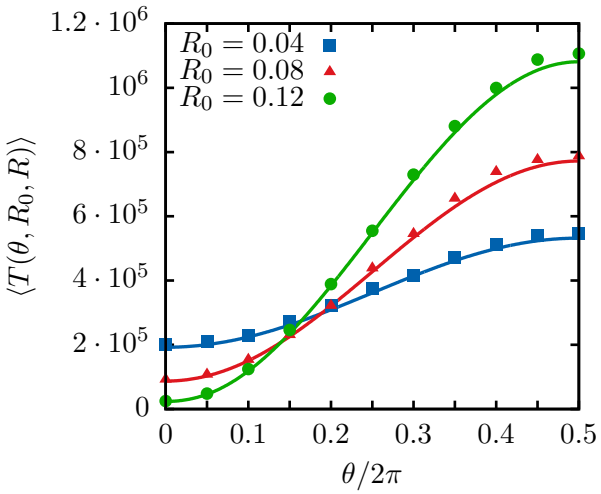

FIGURE 5.6. Mean time to absorption for a Brownian process starting inside a two-dimensional circle for different initial conditions (R_0, θ_0). The points were determined by a Monte-Carlo simulation with $D_2 = 10^{-6}$, $2D_1 = D_2$ and $R = 1/2\pi$. The lines correspond to our theoretical values for these parameters.

easily given by using an electrostatics analogy [**94**] which leads to

$$p(\theta; \theta_0, R_0) = \frac{1 - \frac{R_0^2}{R^2}}{2\pi R\Big(1 - \frac{2R_0 \cos(\theta - \theta_0)}{R} + \frac{R_0^2}{R^2}\Big)}. \tag{5.36}$$

Now let's say that x_0 is the point on the boundary of the circle that lies on the line connecting the initial position $\vec{R}_0 = (\theta_0, R_0)$ to the center of the circle and is closest to the initial position. We can switch between the polar and Cartesian coordinate system by setting $R(\theta - \theta_0) = (z - x_0)$. By this transformation we can now write $p_G(z) = p(\theta; \theta_0, R_0)$. Inserting this expression in Eq. (5.5) we can get following backward equation for the MTA for a process starting on the boundary at the position x,

$$0 = D_1 \frac{\partial^2}{\partial x^2} T(x) - rT(x) + 1 + r \int \mathrm{d}z \, p_G(z) T(z). \tag{5.37}$$

Using the boundary condition $T(0) = T(2\pi R) = 0$ together with Eq. (5.17) the solution to this non-homogeneous differential equation of second order is easily delivered

$$T(x) = \left(\frac{1}{r} + \int \mathrm{d}z \, p_G(z) T(z)\right) \left(1 - \frac{\cosh \ell^{-1}(x - \pi R)}{\cosh \ell^{-1} \pi R}\right). \tag{5.38}$$

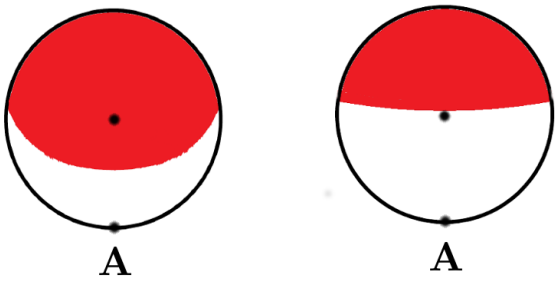

FIGURE 5.7. Different regimes with regard to the existence of an optimal resetting rate for different initial position for a Brownian particle in search for a target located at **A**. The left figure corresponds to the choice of parameters with $D_2/D_1 = 0.25$ and on the right to $D_2 = D_1$. The shaded area (red) describes initial positions for which no positive optimal resetting rate can be found. We can see that for $D_2/D_1 = 1$ a particle starting from the center of the circle can be optimized through a positive resetting rate.

If we multiply now both sides of this formula with $p_G(x)$ and integrate over the interval $[0, 2\pi R]$ we can see that

$$T(x) = \frac{\cosh\sqrt{\frac{r}{D}}\frac{L}{2} - \cosh\sqrt{\frac{r}{D}}\,(x - L/2)}{r\int \mathrm{d}z\, p_G(z)\cosh\sqrt{\frac{r}{D}}\,(z - L/2)} \tag{5.39}$$

holds.

The MTA is hence given by the expression

$$T_1 = \int \mathrm{d}z\, p_G(z) T(z). \tag{5.40}$$

Inserting all of these results in Eq. (5.4) we get

$$T = \frac{R^2 - R_0^2}{4D_2} + \left(\frac{1}{r} + \frac{R^2 - R_0^2}{4D_2}\right) \times$$
$$\times \int \mathrm{d}x\, p_G(x) \frac{\cosh\sqrt{\frac{r}{D_1}}\pi R - \cosh\sqrt{\frac{r}{D_1}}\,(x - \pi R)}{\int \mathrm{d}z\, p_G(z)\cosh\sqrt{\frac{r}{D_1}}\,(z - \pi R)}. \tag{5.41}$$

In Fig. 5.6 we can observe a very good agreement between this formula and the results of Monte-Carlo simulations.

The derived equation enables us to characterize the different regimes inside the circle for which an optimal resetting rate that is non-zero can be found. In Fig. 5.7 we represent the respective areas for the specific ratios

of $D_2 = 0.25D_1$ and $D_2 = D_1$. Two values that are below and above the characteristic value of $D_2 = 0.38D_1$, that was determined in the last section. In both figures we can see that in the limit of $R_0 = R$ a crossover is expected at the value of $\theta = 0.56\pi$. This expectation is in perfect agreement with the results of the third section of this chapter.

5.5. Persistent Resetting

In the previous section we could determine different regimes for which a resetting from the boundary could be beneficial. This was of course only possible by specifying the values of the ratio D_2/D_1. In this section we generalize the previous model and allow for resetting to take place from anywhere inside the circle. We consider also a permanent resetting field and characterize in the following the process as *persistent reset process*. Our analysis relies on the approach introduced in the previous sections.

One has to note here that while the formalism and approach of the previous sections is surely useful, special care with regard to two characteristics of the present problem have to be regarded. The first is the effect of the resetting mechanism on the MTB, τ_2. The second is the modification of the hitting angle distribution due to the constant resetting.

Let us start with the first point. Our goal is hereby the determination of the conditions under which the MTB τ_2 can be minimized by an optimal resetting rate that is positive. Let $\vec{x}_r$ be the position of the particle after each resetting event then our backward equation formalism for the two-dimensional excursions of the particle is described by

$$D_2\partial_{\vec{x}}^2\tilde{q}(\vec{x},s) - (r+s)\tilde{q}(\vec{x},s) = -1 - r\tilde{q}(\vec{x}_r,s) \tag{5.42}$$

with the boundary condition

$$\tilde{q}\left(\vec{x},s\right)|_{|\vec{x}|=R} = 0. \tag{5.43}$$

We start by finding the solution to the homogeneous equation

$$D_2\partial_{\vec{x}}^2\tilde{q}(\vec{x},s) - (r+s)\tilde{q}(\vec{x},s) = 0. \tag{5.44}$$

The solution to this equation is of course expected to be radially symmetric about the origin and to have a vanishing derivative at $|\vec{x}| = 0$

$$\nabla\tilde{q}(\vec{x},s)|_{\vec{x}=\vec{0}} = 0. \tag{5.45}$$

These conditions are fulfilled by the equation

$$\tilde{q}_{hom}(\vec{x},s) = I_0\left(\sqrt{\frac{r+s}{D_2}}|\vec{x}|\right) \tag{5.46}$$

where I_n is the modified Bessel function of the first kind.

Now by knowing the homogeneous solution we can derive the inhomogeneous solution which fulfills the differential equation (5.42), by considering,

as before, the Ansatz

$$\tilde{q}\left(\vec{x},s\right)=AI_0\left(\sqrt{\frac{r+s}{D_2}}|\vec{x}|\right)+B. \tag{5.47}$$

In combination with the boundary condition we can derive the solution

$$\tilde{q}\left(\vec{x},s\right)=\frac{I_0\left(\ell_s^{-1}R\right)-I_0\left(\ell_s^{-1}|\vec{x}|\right)}{rI_0\left(\ell_s^{-1}|\vec{x}_r|\right)+sI_0\left(\ell_s^{-1}R\right)} \tag{5.48}$$

with $\ell_{2,s}^{-1}=\sqrt{(r+s)/D_2}$. The problems studied in this work have the special characteristic that the resetting position $\vec{x}_r$ is equal to the starting position which allows us to simplify our solution to

$$\tilde{q}\left(\vec{x},s\right)=\frac{I_0\left(\ell_{2,s}^{-1}R\right)-I_0\left(\ell_{2,s}^{-1}|\vec{x}|\right)}{rI_0\left(\ell_{2,s}^{-1}|\vec{x}|\right)+sI_0\left(\ell_{2,s}^{-1}R\right)}. \tag{5.49}$$

The MTB for this process is provided by the formula

$$\tau_2(R_0)=\tilde{q}\left(R_0,s=0\right)=\frac{1}{r}\left(\frac{I_0\left(\ell_2^{-1}R\right)}{I_0\left(\ell_2^{-1}R_0\right)}-1\right) \tag{5.50}$$

with $\ell_2=\sqrt{D_2/r}$. This analytical result agrees quite well with the Monte-Carlo simulations as can be seen by Fig. 5.8. Furthermore our formula can be used in order to specify the value of the optimal resetting rate for a large range of values of the ratio R_0/R. The results of this calculation can be seen in Fig. 5.9. It is remarkable that an optimal resetting rate r^* with $r^*\neq 0$ can be found only for $R_0>0.578R$.

We can now assume that the diffusive particle starts from the center of the circle and calculate the ratio D_2/D_1 for which the effect of resetting is beneficial. In this case we have of course the gain potential $\mathcal{P}_G(x)=L^{-1}$ and thus we get the equation

$$\begin{aligned}T=&\frac{1}{r}\left(\frac{I_0\left(\ell_2^{-1}R\right)}{I_0\left(\ell_2^{-1}R_0\right)}-1\right)+\frac{I_0\left(\ell_2^{-1}R\right)}{I_0\left(\ell_2^{-1}R_0\right)}\times\\&\times\frac{\coth L(2\ell_1)^{-1}}{2r\ell_1}\left(L-2\ell_1\tanh L\left(2\ell_1\right)^{-1}\right)\end{aligned} \tag{5.51}$$

Inserting now $R_0=0$ in the formula derived above and using the fact that $I_0(0)=1$ gives us the MTA

$$T=\frac{1}{r}\left(I_0\left(\ell_2^{-1}R\right)-1\right)+I_0\left(\ell_2^{-1}R\right)\frac{\coth L(2\ell_1)^{-1}}{2r\ell_1}\left(L-2\ell_1\tanh L\left(2\ell_1\right)^{-1}\right) \tag{5.52}$$

with $\ell_1=\sqrt{D_1/r}$. In Fig. 5.10 we can see an excellent agreement between this formula and the numerical simulation for the special case of $\ell^{-1}=\ell_1^{-1}=\ell_2^{-1}$. The necessary condition $D_2>0.4D_1$ for the existence of an positive optimal resetting rate can be easily derived from this equation.

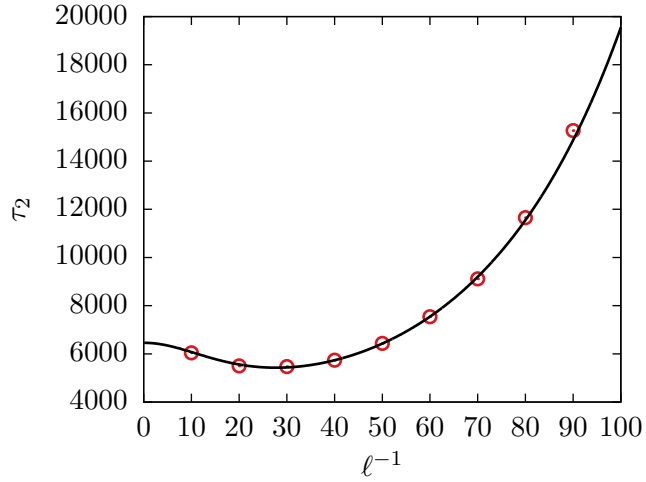

FIGURE 5.8. MTB for two-dimensional Brownian motion in a circle of radius $R = 1$ starting from the radius $R_0 = 0.9$ for different inverse mean path lengths. We can clearly see that there exists an optimal resetting rate for which this time is minimized.

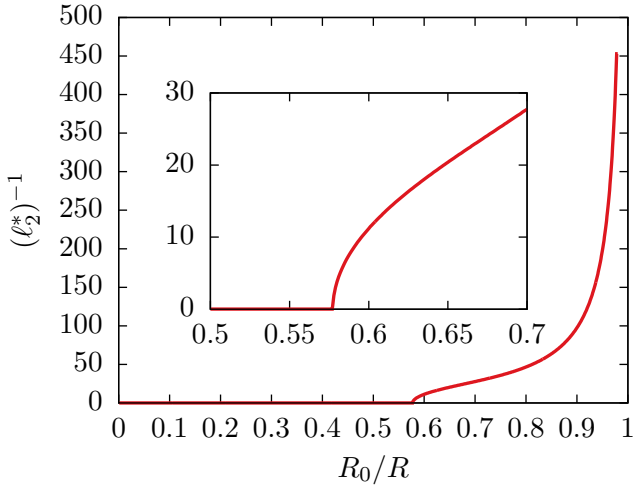

FIGURE 5.9. Inverse of the optimal mean free path length for different ratios of the initial radius to the total radius of the circle. We can see that for $R_0 > 0.578R$ the optimal resetting rate is greater than zero. We have used here a circle of radius $R = (2\pi)^{-1}$.

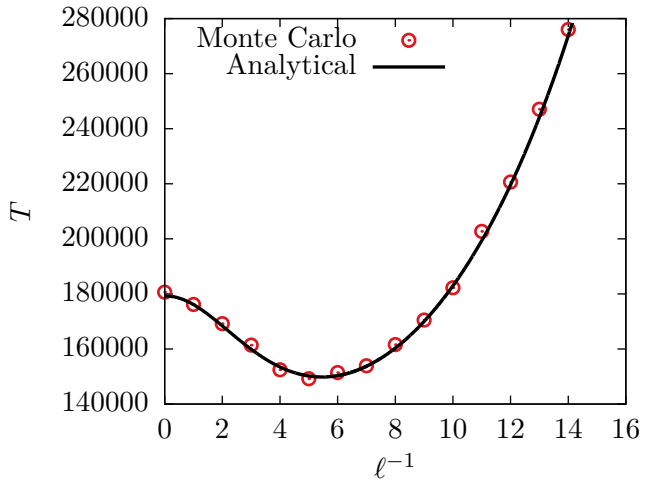

FIGURE 5.10. MTA for a particle starting from the center of the circle of radius $R = (2\pi)^{-1}$ for different inverse mean path lengths and $D_2 = D_1$. We can clearly see that there exists an optimal resetting rate for which this time is minimized. The results of the Monte-Carlo simulation show a very good agreement to the analytical expectations derived from the formula (5.52).

This value is slightly bigger than the value ($D_2 > 0.38D_1$) calculated in the last section. This is not surprising if we consider that for the special case of a resetting field that acts only on the boundary of the system the delay of the first passage time caused by resetting is weaker than the one caused by a persistent resetting field.

Now we focus on the second point, namely the effect of the resetting on the hitting angle. In the past the impact of a resetting mechanism on the outcome of an absorption process has been studied [**134**]. This impact can be understood by considering that the stochastic paths of the particle influenced by resetting are the paths of a renewal process. The mean length of these paths is reduced to a scale proportional to $r^{-1/2}$. This implies an additional condition that has to be considered when determining the hitting angle distribution.

The method introduced in [**134**] is rather general and can also be used here in order to quantify the effect. Let therefore $p(\theta, t)$ describe the probability density function of the event: the diffusive particle crosses the boundary at the time-point t and at a point that corresponds to the angle θ. The probability density function for the same outcome with a positive resetting rate r is given by

$$p_r(\theta) = \frac{\tilde{p}(\theta, r)}{\tilde{p}(r)}, \tag{5.53}$$

where $\tilde{p}(\theta, r)$ and $\tilde{p}(r)$ denote the Laplace Transforms of $p(\theta, t)$ and $p(t) = \int \mathrm{d}\theta\, p(\theta, t)$ evaluated at r, respectively. Unfortunately an analytical expression of the function $p(\theta, t)$ is still missing and we could not evaluate the corresponding Laplace Transform and hence provide an exact form for $p_{G,r}(x) = p_r(\theta)$.

Nevertheless it is possible here the Laplace Transform $\tilde{p}(r)$, since

$$\tilde{p}(r) = -\int_0^\infty \mathrm{d}t\, \frac{\partial Q(R_0, t)}{\partial t} e^{-rt} =$$

$$= -e^{-rt} Q(R_0, t)|_0^\infty - r \int_0^\infty \mathrm{d}t\, e^{-rt} Q(R_0, t) =$$

$$= \frac{2 I_0(\ell_2^{-1} R_0)}{I_0(\ell^{-1} R) + I_0(\ell_2^{-1} R_0)}. \tag{5.54}$$

In the Appendix C we illustrate how the provided formulas can be used in order to calculate the exact effect of resetting on the outcome of a simple one-dimensional diffusion with two absorbing boundary conditions.

The results of the present section can be summarized as

$$T = \frac{1}{r}\left(\frac{I_0\left(\ell_2^{-1} R\right)}{I_0\left(\ell_2^{-1} R_0\right)} - 1\right) + \frac{I_0\left(\ell_2^{-1} R\right)}{I_0\left(\ell_2^{-1} R_0\right)} \times$$

$$\times \int \mathrm{d}x\, p_{G,r}(x) \frac{\cosh \ell_1^{-1} \pi R - \cosh \ell_1^{-1}(x - \pi R)}{\int \mathrm{d}z\, p_{G,r}(z) \cosh \ell_1^{-1}(z - \pi R)}. \tag{5.55}$$

This expression is in good agreement with our previous results. For example it is not hard to see that in the limiting case of $D_2 \to \infty$ the present formula is equivalent to Eq. (5.41).

5.6. Monte Carlo simulation

In order to test our analytical findings we compared them with numerical results derived from Monte-Carlo simulations. We used hereby a simple method by which we simulate a Brownian-like motion by creating and monitoring a discrete time random walk x_t with $t \in \mathbb{N}$, defined by

$$x_t = x_0 + \sum_{k=0}^{t} \xi_k \tag{5.56}$$

whereas the random variables ξ_k are drawn from a normal distribution with mean 0 and variance σ^2.

The mean variance of the random walk is given by the formula

$$\mathbb{E}\left[x_t^2 - x_0^2\right] = \mathbb{E}\left[\sum_{i=1}^{t} (x_i - x_{i-1})^2\right] = \sigma^2 t. \tag{5.57}$$

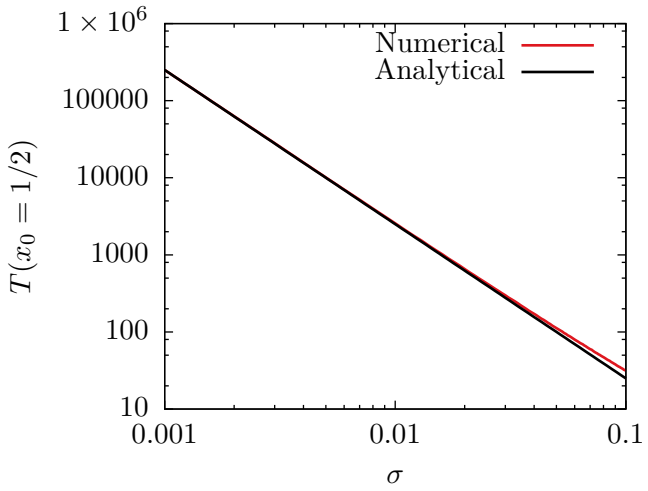

FIGURE 5.11. Numerical and analytical evaluation of the targeting problem with no resetting. We calculate the mean time to absorption for a Brownian particle starting from $x_0 = 1/2$ with two absorbing boundary conditions $T(0) = T(1) = 0$. We can see that a comparison between our analytical and numerical results is only possible for low values of σ.

By comparing this expression to the Green's function we see that $\sigma^2 = 2D_1$. These two scales (analytical and numerical) define the respective characteristic scales for both our methods and allows us to directly compare our numerical results to the derived analytical expressions.

Special care has to be taken here with regard to the choice of standard deviation, since higher values of volatility may lead to discrepancies between the numerical and analytical approach. This is expected due to the fundamentally different nature of the continuum (analytical) and the discrete (numerical) time-step processes and shown in Fig. 5.11 where the expected time to absorption for a process with no resetting and two perfectly absorbing boundary conditions is plotted for both numerical and analytical methods.

In the latter sections 5.3-5.5 the implementation and understanding of the dynamics of two-dimensional Brownian motions became necessary. In order to achieve that, we considered a two-dimensional random walk described by the equation

$$\vec{x}_t = \left(x_0 + \sum_{k=0}^{t} \xi_k \right) \vec{e_x} + \left(y_0 + \sum_{n=0}^{t} \xi_n \right) \vec{e_y}, \tag{5.58}$$

whereas ξ_k is a white noise process derived from the Gaussian distribution $\mathcal{N}(0, \sigma)$. For the presented two-dimensional process we have a standard

deviation given by $2D_2 = \sigma^2$. This allows us to determine numerically the stopping time

$$\tau_2 = \inf\left\{t \in \mathbb{N} : x_t^2 + y_t^2 \geq R^2\right\}. \tag{5.59}$$

For two-dimensional systems the offset is extremely hard to reduce in comparison to the one-dimensional processes. Fortunately we can rely hereby on two methods: using processes with a smaller volatility and/or introduce a finer time-scale. The first method is non-optimal since it leads to an increase of the mean time to absorption and correspondingly to higher running times.

We decided therefore to use the second method. We considered hereby that each time step consists of δ^{-2} smaller steps during which jumps of length $\xi\delta$ are performed. It is easy to see that by sending δ to zero the desired Wiener process can be approximated, but even for $\delta > 0$ this method leads to a great improvement of the derived results. For sections 5.3 and 5.4 we have chosen $\delta = 0.25$ and for section 5.5 $\delta = 0.1$.

In order to simulate the resetting mechanism we introduced the resetting probability $r_n \in [0, 1]$. After each jump the walker is reset to a new position with a probability r_n according to the gain distribution $\mathcal{P}_G$. The mean time between two resets τ_r for this process is consequently given by the formula

$$\tau_{r,n} = 1 + \sum_{k=0}^{\infty} k r_n (1 - r_n)^k = 1 + \frac{1 - r_n}{r_n} = \frac{1}{r_n}. \tag{5.60}$$

In our analytical calculations we know that the times intervals between two resets have an exponential distribution

$$p(t) = re^{-rt} \tag{5.61}$$

for which then the mean time is given by $\tau_{r,a} = \frac{1}{r}$.

As already seen in the last chapter a comparison between our analytical findings and the Monte-Carlo approach is made possible by the requirement that the two time scales, $\tau_{r,a}$ and $\tau_{r,n}$, are equal. This is accomplished by adjusting the two parameters, r_n and r.

5.7. Discussion and Conclusions

In this chapter we studied the dynamics of a diffusive searcher which combines two different types of diffusive behavior. Two distinct modes are considered hereby, one where the searcher undergoes a two-dimensional diffusion and one where an one-dimensional diffusion process along the boundary of the domain is performed. We also assumed that the evolution of the process involves restarts which allow the searcher to return to its initial position.

We started by a Fokker-Planck formalism and used the Laplace Transform to calculate the mean time to absorption for several variations of the process. This allowed us to have a better evaluation of the properties of random search processes with restarts in two-dimensional bounded domains. In the last chapter we proved that resetting can be beneficial for the case of

an one-dimensional diffusion process in a bounded domain [**135**]. The work presented here allows us to assert that resetting may be beneficial for a diffusive search process inside a two-dimensional bounded domain.

Before we go over to the properties of the two-dimensional model we have to note that while in the last chapter we considered an one-dimensional model with reflecting boundary conditions and derived the necessary conditions for the existence of a positive resetting rate here we could show that for a one-dimensional process taking place in a periodic domain of length L an optimal positive resetting rate exists as long as the distance between the initial position and the target is smaller than $0.276L$. Furthermore if the resetting does not lead back to the initial position but sets the searcher at random position of the whole interval $[0, L]$, then the optimal resetting rate is equal to ∞.

These results helped us greatly when analyzing the process that switches between two-dimensional diffusion and one-dimensional excursion. Firstly we considered the case where a resetting field applies only on the boundary. For this problem several regions with an optimal resetting rate that was bigger than zero could be found. Of course this was only possible by considering specific values of the ratio D_2/D_1 between the two diffusion constants. Our approach also showed that for a process starting from the center of the circle an optimal resetting rate can be found as long as $D_2 > 0.38D_1$. This result agrees perfectly with the past works which followed a diverse framework since they were occupied with processes exhibiting intermittent behavior [**107**]. In the last section we generalized the resetting field and considered the possibility of a reset from inside the circle. These resetting dynamics can only have a positive effect for the special case of a process starting from the center of the circle only when $D_2 > 0.4D_1$.

The present formalism could also been generalized in order to analyze search processes where the target is not a point but an extended area on the boundary. This model would correspond to a Brownian particle trying to escape from a bounded domain through a small window while under the effect of a resetting potential. We have also a variation of the narrow escape problem [**136**] where we can ask ourselves if a positive resetting rate can accelerate this process.

Another property of search processes that arises in several realizations but has not been considered here is the existence of several searchers. The relevance of many searchers for diffusion with resetting has been considered in the past [**113, 79, 115**]. Such a consideration would surely be interesting also in the present setting. This implementation also allows one to consider the effect of resetting on interacting particles. One could as example consider the case of a single file diffusion on the boundary of the circle [**143**].

CHAPTER 6

Conclusions

In this work we studied two distinct classes of non-equilibrium models, random average process and diffusion with resetting. Despite the significant differences between them a stochastic analytical approach proved essential in both cases. In chapter 3 for example the analysis of the random average process with $\gamma = -\infty$ became possible only by the study of the time evolution of the mass at a single site and the determination of the probability distribution function of the random variable m_τ. For the diffusion process on the other hand the vast majority of the presented results in chapters 4 and 5 were based on established stochastic analytical methods of the past. This fact underlines the general importance of stochastic calculus in non-equilibrium physics.

In chapter 2 and 3 we focused on the random average process that is related to stochastic driven lattice gas models with stochastic nearest neighbor interactions like the zero range process. In contrast to the lattice gas models the state of the random average process is described by continuous and unbounded random variables. Here we studied the specific example of a truncated random average process where the fraction density ϕ and hence the dynamics of the system are influenced by the state of the system. For this special class of stochastic mass transport models an analytical approach is difficult and in some cases even impossible.

The limits of the analytical methods became apparent when dealing with three different models of truncated stochastic mass transport in chapter 2. For example a mean field ansatz proved to be misleading due to the existence of strong two-point mass correlations. In addition the derivation of a critical density by a grand-canonical formalism was not possible. These difficulties made an analytical evaluation of the broken ergodicity property of the TARAP impossible. Nevertheless an order statistics approach may prove to be successful in a future study of the condensation transition for truncated models in the thermodynamic limit (see Appendix B).

Nevertheless it was possible to gain some analytical results for a new kind of truncated random average process where only sites with masses above a certain cutoff (which we chose to set equal to 1) contribute to the flow in the system. For this model an absorbing state appears for $\rho < 1$ that can be determined by a canonical ensemble formalism for a relatively broad class of fraction densities ϕ. It is given that the determination of this state is very crucial in the understanding of the properties for the system with $\rho > 1$.

It is also notable that the derived results provide an algorithm that can create rather efficiently a large set of independently and identically distributed random variables that fulfill two kind of constraints. The first constraint determines the maximal value of those variables and the second fixes their total sum. A naive computer algorithm trying to accomplish the same task has a much higher running time that our proposed method. Furthermore it was possible to show that the described absorbing state also exists when the dynamics are partial asymmetric. These findings prove that large deviation theory is a very useful tool in the analysis of non-equilibrium systems and probably can contribute to the understanding of condensation transitions in such models.

The study of the effect of stochastic resetting on diffusing search processes that take place in bounded domains has revealed some very interesting findings. We could see in chapter 4 that for an one-dimensional partial absorption process with two reflecting boundaries the option of stochastic resetting to the initial position is not always advantageous. The optimal resetting rate r that minimizes the Mean Time to Absorption (MTA) is a continuous function of the distance between the target and the initial position of the stochastic searcher. The exact regions inside this one-dimensional bounded domain for which the optimal resetting rate is bigger than zero could be defined for different values of the absorption rate α. Furthermore we were in the position to determine analytically the MTA for a random walk in a discrete lattice with a perfectly absorbing target $\alpha \to \infty$.

In chapter 5 we present a new random search model formulated again as a stochastic first passage time problem. The model consists of two components, each of which are not individually new, but the combination of the two is novel and interesting. First, the searcher is able to move (by Brownian motion) in 2D when in the interior of a bounded domain and switches to 1D Brownian motion (with a different diffusivity) when on the boundary of the domain. The second component is that the search randomly resets to its initial position. The counterintuitive result is that random resetting can speed up the random search, particularly when motion on the boundary is slower. It is also possible to show that there is a region within the disc where starting positions support a positive optimal resetting rate.

First passage scenarios like the one explored in this work have been essential in the development of our theoretical understanding of cell biology, foraging behavior, stock markets and chemical or biochemical reactions. Furthermore they may find applications in data analysis methods that rely on stochastic search algorithms. In all of these different fields the properties of stochastic search processes that take place inside bounded domains play a very important role. It would be surely interesting to test the existence of an optimal resetting rate in more complex geometries than the one presented in this work.

Additionally our findings support the idea that random walk, in search for a target site inside a finite size network, may profit from the implementation of a restart mechanism. Such a restart mechanism is easily implemented for a complex network by inserting several directed links. The effect of this resetting mechanism can then be estimated by analyzing the spectral properties of the two networks, the original and the modified one.

We have seen in this work that stochastic processes with resetting were inspired by the adoption of memory effects in the evolution of those processes. Here we introduced a very basic form of memory where the searcher only remembers its initial position. It is therefore natural to try to encompass a more complicated version of this memory effect in a future work. This possible interplay between resetting to previous preferential positions and surface mediated diffusion is surely a very interesting subject.

One last question that arose from this work relates to the probability distribution function of the escape time from inside a circular domain for a two-dimensional Brownian motion. It was not possible to find or to derive an exact expression for the pdf of the escape times under the condition that the crossing of the boundary took place at a specific angle of the circle. Of course such a question is only meaningful if the Brownian motion started from a point, that it is not the center of the circle. This mathematical problem seems to be rather simple but due to time reasons its solution is not part of this work. The exact calculation of this probability density function would allow us to predict the effect of resetting on the hitting angle distribution and therefore complete our stochastic analytical endeavor of chapter 5.

APPENDIX A

Mean Field Approach for the Random Average Process

In this chapter we will see how the mean field ansatz can be applied for a special case of the random average processes. We consider namely the case where at each time-step a random fraction of the mass at each site i is chipped off. A fraction equal to $(1+\alpha)/2$ of this chipped off mass is then transported to site $i+1$ and the rest, $(1-\alpha)/2$, to the site $i-1$. The evolution of the state at a specific time-point $(m_{1,t}, ..., m_{L,t})$ is thus described by the following equations

$$m_{i,t+1} = (1-r_{i,t})m_{i,t} + \frac{1+\alpha}{2} r_{i-1,t} m_{i-1,t} + \frac{1-\alpha}{2} r_{i+1,t} m_{i+1,t}, \quad \forall i : 1 < i < L \tag{A.1}$$

$$m_{1,t+1} = (1-r_{1,t})m_{1,t} + \xi_{\ell,t} + \frac{1-\alpha}{2} r_{2,t} m_{2,t} \tag{A.2}$$

$$m_{L,t+1} = (1-r_{L,t})m_{L,t} + \xi_{r,t} + \frac{1+\alpha}{2} r_{L-1,t} m_{L-1,t} \tag{A.3}$$

The elements $\xi_{\ell,t}$ and $\xi_{r,t}$ can also be used to describe hereby the left and right boundary of the system respectively. The parameter α serves as an indicator of the asymmetry in the system. For $\alpha = 0$ the update process has symmetrical dynamics, while setting $\alpha = 1$ allows us to study the properties of the totally asymmetrical process.

In order to analyze the effect of closed boundaries in the system we can simply set

$$\xi_{\ell,t} = \frac{1+\alpha}{2} r_{L,t} X_{L,t} \quad \text{and} \quad \xi_{r,t} = \frac{1-\alpha}{2} r_{1,t} X_{1,t}. \tag{A.4}$$

From the Master Equation (A.1) we can see that the two-point correlation functions in the steady state limit

$$C_j = \langle m_i m_{i+j} \rangle \tag{A.5}$$

fulfill following equations:

$$C_0 \left(\mu_2 \left(1 + \frac{1+a^2}{2} \right) - 2\mu_1 \right) + 2C_1 \mu_1 (1-\mu_1) + 2C_2 \mu_1^2 \frac{1-a^2}{4} = 0$$

$$C_0\left(\frac{1+a}{2}(\mu_1-\mu_2)+\frac{1-a}{2}(\mu_1-\mu_2)\right)+C_1\mu_1\left(-2+\mu_1\frac{3+a^2}{4}\right)+$$
$$+C_2(\mu_1-\mu_1^2)+C_3\frac{1-a^2}{4}\mu_1^2=0$$
$$C_0(\mu_1-\mu_2)+C_1\mu_1\left(\frac{7-a^2}{4}\mu_1-2\right)+C_2\mu_1(1-\mu_1)+C_3\frac{1-a^2}{4}\mu_1^2=0$$
$$C_{j-2}\frac{1-a^2}{4}\mu_1^2\quad+C_{j-1}\mu_1(1-\mu_1)+C_j\mu_1\left(\tfrac{1+a^2}{2}\mu_1-2\right)+C_{j+1}\mu_1(1-\mu_1)+$$
$$+C_{j+2}\tfrac{1-a^2}{4}\mu_1^2,\quad \text{for}\quad j\geq 4. \tag{A.6}$$

It is not possible to solve this set of equations and we have to use a different approach.

By applying the product measure ansatz and equation (A.1) we can see that the evolution of the probability distribution function for a single site is given by the following master equation

$$\begin{aligned}P_t(m_i)=\ & \int_0^\infty \mathrm{d}m'_{i-1}\int_0^1 \mathrm{d}r_{i-1}\int_0^\infty \mathrm{d}m'_i\int_0^1 \mathrm{d}r_i\int_0^\infty \mathrm{d}m'_{i+1}\int_0^1 \mathrm{d}r_{i+1}\\ &\times P_{t-1}(m'_{i-1},m'_i,m'_{i+1})\phi(r_{i-1})\phi(r_i)\phi(r_{i+1})\\ &\times\delta\left(m_i-m'_i(1-r_i)-\tfrac{1+\alpha}{2}r_{i-1}m'_{i-1}-\tfrac{1-\alpha}{2}r_{i+1}m'_{i+1}\right)\end{aligned} \tag{A.7}$$

We will consider in the following the fraction density $\phi(r)=1$. For this special choice with regard to the fraction density we can see that in the stationary limit $t\to\infty$, following equation

$$Q(s)=\int_0^1 \mathrm{d}r\,Q(rs)\int_0^1 \mathrm{d}r\,Q\left(\frac{1-\alpha}{2}rs\right)\int_0^1 \mathrm{d}r\,Q\left(\frac{1+\alpha}{2}rs\right). \tag{A.8}$$

for the Laplace transform, $Q(s)=\int_0^\infty \mathrm{d}xP(x)\exp(-xs)$ is fulfilled. For $\alpha=\pm 1$, this equation can be solved in closed form and we get $Q(s)=\frac{4}{(s+2)^2}$ leading to the well known result $P(x)=4x\exp(-2x)$ [**16**].

For other values of α a closed form expression is impossible. Nevertheless we are in the position to derive the different moments of the distribution. Differentiating two times of Equation (A.8) and setting $s=0$ allows us to determine the second moment of the distribution,

$$\langle x^2\rangle=\frac{3}{4}\frac{5-\alpha^2}{3-\alpha^2}. \tag{A.9}$$

From the numerical simulations one can see clearly a deviation from the predicted behavior for $|\alpha|<1$ (see Fig. 1). This fact clearly shows that the mean field approach for systems with $|\alpha|<1$ is false. Similar results have been derived for a different version of the symmetrical random average process [**17**]. It seems also impossible to define the distribution for general α. Nevertheless it is viable to define a symmetric process for which the mean field approach applies.

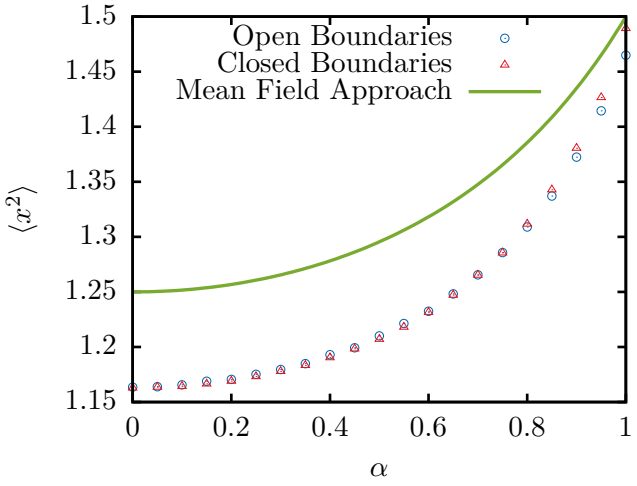

FIGURE A.1. Second moment for random average process defined by Eq. (1) for different asymmetry coefficient and two distinct boundary conditions. We see a clear discrepancy between the mean field solution and the numerical results for $\alpha < 1$. We are therefore inclined to declare the product measure ansatz for $\alpha < 1$ as invalid. In the case of open boundary conditions we have chosen $\xi_{\ell,t}, \xi_{r,t}$ to have a uniform distribution in the interval $[0, 1]$.

We see also that the mean field approach does not apply for the special case of $\alpha = 0$ for the master equation defined above. This fact is independent from the symmetric nature of the system, as one can introduce a symmetric system, for which the mean field approach is fruitful. We present here such a process and prove numerically that the predicted probability distribution is the correct one. We define therefore a system of stochastic differential equations where at each time the fraction of the masses transported to the two neighboring sites are both chosen from a uniform probability distribution. The process is described by the master equation

$$m_{i,t+1} = r_{i,s,t} m_{i,t} + r_{i-1,r,t} m_{i-1,t} + r_{i+1,\ell,t} m_{i+1,t}. \tag{A.10}$$

With

$$\phi(r_r, r_\ell, r_s) = 2\delta(r_{\ell,t} + r_{r,t} + r_{s,t} - 1) \tag{A.11}$$

leading to

$$\phi(r_r) = \phi(r_\ell) = \phi(r_s) = \phi(r) = 2(1 - r). \tag{A.12}$$

It is not hard to see that in this case the Laplace transform of the mass distribution is given by

$$Q(s) = \left[\int \mathrm{d}r \, 2(1 - r) Q(sr) \right]^3, \tag{A.13}$$

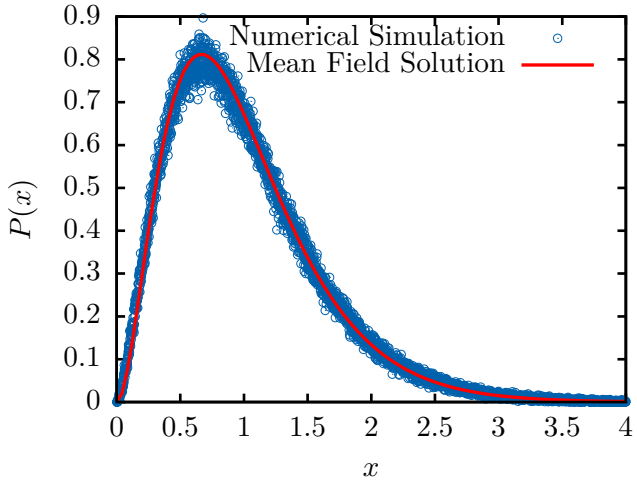

FIGURE A.2. Probability distribution for the process described by Equations (A.10)-(A.12). We can see a very good agreement between the predicted distribution, Eq. (A.14), and the Monte Carlo simulation. The Monte Carlo simulation is based on 10^4 different realizations.

which can be easily solved to deliver

$$P(x) = \frac{27}{2} x^2 \exp(-3x) . \tag{A.14}$$

APPENDIX B

Extreme Value Distribution of the Random Average Process

In the following section we consider the order statistics of the free ARAP. This study can eventually be used in order to understand the ergodicity breaking observed in [**36**]. We consider also in the following the set $\{\ell_k(t)\}$, where $\ell_k(t)$ is the k-largest mass at the time-point t in the system, instead of the mass configuration $\{m_i(t)\}$. Hence we use the notation $\ell_k(t)$ with

$$\ell_L(t) < \ell_{L-1}(t) < ... < \ell_1(t) = \max_{1\leq i\leq L} m_i(t). \tag{B.1}$$

In Chapter 2 we derived a diagram for the states of three different truncation models with finite lengths. One question that naturally arises is if the observed structure survives in the thermodynamic limit. Here we will try to answer this question by focusing on the properties of the largest value $\ell_1(t)$ in the thermodynamic limit. Since in the following we consider only free ARAP update rules the distribution of the masses is stationary. Hence we can use in the following the characterization ℓ_1 instead of $\ell_1(t)$.

We know from [**45**] that the probability of $\ell_1 \leq x$ is given by

$$P(x, M, L) = \frac{I(x, M, L)}{Z(M, L)} \tag{B.2}$$

where

$$I(x, M, L) = \prod_{i=1}^{L} \int_0^x \mathrm{d}m_i \, f(m_i)\delta\left(\sum_{i=1}^{L} m_i - M\right) \tag{B.3}$$

and $Z(M, L)$ is given by $Z(M, L) = I(\infty, M, L)$ (see equation (5) above).

The Laplace transform of $I(x, M, L)$ is easily computed by

$$\int_0^\infty \mathrm{d}M \, I(x, M, L)e^{-sM} = \left[\int_0^x \mathrm{d}m \, f(m)e^{-sm}\right]^L. \tag{B.4}$$

The critical density for a condensation phase transition of the free ARAP is infinite and we can apply the Bromwich integral in order to invert the expression (B.4) in order to get

$$P(x, M, L) = \frac{\int_{c-i\infty}^{c+i\infty} \mathrm{d}s \, \exp\left[L\left(\rho s + \ln g(s)\right)\right]}{\int_{c-i\infty}^{c+i\infty} \mathrm{d}s \, \exp\left[L\left(\rho s - 2\ln s\right)\right]} \tag{B.5}$$

with $M = \rho L$ and

$$g(s) = s^{-2}(1 - e^{-sx} - sxe^{-sx}). \tag{B.6}$$

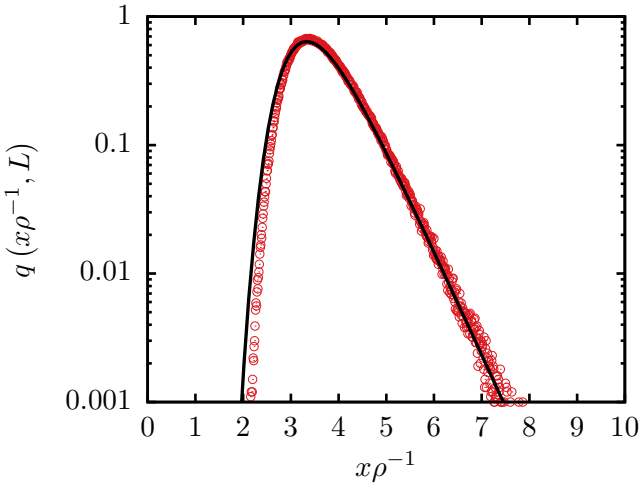

FIGURE B.1. Numerical (red circles) and analytical (black line) derivation of the largest value distribution density for a free ARAP system with $L = 100$ and $\rho = 1$.

The integration is performed along the vertical line $\Re(s) = c$ in the complex plane such that c is greater than the real part of all singularities of the integrand. Since we are in the fluid phase we can use a saddle point approximation as the one presented in [**47**] where to leading order the saddle point, s_0, of the integrand is independent of x and is given by the equation

$$\rho = \frac{\int_0^\infty \mathrm{d}m\, m^2 e^{-s_0 m}}{\int_0^\infty \mathrm{d}m\, m e^{-s_0 m}} = \frac{2}{s_0}. \tag{B.7}$$

Inserting this formula in

$$P(x, M, L) = \exp\left[-L\frac{\int_x^\infty \mathrm{d}m\, m e^{-s_0 m}}{\int_0^\infty \mathrm{d}m\, m e^{-s_0 m}}\right] \tag{B.8}$$

leads finally to the approximate solution

$$P\left(x, M, L\right) = P\left(x\rho^{-1}, L\right) = \exp\left[-L\left(\frac{2x}{\rho} + 1\right)e^{-\frac{2x}{\rho}}\right]. \tag{B.9}$$

Although the derived equations are approximations they can be still useful even for finite systems as shown in Figure B.1 where we can see a good agreement between the Monte Carlo simulation and our analytical prediction for the probability density function of the largest value

$$q\left(x\rho^{-1}, L\right) = \rho\frac{\partial}{\partial x}P\left(x\rho^{-1}, L\right). \tag{B.10}$$

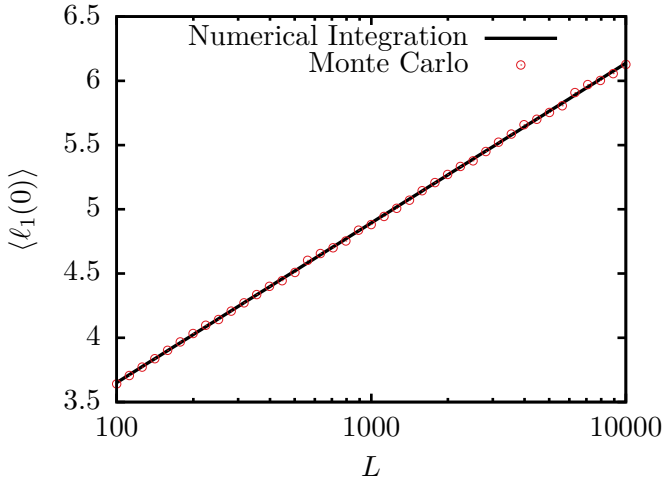

FIGURE B.2. Mean largest value for different lengths in the special case of $\rho = 1$. Each data point was calculated by averaging over 10^4 different Monte Carlo simulations. We have evolved hereby a periodic boundary system with random initial condition according of the dynamics of the free ARAP. The blue line was derived by a numerical evaluation of the integral in Eq. (B.11).

We can use now this expression to calculate the mean largest value in the system

$$\frac{\langle \ell_1 \rangle}{\rho} = \int_0^\infty \mathrm{d}y\, y q\,(y, L) = \rho^{-1} \int_0^\infty \mathrm{d}x\, x \tfrac{\partial}{\partial x} P\left(x\rho^{-1}, L\right) = \\ = -\sum_{n=1}^{\infty} \left(\tfrac{-L}{n}\right)^n \tfrac{1}{2n} \sum_{k=0}^{n} \tfrac{n^k}{k!}. \tag{B.11}$$

We preferred here a numerical evaluation of the integral in Eq. (B.11). The results of which are presented in Figure B.2 where we also plotted the results of a Monte Carlo of a free ARAP system. The derived curve is best approximated by the function

$$\langle \ell_1 \rangle = 0.54\rho \ln(8.63L + 1). \tag{B.12}$$

Now if we set $L = 100$ then we can derive

$$\langle \ell_1 \rangle = 3.65\rho = 100\rho\ell^*, \tag{B.13}$$

whereas ℓ^* is the value for $\langle \ell_1 \rangle \rho^{-1} L^{-1}$ that we could observe in the fluid state for all of the truncated models studied in Chapter 2. Unfortunately the extreme value distribution can be determined analytically only for the fluid case.

Nevertheless the presented approximations prove extremely useful in the analysis of the broken ergodicity property of truncated models. This characteristic was first noticed in [**36**] where the divergence of the lifetimes of the high flow and the low flow states in the thermodynamic limit could be observed. An ergodicity breaking is also to be expected for the TARAP and the ZRRAP in the case of $\gamma > 0$ and for the SRAP if we assume that $\gamma > 1$.

This statement relies on two facts, the stability of condensates for truncated models and the degeneracy of the extreme value distribution in the thermodynamic limit.

In Chapter 2 we characterized the condensate phase by the large deviation of the mean largest value from the derived expectation of Eq. (B.12). By using Monte Carlo simulations we could see that for increasing times this deviation is also increasing. Specifically we could say that for large time intervals following property becomes evident

$$\left\langle \frac{\partial \ell_1(t)}{\partial t} \right\rangle \geq 0 \quad \text{as long as} \quad \ell_1(t) > 1. \tag{B.14}$$

This assumption would of course not hold for all time-points in a finite system due to the conservation of the mass, M, but it becomes reasonable if we consider the case of $L \to \infty$. Now for $\ell_1(t) \gg 1$ this would lead to a condensate with infinite lifetime, meaning that the probability of the mass on this site to return to values below 1 is becoming zero. This condition alone is not sufficient for the appearance of condensates in the studied systems since no guarantee for the survival of states with $\ell_1(t) = 1 + \varepsilon$ can be made. Therefore we have to consider the order statistics of the free ARAP.

We note here that the position of the largest value in the fluid state is neither stable nor does it perform a continuous drift but shows irregular jumps. It is therefore appropriate to consider this as a resetting of the largest value to a random position constantly during the evolution of the system. Due to this resetting it is important to calculate the distribution of the second largest value in order to describe the properties of the transition $\{\ell_1(t) < 1\} \leftrightarrow \{\ell_1(t+1) > 1\}$.

We start therefore by the formula

$$\Pr\{\ell_2 < x\} = \Pr\{\ell_1 < x\} + \Pr\{\ell_2 < x < \ell_1\}. \tag{B.15}$$

Since the term $\mathrm{P}\{\ell_1 < x\}$ has been calculated above we concentrate now on the second term [**48**]

$$\Pr\{\ell_2 < x < \ell_1\} = L \int_x^\infty \mathrm{d}m_1 \, f(m_1) \times \frac{\prod_{i=2}^{L} \int_0^x \mathrm{d}m_i \, f(m_i) \delta\left(\sum_{i=2}^{L} m_i - M - m_1 \right)}{\prod_{i=1}^{L} \int_0^\infty \mathrm{d}m_i \, f(m_i) \delta\left(\sum_{i=1}^{L} m_i - M \right)}. \tag{B.16}$$

In order to evaluate this expression we use, as before, a saddle point approximation of the inverse Laplace transform by determining the minimum

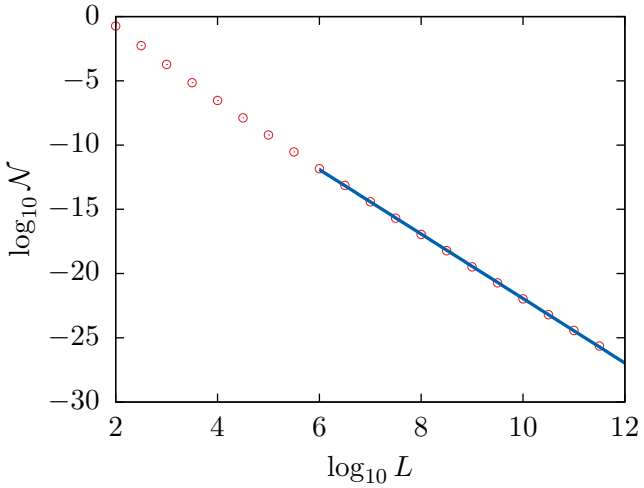

FIGURE B.3. $\mathcal{N} = \int \mathrm{d}\rho \Pr\{\ell_2 < 1 < \ell_1\}$ vs the length of the system L. We find that for increasing lengths this weight tends to zero with an algebraic law. Numerically we find $\mathcal{N} \propto L^{-2.5}$ for $L \to \infty$. The blue line correspond to our numerical fit.

of the function

$$h(s) = \rho s \quad + \tfrac{1}{L} \ln \int_x^\infty \mathrm{d}m\, f(m) e^{-sm} + \\ + \tfrac{L-1}{L} \ln \int_0^x \mathrm{d}m\, f(m) e^{-sm}. \tag{B.17}$$

Using a numerical calculation we can see that

$$\lim_{L\to\infty} \Pr\{\ell_2 < x\} \sim \lim_{L\to\infty} \Pr\{\ell_1 < x\}. \tag{B.18}$$

This follows from the fact that the expression $\Pr\{\ell_2 < x < \ell_1\}$ vanishes faster than $\Pr\{\ell_1 < x\}$ when $L \to \infty$. One can use the same approach in order to show that

$$\lim_{L\to\infty} \Pr\{\ell_{k+1} < x\} \sim \lim_{L\to\infty} \Pr\{\ell_k < x\} \quad \forall k \ll L. \tag{B.19}$$

The dependency of the probability $\Pr\{\ell_2 < x < \ell_1\}$ on the length of the system is reflected in Figure B.3 where the quantity

$$\mathcal{N} = \int \mathrm{d}\rho \Pr\{\ell_2 < 1 < \ell_1\} \tag{B.20}$$

is shown as function of the length of the system. We choose $\mathcal{N}$ in order to show that the likelihood of a transition $\{\ell_1(t) > 1\} \leftrightarrow \{\ell_1(t+1) < 1\}$, which strongly depends on $\Pr\{\ell_2 < x < \ell_1\}$, is vanishing for all densities.

On the other side if we consider the density ρ^* for which the expression $\Pr\{\ell_2 < 1 < \ell_1\}$ is maximal,

$$\frac{d}{d\rho} \Pr\{\ell_2 < 1 < \ell_1\}\,|_{\rho^*} = 0, \tag{B.21}$$

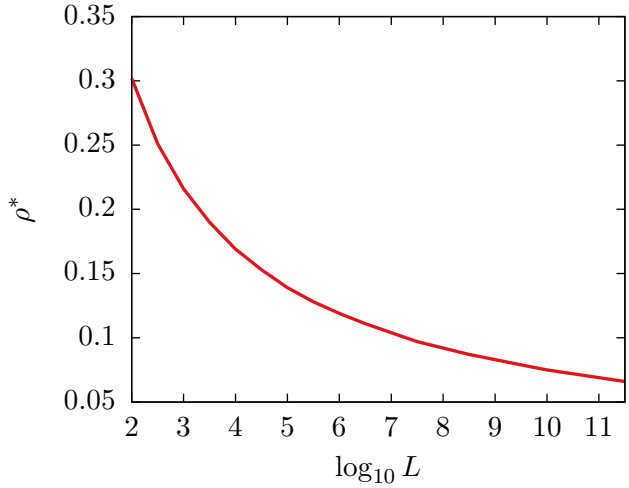

FIGURE B.4. Density ρ^* as function of the length of the system.

we can see in Figure B.4 that the behavior of the function $\rho^*(L)$ is described by a monotone decreasing function for increasing lengths.

In detail we show that for sufficiently high densities ($\rho > (\ln L)^{-1}$) in the thermodynamic limit we arrive at a state where a macroscopic number of sites have a mass above 1. If we assume that these states have a survival probability (meaning the probability of remaining above 1) that is higher than zero, then the existence of a macroscopic number of such states in combination with the increasing survival probabilities for increasing masses when truncation dynamics apply is a sufficient condition for the creation of a condensate in the system.

Similarly for $\rho \ll (\ln L)^{-1}$ we almost surely can observe states with $\ell_1(t) < 1$ and a vanishing transition probability $\{\ell_1(t) < 1\} \to \{\ell_1(t+1) > 1\}$ for $L \to \infty$ and $\forall t \in \mathbb{N}$. By taking into account these two facts the broken ergodicity property for truncated models in the thermodynamic limit becomes evident.

We were unfortunately not in the position to derive any analytical results. This is of course due to the complex nature of the fraction density. Nevertheless we think that the presented approach can prove rather useful in the future when discussing the broken ergodicity property or in general condensation transitions arising out of single site deviations. Specifically we are convinced that when truncated dynamics apply the system in the thermodynamic limit can be in either of two states: no site has a mass above the cutoff or a macroscopic number of sites has a mass above the cutoff.

APPENDIX C

Effect of Resetting on the Hitting Probability

In order to visualize the effect of resetting on the hitting probability we decided to present here the effect of a resetting mechanism on the simple one-dimensional diffusion process with two absorbing boundary conditions.

Let us also consider a Brownian Motion with resetting that takes place in the one-dimensional interval $[0, L]$ with two perfectly absorbing traps on $x = 0, L$. Let $P_r(x_0)$ describe hereby the probability for the process starting at the position x_0 to terminate on the boundary $x = L$. If we set the resetting rate r equal to zero, then we know that the expression

$$P_{r=0}(x_0) = \frac{x_0}{L} \tag{C.1}$$

is to be expected. Now we have to ask ourselves how this expression might change if the process resets to its initial position with a resetting rate $r > 0$.

We use here the method introduced in [**134**] in order to calculate the effect. Let $p(x_0, t)$ describe the probability density function of the absorption time and $p^s(x_0, t)$ the pdf of the absorption times with a successful outcome, namely an absorption at $x = L$, then the probability for a positive outcome with a resetting rate r is given by the formula

$$P_r(x_0) = \frac{\tilde{p}^s(x_0, r)}{\tilde{p}(x_0, r)}. \tag{C.2}$$

Whereas $\tilde{p}^s(x_0, r)$ and $\tilde{p}(x_0, r)$ denote the Laplace Transforms of $p^s(x_0, t)$ and $p(x_0, t)$

$$\tilde{p}^s(x_0, r) = \int \mathrm{d}t\, \mathrm{e}^{-rt} P^s(x_0, t), \quad \tilde{p}(x_0, r) = \int \mathrm{d}t\, \mathrm{e}^{-rt} P(x_0, t) \tag{C.3}$$

evaluated at r respectively. In order to calculate the probability distribution functions, $p^s(x_0, t)$ and $p(x_0, t)$, we first calculate the pdfs $\psi(x, t; x_0)$ for the Brownian particles by using the image method [**144**]

$$\psi(x,t;x_0) = \sum_{k=0}^{\infty} \frac{\exp\left(-\frac{(x-x_0-2k)^2}{4Dt}\right) - \exp\left(-\frac{(x+x_0-2(k+1))^2}{4Dt}\right)}{\sqrt{4\pi Dt}} - \frac{\exp\left(-\frac{(x+x_0+2k)^2}{4Dt}\right) + \exp\left(-\frac{(x-x_0+2(k+1))^2}{4Dt}\right)}{\sqrt{4\pi Dt}}.$$

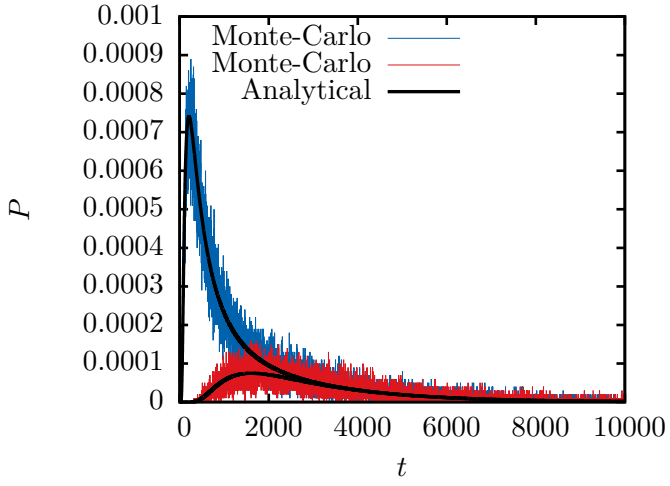

FIGURE C.1. Evaluation of the probability density functions $p^s(t)$ and $p^f(t)$ for process starting at $x_0 = 0.75$ with $L = 1$ and $D = 5 \cdot 10^{-4}$. The blue lines corresponds to the results of the Monte-Carlo simulation which ends at the boundary $x = L$ while the red lines describe the distribution of the absorption times for process who end in fails (at the boundary $x = 0$). We can see a very good agreement between our numerical and analytical results.

Now we can calculate the probability density function for success or fail as function of the time by the derivative

$$p^s(x_0, t) = \frac{\partial}{\partial x}\psi(x, x_0; t)|_{x=L} = p(x_0, t) - p^f(x_0, t). \tag{C.4}$$

We use here the notation $p^f(x_0, t)$ to describe the pdf of the absorption times for Brownian particles that get absorbed at $x = 0$. The pdf is consequently given by

$$p(x_0, t) = \frac{\partial}{\partial x}\psi(x, x_0; t)|_{x=0} + \frac{\partial}{\partial x}\psi(x, x_0; t)|_{x=L} = p^s(x_0, t) + p^f(x_0, t). \tag{C.5}$$

By using these expressions we are in the position to calculate analytically the expression $p^s(x_0), p(x_0, r)$ and hence $P_r(x_0)$. In Figure C.2 we can see an excellent agreement between our numerical and analytical results.

The same method was used in chapter 5 in order to calculate the effect of the resetting on the hitting probability for a two dimensional process inside a circle. For a process starting from the center of the circle the Laplace transform of the probability distribution of the hitting times is given by the expression

$$\tilde{p}(r) = \frac{2I_0(R_0)}{I_0(R) + I_0(R_0)}. \tag{C.6}$$

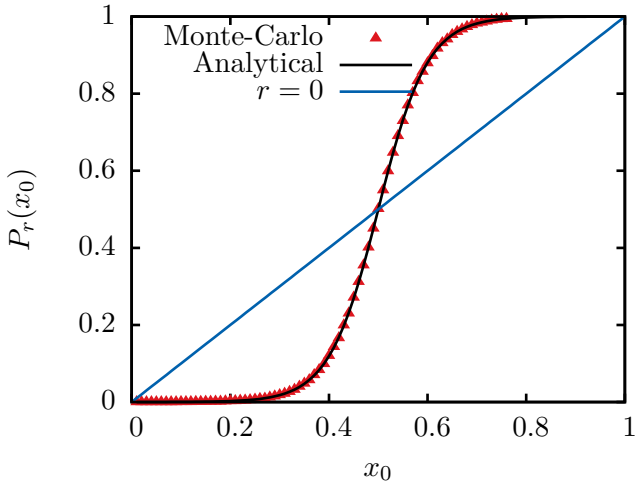

FIGURE C.2. Probability for a process to end at the boundary $x = 1$ if it started from the position x_0 with $D = 5 \cdot 10^{-5}$ and $r = 5 \cdot 10^{-3}$.

Unfortunately it was impossible to define the Laplace transform of the same function for the specific value of a certain angle outcome θ for $p_r(\theta)$ given by

$$p_r(\theta) = \frac{\tilde{p}(\theta, r)}{\tilde{p}(r)} = \frac{\int \mathrm{d}t\, e^{-rt} p(\theta, t)}{\int \mathrm{d}t \int \mathrm{d}\theta\, e^{-rt} p(\theta, t)}. \tag{C.7}$$

Here the term $p(\theta, t)$ describes the pdf of the absorption times that happen at a specific angle θ. This expression is hardly approachable analytically and hence we were not in the position to provide a fully analytical expression for the general case of the mean to absorption for Brownian particle starting from a random position inside the circle.

APPENDIX D

Optimal Search Strategy for Intermittent Search Process

In the last two chapters of our work we occupied ourselves with the search properties of diffusion processes with resetting dynamics. One question that arose during our work was related to the existence of an optimal search strategy for Brownian motion process taking place in a periodic domain. We have seen hereby in chapter 4 that an optimal searching time for a resetting process inside a periodic domain is achieved when we combine a uniform gain potential with an infinitely high resetting rate.

In this chapter we describe the properties of search process not in terms of resetting dynamics but that of an intermittent search process that combines short range excursions with long range jumps. Let φ characterize hereto the probability distribution of these long range jumps. The time intervals between two such long range jumps are described by the exponential

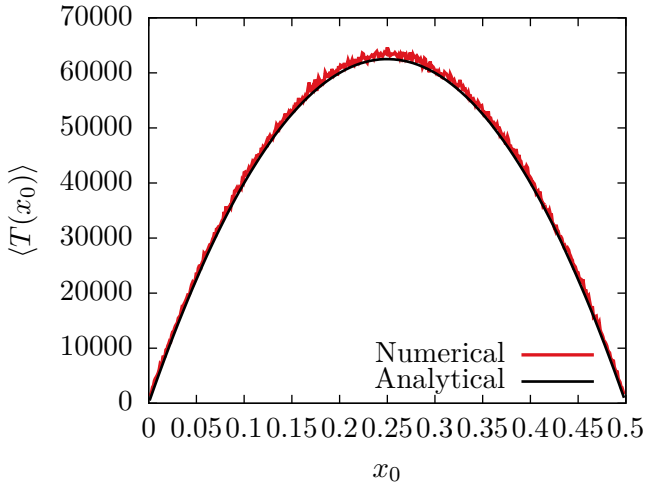

FIGURE D.1. Mean time to absorption for a resetting process that performs a maximum jump of $a = 2R$. The numerical results were derived by a discrete time Monte-Carlo simulation where after each time-step the searcher performed a long range jump.

distribution function $\lambda e^{-\lambda t}$. For the special case of

$$\varphi(x) = 1, \quad \forall x \in [0, 2\pi R]. \tag{D.1}$$

an optimal search strategy would require an infinite high jump rate λ.

Now let us focus on the case where these long range jumps are described by a δ function

$$\varphi(x) = \delta(x - b). \tag{D.2}$$

Naturally the question arises how the parameter b has to be chosen in order for the quantity

$$\mathcal{I} = \int \mathrm{d}x\, T(x), \tag{D.3}$$

with $T(x)$ being the mean time to absorption for a process starting at x, to be minimized?

Let us here consider the choice of $b = L/2$. Fortunately this case can be described analytically and an optimal strategy for this jump distribution can be found. One has to consider hereby that the mean time to absorption for this process is equal to that of one particle bounded in the region $[0, L/2]$ with one reflecting and one perfectly absorbing boundary condition whereas the position of these boundaries is exchanged with a rate λ. We also have to deal with a target problem with a radiation boundary condition [**115, 131**]. After this unconventional yet simple realization it is easy to see that the Laplace transform of the survival probability reads

$$\tilde{q}(z, s) = \frac{\lambda \cosh \alpha L/4 - \left(\lambda - \sqrt{Ds}\right) \cosh \alpha \left(z - L/4\right)}{\lambda s \cosh \alpha L/4} \tag{D.4}$$

with $\alpha = \sqrt{s/D}$. Now if we consider the limit $\lambda \to \infty$ and do a series expansion of cosh up to $\mathcal{O}(s)$ then this equation transforms into

$$\lim_{\lambda\to\infty} T(z) = \lim_{\lambda\to\infty} \lim_{s\to 0} \tilde{q}(z, s) = \frac{2 + (\alpha L/4)^2 - 2 - \alpha^2 \left(z - L/4\right)^2}{2s} =$$

$$= \frac{z\left(z - L/2\right)}{2D} \quad \text{for} \quad z \in [0, L/2]. \tag{D.5}$$

We see also that the mean time $T(z) = \tilde{q}(z, 0)$ is in the limit of $\lambda \to \infty$ that of a particle between two perfect absorbing boundaries at $0, L$ or equivalently to that of two particles performing the same random motion in the interval $[0, L]$ while being at a distance $L/2$ from each other. The relative good agreement between the analytical and the numerical solution is shown in Figure D.1. We simulated hereby a random walk process that evolves in a discrete time setting. After each jump a long range jump is performed.

Bibliography

[1] O. Penrose, Foundations of Statistical Mechanics (Pergamon, Braunschweig, 1970).
[2] A. Griffin, D. W. Snoke, and S. Stringari, Bose-Einstein Condensation (Cambridge University Press, Cambridge, 1996).
[3] O. J. O'Loan, M. R. Evans, and M. E. Cates, *Phys. Rev. E* **58**, 1404 (1998).
[4] D. Chowdhury, L. Santen, and A. Schadschneider, *Phys. Rep.* **329**,199 (2000).
[5] J. Kaupuzs, R. Mahnke, and R. J. Harris, *Phys. Rev. E* **72**, 056125 (2005).
[6] P. Bialas, Z. Burda, and D. Johnston, *Nucl. Phys. B* **493**, 505 (1997).
[7] P. L. Krapivsky, S. Redner, and F. Leyvraz, *Phys. Rev. Lett.* **85**, 4629 (2000).
[8] G. Bianconi and A. L. Barabási, *Phys. Rev. Lett.* **86**, 5632 (2001).
[9] J. P. Bouchaud and M. Mézard, *Physica A* **282**, 536 (2000).
[10] Z. Burda, D. Johnston, J. Jurkiewicz, M. Kaminski, M. A. Nowak, G. Papp, and I. Zahed, *Phys. Rev. E* **65**, 026102 (2002).
[11] K. van der Weele, D. van der Meer, M. Versluis, and D. Lohse, *Europhys. Lett.* **53**, 328 (2001).
[12] N. Pottier, Nonequilibrium Statistical Physics *Linear Irreversible Processes* (Oxford University Press, New York, 2011)
[13] R. Livi and P. Politi, Nonequilibrium Statistical Physics: *A Modern Perspective* (Cambridge University Press, Cambridge, 2017)
[14] M. R. Evans and B. Waclaw, *J. Phys. A: Math. Theor.* **47**, 095001 (2014).
[15] M. R. Evans and T. Hanney, *J. Phys. A: Math. Gen.* **38**, R195 (2005).
[16] S. N. Coppersmith, C.-h. Liu, S. N. Majumdar, O. Narayan, and T. A. Witten, *Phys. Rev. E* **53**, 4673 (1996).
[17] R. Rajesh and S. Majumdar, *J. Stat. Phys.* **99**, 943 (2000).
[18] J. Krug and J. Garcia, *J. Stat. Phys.* **99**, 31 (2000).
[19] P. A. Ferrari and L. Fontes, *J. Probab.* **3**, 34 (1998).
[20] R. Rajesh and S. N. Majumdar, *Phys. Rev. E* **64**, 036103 (2001).
[21] F. Zielen and A. Schadschneider, *J. Stat. Phys.* **106**, 173 (2002).
[22] F. Zielen and A. Schadschneider, *J. Phys. A: Math. Gen.* **36**, 13 (2002).
[23] J. Cividini, A. Kundu, S. Majumdar, and D. Mukamel, *J. Phys. A: Math. Theor.* **49** (8), 085002 (2016).
[24] J. Cividini, A. Kundu, S. Majumdar, and D. Mukamel, *J. Stat. Mech.* , 053212 (2016).
[25] A. Kundu and J. Cividini, *Europhysics Letters* **115**, 54003 (2016).
[26] J. Szavits-Nossan, M. R. Evans, and S. N. Majumdar, *Phys. Rev. Lett.* **112**, 020602 (2014).
[27] S. Chatterjee, P. Pradhan, and P. K. Mohanty, *Phys. Rev. Lett.* **112**, 030601 (2014).
[28] A. Das, S. Chatterjee, and P. Pradhan, *Phys. Rev. E* **93**, 062135 (2016).
[29] S. Chakraborti, S. Mishra, and P. Pradhan, *Phys. Rev. E* **93**, 052606 (2016).
[30] A. Das, A. Kundu, and P. Pradhan, *Phys. Rev. E* **95** F, 062128 (2017).
[31] E. Levine, D. Mukamel, and G. M. Schütz, *J. Stat. Phys.* **120**, 759 (2005).
[32] P. Greulich and A. Schadschneider, *J. Stat. Mech.* P04009 (2008).
[33] Y. Sinai, Lectures in Ergodic Theory (Princeton University, Princeton, 1977).
[34] S. Grosskinsky, G. M. Schütz, and H. Spohn, *J. Stat. Phys.* **113**(3/4), 389 (2003).

[35] A. Schadschneider, D. Chowdhury, and K. Nishinari, Stochastic Transport in Complex Systems: from Molecules to Vehicles (Elsevier, Amsterdam, 2011).
[36] F. Zielen and A. Schadschneider, *Phys. Rev. Lett.* **89**, 090601 (2002).
[37] C. Godreche and J.M. Luck, *J. Phys. A* **38** 7215 (2005).
[38] P. Chleboun and S. Grosskinsky, *J. Phys. A* **48**, 055001 (2015).
[39] O. Hirschberg, D. Mukamel, and G. M. Schütz, *Phys. Rev. E* **87** 052116 (2013).
[40] C. Landim, *Commun. Math. Phys.* **330** 1 (2014).
[41] B. Waclaw and M. R. Evans, *Phys Rev. Lett.* **108** 070601 (2012).
[42] S. Majumdar, M. R. Evans, and R. K. P. Zia, *J. Phys. A: Math. Gen.* **37**, 25 (2004).
[43] S. Majumdar, M. R. Evans, and R. K. P. Zia, *J. Stat. Mech.: Theor. Exp.* L10001 (2004).
[44] S. N. Majumdar, M. R. Evans, and R. K. P. Zia, *Phys. Rev. Lett.* **94**, 180601 (2005).
[45] M. R. Evans, S. N. Majumdar, and R. K. P. Zia, *J. Stat. Phys.* **123**, 357 (2006).
[46] M. R. Evans, *J. Phys. A: Math Gen.* **30**, 5669 (1997).
[47] M. R. Evans and S. N. Majumdar, *J. Stat. Mech.* P05004 (2008).
[48] H. A. David, Order Statistics (John Wiley and Sons, Hoboken, 1970).
[49] T. Ligett, Interacting Particle Systems (Springer-Verlag, Berlin Heidelberg, 1995).
[50] V. Privman, Non-equilibrium Statistical Physics in one Dimension, (Cambridge University Press, Cambridge, 2005).
[51] T. Bodineau and B. Derrida, *Phys. Rev. Lett.* **92**, 180601 (2004).
[52] R. S. Ellis, *Scand. Actuarial. J.* **1**, 97 (1995).
[53] S. R. S. Varadhan, Large Deviations and Applications (SIAM, Philadelphia, 1984).
[54] R. S. Ellis, Entropy, Large Deviations, and Statistical Mechanics (Springer, New York, 1985).
[55] A. Dembo and O. Zeitouni, Large Deviations Techniques and Applications, (Springer, New York, 2010).
[56] H. Touchette, *Phys. Rep.* **478**, 1 (2009).
[57] H. Touchette, arXiv:1106.4146 (2011).
[58] D. Sornette, Critical Phenomena in Natural Sciences: *Chaos, Fractals, Selforganization and Disorder: Concepts and Tools* (Springer Verlag, Heidelberg, 2004)
[59] F. Spitzer, *Adv. Math.* **5**, 246 (1970).
[60] M. Henkel, H. Hinrischen, S. Lübeck, Non-Equilibrium Phase Transitions, (Springer, Berlin Heidelberg, 2008).
[61] J. Szavits-Nossan, M. R. Evans, and S. N. Majumdar, *Phys. Rev. Lett.* **112**, 020602 (2014).
[62] J. Szavits-Nossan, M. R. Evans, and S. N. Majumdar, *J. Phys. A: Math. Theor.* **47** 455004 (2014).
[63] D. R. Cox and H. D. Miller, The Theory of Stochastic Processes, (CRC Press, New York, 1977).
[64] G. Gallavotti and E. G. D. Cohen, *Phys. Rev. Lett.* **74**, 2694 (1995).
[65] Y. Oono and M. Paniconi, *Prog. Theor. Phys. Supp.* **130**, 29 (1998).
[66] J. L. Lebowitz and H. Spohn, *J. Stat. Phys.* **95**, 333 (1999).
[67] L. Bertini, A. De Sole, D. Gabrielli, G. Jona-Lasinio, and C. Landim, *Rev. Mod. Phys.* **87**, 593 (2015).
[68] T. Hatano and S.-I. Sasa, *Phys. Rev. Lett.* **86**, 3463 (2001).
[69] S. Sasa and H. Tasaki, *J. Stat. Phys.* **125**, 125 (2006).
[70] E. Bertin, K. Martens, O. Dauchot, and M. Droz, *Phys. Rev. E* **75**, 031120 (2007).
[71] K. Hayashi and S.-I. Sasa, *Phys. Rev. E* **68**, 035104 (2003).
[72] R. Durrett, Probability: Theory and Examples, (Cambridge University Press, Cambridge, 2010).
[73] A.J. Bray and R.A. Blythe, *Phys. Rev. Lett.* **89**, 150601 (2002).
[74] S. Condamin, O. Bénichou, V. Tejedor, R. Voituriez and J. Klafter, *Nature* **450**, 77-80 (2007).

[75] A. Blumen, G. Zumofen, and J. Klafter, *Phys. Rev. B* **30**, 5379 (1984).
[76] L. Mirny, M. Slutsky, Z. Wunderlich, A. Tafvizi, J. Leith and A. Kosmrlj, *J. Phys. A: Math. Theor.* **42**, 434013 (2009).
[77] S. Redner and P. L. Krapivsky, *Am. J. Phys.* **67**, 12 (1999).
[78] D. Toussaint and F. Wilczek, *J. Chem. Phys.* **78**, 2642 (1983).
[79] M. R. Evans and S. N. Majumdar, *J. Phys. A: Math. Theor.* **47**, 285001 (2014).
[80] A. Montanari and R. Zecchina, *Phys. Rev. Lett.* **88**, 178701 (2002).
[81] S. Janson and Y. Peres, *SIAM J. Discrete Math.* **26**, 537 (2012).
[82] I. Dumitriou, P. Tetali, and P. Winkler, *SIAM J. Discrete Math.* **16**, 604 (2003).
[83] E. Gelenbe, *Phys. Rev. E* **82**, 061112 (2010).
[84] O. Bénichou, C. Loverdo, M. Moreau, and R. Voituriez, *Rev. Mod. Phys.* **83**, 81 (2011).
[85] S. Condamin, O. Bénichou, and M. Moreau, *Phys. Rev. Lett.* **95**, 260601 (2005).
[86] O. Bénichou, M. Moreau, P.-H. Suet, and R. Voituriez, *J. Chem. Phys.* **126**, 234109 (2007).
[87] M. R. Evans, S. N. Majumdar and K. Mallick, *J. Phys. A: Math. Theor.* **46**, 185001 (2013).
[88] X. Durang, M. Henkel, and H. Park, *J. Phys. A: Math. Theor.* **47**, 045002 (2014).
[89] J. Whitehouse, M. R. Evans and S. N. Majumdar, *Phys. Rev. E* **87**, 022118 (2013).
[90] T. G. Mattos, C. Mejía-Monasterio, R. Metzler and G. Oshanin, *Phys. Rev. E* **86**, 031143 (2012).
[91] A. Szabo, G. Lamm and G. H. Weiss, *J. Stat. Phys.* **34**, 225 (1984).
[92] D. A. Atkinson and H. W. Crater, *Am. J. Phys.* **43**, 301-304 (1975).
[93] A. Pal, *Phys. Rev. E* **91**, 012113 (2015).
[94] S. Redner, *A Guide to First-Passage Processes* (Cambridge University Press, Cambridge, 2001).
[95] L. Kusmierz, S. N. Majumdar, S. Sabhapandit, and G. Schehr, *Phys. Rev. Lett.* **113**, 220602 (2014).
[96] J. Lörinzsci, F. Hiroshima, and V. Betz, *Feynmann-Kac-Type Theorems and Gibbs Measures on Path Space: With Applications to Rigorous Quantum Field Theory* (Walter de Gruyter, Berlin, 2010).
[97] M. Reed and B. Simon, *Methods of Modern Mathematical Physics, Volume 1: Functional Analysis* (Academic Press, London, 1980).
[98] B. Simon *Bull. Amer. Math. Soc. (N.S.)* **7** 3, 447 (1982).
[99] W. Feller, *An Introduction to Probability Theory and Its Applications* (Wiley, Hoboken, 1971).
[100] B. Simon, *J. Math. Phys.* **12**, 140-148 (1971).
[101] S. Condamin, O. Bénichou and M. Moreau, *Phys. Rev. E* **72**, 016127, (2005).
[102] D. K. Park, *J. Math. Phys.* **36**, 5453 (1995).
[103] B. Gaveau and L. S. Schulman, *J. Phys. A: Math. Gen.* **19**, 1833-1846 (1986).
[104] B. Davies, *Integral Transforms and Their Applications* (Springer, Belrin Heidelberg 2001).
[105] T. Guérin, N. Levernier, O. Bénichou, and R. Voituriez, *Nature* **534**, 356 (2016).
[106] R. Metzler, G. Oshanin, and S. Redner, First-Passage Phenomena and their Applications (World Scientific, Singapore, 2014) Vol **35**.
[107] O. Bénichou, D. Grebenkov, P. Levitz, C. Loverdo, and R. Voituriez, *Phys. Rev. Lett.* **105**, 150606 (2010).
[108] J.-P. Bouchaud and M. Potters, Theory of Financial Risk and Derivative Pricing *From Statistical Physics to Risk Management* (Cambridge University Press, Cambridge, 2000).
[109] O. Bénichou, Y. Kafri, M. Sheinman, and R. Voituriez, *Phys. Rev. Lett.* **103**, 138102 (2009).

[110] O. Bénichou, D. S. Grebenkov, L. Hillairet, L. Phun, R. Voituriez, and M. Zinsmeister, *Analysis and Mathematical Physics* **5**, 321-362 (2015).
[111] S. C. Manrubia, and D. H. Zanette, *Phys. Rev. E* **59**, 4945 (1999).
[112] M. Montero, and J. Villarroel, *Phys. Rev. E* **87**, 012116 (2013).
[113] M. R. Evans, and S. N. Majumdar, *Phys. Rev. Lett.* **106**, 160601 (2011).
[114] M. R. Evans, and S. N. Majumdar, *J. Phys. A: Math. Theor.* **44**, 435001 (2011).
[115] J. Whitehouse, M. R. Evans and S. N. Majumdar, *Phys. Rev. E* **87**, 022118 (2013).
[116] R. Hołyst, M. Błaźejczyk, K. Burdzy, G. Góralski, L. Bocquet, *Physica A: Stat. Mech. Appl.* **277**, 71 (2000).
[117] A. Pal *Phys. Rev. E* **91**, 012113 (2014).
[118] D. Boyer and Solis-Salas, *Phys. Rev. Lett.* **112**, 240601 (2014)
[119] D. Boyer, M. R. Evans, and S. N. Majumdar, *J. Stat. Mech.* 023208, 2017.
[120] L. Kuś mierz, S. N. Majumdar, S. Sabhapandit, and G. Schehr, *Phys. Rev. Lett.* **113**, 220602 (2014).
[121] S. Gupta, S. N. Majumdar, and G. Schehr, *Phys. Rev. Lett.* **112**, 220601 (2014).
[122] F. Bartumeus, and J. Catalan, *J. Phys. A: Math. Theor.* **42**, 43 (2009).
[123] O. Bénichou, C. Loverdo, M. Moreau, and R. Voituriez, *Rev. Mod. Phys.* **83**, 81 (2011).
[124] S. Gupta, and A. Nagar, *J. Phys. A: Math Theor.* **49**, 445001 (2016).
[125] J. Fuchs, S Goldt, and U. Seifert, *Europhys. Lett.* **113**, 60009 (2016).
[126] A. Pal, and S. Reuveni, Phys. Rev. Lett. **118**, 030603 (2017).
[127] R. Falcao and M. R. Evans, *J. Stat. Mech.* **17**, 023204 (2017).
[128] R. J. Harris, and H. Touchette, *J. Phys. A: Math. Theor.* **50**, 10LT01 (2017).
[129] A. Pal, A. Kundu, and M. R. Evans, *J. Phys. A: Math. Theor.* **49**, 225001 (2016).
[130] J. M. Meylahn, S. Sabhapandit, and, H. Touchette *Phys. Rev. E* **92** , 062418 (2015).
[131] H. Sano and M. Tachiya, *J. Chem. Phys.* **71**, 1276 (1979).
[132] B. Mukherjee, K. Sengupta, and S. N. Majumdar, arXiv:1806.00019 (2018).
[133] D. C. Rose, H. Touchette, I. Lesanovsky, and J. P. Garrahan, arXiv:1806.01298 (2018).
[134] S. Belan, *Phys. Rev. Lett.* **120**, 080601 (2018).
[135] C. Christou and A. Schadschneider, *J. Phys. A: Math Theor.* **48**, 28 (2015).
[136] O. Bénichou and R. Voituriez, *Phys. Rev. Lett.* **100**, 168105 (2008).
[137] A. Pal and S. Reuveni, *Phys. Rev. Lett.* **118**, 030603 (2017).
[138] V.P. Shkilev, *Phys. Rev. E* **96**, 012126 (2017)
[139] L . Kuśmierz, M. Bier and E. Gudowska-Nowak *J. Phys. A: Math Theor.* **50**, 18 (2017)
[140] A. Scacchi and A. Scharma, arxiv:1708.05591 (2017).
[141] L. Lovasz, *Random Walks on Graphs: A Survey in Combinatronics* (Bolyai Society for Mathematical Studies, Keszthely, 1996).
[142] R. Manella, *Phys. Lett. A* **254** (5), 257 (1999).
[143] A. Taloni and F. Marchesoni, *Phys. Rev. Lett.* **96**, 020601 (2006).
[144] I. Karatzas and S. Shreve, Brownian Motion and Stochastic Calculus (Springer-Verlag, New York, 1988).

Danksagung

Zum Schluss möchte ich mich bei allen Leuten bedanken, die die Erstellung dieser Arbeit möglich gemacht haben. (Hoffe ich vergesse dabei niemanden!)

An erster Stelle möchte ich mich bei Prof. Dr. Schadschneider bedanken, der mir die Promotionsstelle angeboten hat. Zudem war seine Betreuung nicht nur hilfreich sondern auch immer ermutigend. Vielen Dank für die exzellente Zusammenarbeit in allen diesen Jahren.

Ich möchte mich auch bei der gesamten Arbeitsgruppe bedanken, bei Cornellia, Steffan, Daniel, Christoph und Johannes. Wir hatten im Laufe der Zeit sehr viele hilfreiche Gesrpäche. Teilweise hatten sie was mit Physik zu tun. Meistens waren sie spannender!

Einen besonderen Dank geht auch an Abhinava Chatterjee. Wir hatten während seines Aufenthaltes in Köln eine sehr gute Zusammenarbeit. Er hat mir auch wesentlich dabei geholfen, meine Gedanken verständlicher zu fassen.

Ich sollte mich auch bei Kostas und Balaji bedanken. Wir hatten während der Raucherpausen immer sehr spannende Gesrpäche. Sie haben mir auch wesentlich bei den technischen Details dieser Arbeit geholfen.

Ich kann bei dieser Danksagung natürlich nicht die Fachschaft Physik vergessen. Sie hatten nicht nur immer ein offenes Ohr für physikalische Probleme, sondern haben auch meine Arbeit im Institut erfeurlicher gestaltet.

Zum Schluss Dionysia und Ioannis, vielen Dank!

Erklärung

Ich versichere, daß ich die von mir vorgelegte Dissertation selbständig angefertigt, die benutzten Quellen und Hilfsmittel vollständig angegeben und die Stellen der Arbeit – einschließlich Tabellen, Karten und Abbildungen –, die anderen Werken im Wortlaut oder dem Sinn nach entnommen sind, in jedem Einzelfall als Entlehnung kenntlich gemacht habe; daß diese Dissertation noch keiner anderen Fakultät oder Universität zur Prüfung vorgelegen hat; daß sie – abgesehen von unten angegebenen Teilpublikationen – noch nicht veröffentlicht worden ist sowie, daß ich eine solche Veröffentlichung vor Abschluß des Promotionsverfahrens nicht vornehmen werde. Die Bestimmungen dieser Promotionsordnung sind mir bekannt. Die von mir vorgelegte Dissertation ist von Prof. Dr. Andreas Schadschneider betreut worden.

Teilpublikationen:
C. Christou and A. Schadschneider, *J. Phys. A: Math Theor.* **48**, 28 (2015)
C. Christou and A. Schadschneider, arXiv:1703.02966 (2017)
A. Chatterjee, C. Christou, and A. Schadschneider, *Phys. Rev. E* **97**, 062106 (2018)

Köln, den 16.04.2019